Investigation towards controlled precipitation of nickel using $H_2S(g)$ by harnessing pH dependent sulphide speciation

Nazneen Karbanee

Thesis presented for the degree of
Master of Science in Engineering
In the Department of Chemical Engineering
University of Cape Town

March 2007

I know the meaning of plagiarism and declare that all the work in the document, save for that which is properly acknowledged, is my own.

In the name of God, the most beneficent, the most merciful

Acknowledgements

I wish to thank a number of people who have contributed to producing this thesis:

To Professor Lewis for her guidance and for granting me the opportunity to further my studies in an excellent research unit known for its good work ethic and for producing excellent research.

To Dr van Hille for his excellent supervision, help and patience. You're cool Rob! ☺

To my colleagues in the Crystallisation and Precipitation Unit, both past and present for their friendship and assistance

To my mother for all her prayers. To my father, Shaheena, Nazir-Ahmed, Farouk and our most special boy, Sa'ad

To Oliver for his understanding, encouragement and support

To the NRF for funding this project

Synopsis

During hydrometallurgical processing to produce Ni(s) a Reduction End Solution (RES) ($Ni(NH_3)_2SO_4$) is generated containing significant concentrations of aqueous nickel (1.20g/L) and cobalt (0.25g/L). The recovery of these heavy metals has the dual advantage of offering significant financial benefit while removing contaminating species from the mother liquor prior to recycling of $(NH_4)_2SO_4$.

Sulphide as a precipitating agent is effective as it facilitates the removal of heavy metals to very low residual concentrations (ppm – ppb levels) over a wide pH range, owing to the low solubilities (K_{SP}) of metal sulphides. However, previous work on metal sulphide precipitation has highlighted a number of challenges. The low solubilities of metal sulphides in combination with the rapid kinetics of sulphide precipitation leads to rapid, uncontrolled metal sulphide precipitate formation. The extremely high supersaturations result in high rates of nucleation, leading to the formation of particles with undesirable characteristics.

In this thesis, to gain insight on the metal sulphide precipitation of nickel and cobalt from the RES, a simplified model system, consisting of a synthetic $NiSO_4$ solution with a concentration of 200ppm Ni^{2+}, was utilised to determine the effect of $H_2S(g)$ as a precipitating agent. Results were evaluated on the basis of efficiency of nickel removal and the properties of the NiS precipitates formed.

The first task was to identify the sulphide species responsible for precipitation of nickel from solution. This was achieved by adjusting the initial pH of the sulphide reagent. The results suggest that $H_2S(aq)$ is not able to effect NiS precipitation.

Owing to extremely high supersaturations, methods of reducing the supersaturation were investigated. The use of $H_2S(g)$ to slow generation of supersaturation was chosen. The mass transfer delay for diffusion of sulphide into solution and the subsequent speciation limited the rate of the precipitation reaction. However, during precipitation the solution pH dropped to acidic values (ie below 6.99) owing to the release of protons from the speciation of sulphide and the subsequent precipitation reaction. Hence, the precipitation of nickel no longer occurred since the majority of sulphide species present in solution were $H_2S(aq)$.

Controlled release of HS^- ions was facilitated, in the semi-batch gaseous experiments, by the addition of alkalinity. Alkalinity, in the form of NaOH, was supplied in low

concentrations initially and it was found that nickel removal occurred at a linear rate, reaching completion within 30-40 minutes. During the continuous nickel removal the aqueous sulphide concentration increased to an equilibrium value and after an initial decrease the pH remained constant between 3 and 4. Thus, the sulphide in solution was present as the $H_2S(aq)$ species and therefore unable to react with nickel.

Resolubilisation of nickel sulphide precipitates was observed, and it was hypothesised that this was due to the formation of aqueous polysulphide complexes. The redissolution effect was tested in batch experiments, varying the molar ratio of Ni:S and significant resolubilsation was observed in the presence of excess HS^- ions.

When NaOH was added at a low concentration the efficiency of sulphide utilisation was low. Aqueous sulphide accumulation was observed within the reactor and the majority of added sulphide passed through the reactor without dissolving. The undissolved sulphide was quantified in a post reactor sulphide trap.

A higher NaOH concentration was supplied to the bubble column so that a greater concentration of $H_2S(aq)$ in solution dissociated to form HS^-. The result was reduced reaction times from 30 to 2.5 minutes, without significant wastage of sulphide reagent. It was attempted to model these experiments using OLI Lab Systems Analyzer. OLI predicted greater Ni^{2+} removal and a greater pH decrease than experimentally observed. For each time interval modelled, OLI predicted the thermodynamic equilibrium, utilising the total free sulphide available. The lower the pH the longer the system took to reach thermodynamic equilibrium and the time scales involved became unrealistic with respect to reactor operation. As a result, the model over-predicted process efficiency. Therefore, thermodynamic based modelling of the system was not appropriate.

The rate of sulphide dissolution was theoretically modelled using Higbie's Penetration Theory. The model was experimentally validated by comparing modelled and experimental aqueous sulphide concentrations and was found to hold for the duration of the experiment. Supersaturation predictions were based on the rate of diffusion as calculated from Higbie's theory and subsequent speciation. It was found that supersaturations decreased when a gaseous sulphide source was employed as opposed to slug-dosing with aqueous sulphide. Typical supersaturation values for the gaseous system were in the region of 10^6 compared to 10^{14} for the batch system.

Particle size distribution (PSD) measurement was attempted in order to carry out population balance modelling of the precipitation reaction. However, due to the flocculation and settling of precipitate particles in the measuring apparatus, robust PSD

measurement was not possible. It was therefore not possible to experimentally determine the controlling particle rate processes; however, empirical data suggests the system is dominated by nucleation and aggregation.

Experiments performed using diluted Reduction end solution (RES) showed that while the complex solution matrix provided significant buffering capacity, the reaction mechanism was similar to that determined for the synthetic nickel sulphate system. Alkalinity input was necessary to facilitate complete precipitation, because the buffering capacity of the diluted RES was insufficient to neutralise all the protons generated during complete precipitation of the nickel and cobalt.

Table of contents

ACKNOWLEDGEMENTS I

SYNOPSIS II

TABLE OF CONTENTS V
LIST OF FIGURES VII
LIST OF TABLES VIII
LIST OF SYMBOLS IX

1. INTRODUCTION 1

1.1. METAL SULPHIDE PRECIPITATION 2
1.2. OBJECTIVES 3
1.3. THESIS OVERVIEW 4

2. PRECIPITATION THEORY 5

2.1 SUPERSATURATION 6
2.2 NUCLEATION 10
2.2.1 Homogeneous nucleation 10
2.2.2 Heterogeneous Nucleation 14
2.2.3 Secondary Nucleation 15
2.3 GROWTH 15
2.3.1 Crystal growth theories 16
2.3.1.1 Two-Dimensional Growth Theories 17
2.3.1.2 BCF (Burton-Cabrera-Frank) surface diffusion Model 18
2.3.1.3 The Diffusion Layer Model 18
2.4 AGGREGATION 19
2.5 BREAKAGE 22

3. SULPHIDE PRECIPITATION 23

3.1. METAL SULPHIDE SOLUBILITIES 24
3.2 SULPHIDE SPECIATION 28
3.3 FORMATION OF AQUEOUS POLYSULPHIDE COMPLEXES/CLUSTERS 30

4. METHODS OF REDUCING LOCAL SUPERSATURATION 33

4.1 MIXING 34
4.2 FLUIDISED BED REACTOR (FBR) 36
4.3 GASEOUS PRECIPITATING REAGENT 38

5. GASEOUS DISSOLUTION AND REACTION OF $H_2S(G)$ 40

5.1 ONE DIMENSIONAL UNSTEADY STATE MOLECULAR DIFFUSION 40
5.2 HIGBIE'S PENETRATION THEORY APPLIED TO METAL SULPHIDE PRECIPITATION 44

6. MATERIALS AND METHODS 48

6.1 SOLUTIONS 48
6.2 ANALYTICAL TECHNIQUES 48
6.3 REACTORS 49
6.3.1 Batch Reactor 49
6.3.2 Bubble Column 50
6.4 EXPERIMENTAL DESIGN 51
6.4.1 Batch Aqueous Experiments 51
6.4.1.1. Control of the sulphide species available for reaction 52
6.4.1.2. Molar ratio of Ni:S 52
6.4.2 Semi-batch gaseous experiments 53
6.4.2.1. Low alkalinity (NaOH) concentrations 54
6.4.2.2. Higher alkalinity (NaOH) concentrations 54
6.4.2.3. RES experiments 55

6.4.3 Modelling *56*

7. EXPERIMENTAL RESULTS AND DISCUSSION 59

7.1. BATCH RESULTS 59
7.1.1 Varying pHi *60*
7.2. SEMI-BATCH RESULTS 66
7.2.1. Low alkalinity (NaOH) concentrations *68*
7.2.2 Varying the Ni:S molar ratio *71*
7.2.3. High alkalinity (NaOH) flowrates *78*
7.2.3.1. Higbie's penetration theory 86
7.2.3.2. Supersaturations 88
7.2.3.3. Particle size distributions (PSDs) 89
7.2.4. Reduction End Solution (RES) *91*

8. CONCLUSIONS AND RECOMMENDATIONS 97

9. REFERENCES 109

APPENDICES 115

APPENDIX A 115
APPENDIX B 116
APPENDIX C 121
APPENDIX D 126
APPENDIX E 126
APPENDIX F 127
APPENDIX G 133
APPENDIX H 133
APPENDIX I 134
APPENDIX J 135

List of figures

Figure 1: Various regions of supersaturation and predominant particle formation mechanisms (Gosele and Kind, 1991) 9
Figure 2: Different mechanisms of nucleation (Söhnel and Garside, 1992) 10
Figure 3: Free energy diagram for nucleation explaining the existence of a 'critical nucleus', free energy vs cluster size (Mullin, 1972) 12
Figure 4: Heterogeneous nucleation; precipitate deposit on a catalyzing foreign surface illustrating the wetting angle 14
Figure 5: Surface structure of a growing crystal (Ohara and Reid, 1973) 16
Figure 6: Development of a growth spiral from the screw dislocation (Mullin, 2002) 18
Figure 7: Concentration profile and concentration driving forces in crystallisation from solution according to the simple diffusion-reaction model (Mullin, 2001; Myerson, 2002) 19
Figure 8: Formation of an aggregate - free particles collide and either disrupt and remain as free particles or cement together via growth of a crystalline bridge between the particles and form an aggregate 20
Figure 9: Metal sulphide precipitation diagram [25°C and 1 atm for $H_2S(g)$] (Jackson, 1986) 26
Figure 10: Solubility of nickel sulphide in solution generated using the OLI Stream Analyzer software (25 July 2005) 27
Figure 11: The pH dependent speciation dissociation of free sulphides 29
Figure 12: Introduction of a reagent feed stream into a stirred, baffled batch reactor showing variations in concentration with spatial position (Vicum et al., 2004) 34
Figure 13: Schematic of an FBR and methods used to decrease local supersaturation (van Hille, 2005; Guillard, 2001) 36
Figure 14: Unsteady state diffusion through a differential volume $A\Delta z$ (Seader and Henley, 1998) 41
Figure 15: Penetration and surface renewal theory for the mass transfer from a fluid-fluid interface into a liquid (Seader and Henley, 1998) 43
Figure 16: Schematic of the diffusion of gaseous hydrogen sulphide into solution, followed by speciation of $H_2S(g)$ and reaction with Ni^{2+} 46
Figure 17: Batch reactor using aqueous sulphide to precipitate Ni^{2+} 50
Figure 18: Semi-batch bubble column using $H_2S(g)$ to precipitate Ni^{2+} 51
Figure 19: Showing the high turbulent dissipation in the vicinity of the impeller in a batch reactor. Three dimensional computational fluid dynamics (CFD) model using the k-ε model in FLUENT 6.1 (Fluent Inc., Lebanon, USA) (Vicum et al., 2004) 59
Figure 20: Nickel sulphide precipitation pHi = 11.59 (unadjusted) showing concentrations of nickel ions and free sulphides in solution and solution pH [B01] 60
Figure 21: Nickel sulphide precipitation pHi = 9.88 showing concentrations of nickel ions and free sulphides in solution and solution pH [B02] 62
Figure 22: Nickel sulphide precipitation when pHi = 4.24 showing concentrations of nickel ions and free sulphides in solution and solution pH [B03] 63
Figure 23: Redox potentials of batch experiments run varying the initial pH of the sulphide solution (B01, B02 and B03) 64
Figure 24: NiS precipitation in the semi-batch bubble column using $H_2S(g)$ (= 0.8L/min) with no addition of alkalinity [L06] 67
Figure 25: NiS precipitation using $H_2S(g)$ comparing low NaOH concentrations (0.100, 0.150 and 0.200mmol/min) used to facilitate reaction at different $H_2S(g)$ flowrates (0.2, 0.6 and 0.8L/min) [L01 - L05] 69
Figure 26: Nickel and sulphide concentrations (mg/L) for batch precipitation of nickel from $NiSO_4$ using Na_2S using varying ratios of Ni:S [B04, B01, B05 and B06] closed symbols = nickel, open symbols = sulphide 72
Figure 27: Ni:S = 1:1.5 [B05] showing the increasing filtrate opacity with time after initial addition of reagents 73
Figure 28: Ni:S = 1:2 [B06] showing the increasing filtrate opacity with time after initial addition of reagents 74
Figure 29: Settling data for the precipitation of NiS using from synthetic $NiSO_4$ (200ppm Ni^{2+}) Na_2S for various ratios of Ni:S 76
Figure 30: Supersaturations based on initial global concentrations for batch nickel precipitation experiments using Na_2S varying the initial pH (pHi) of the sulphide solution [B01, B02, B03] and varying the ratio of Ni:S [B04, B05, B06] 77

Figure 31: NiS precipitation using $H_2S(g)$ comparing different $H_2S(g)$ flowrates (0.1, 0.3, 0.5 and 0.8L/min) when NaOH = 2.23mmol/min [T01 – T04] 79
Figure 32: Nickel Precipitation with $H_2S(g)$: nickel removal and pH with time NaOH = 2.23mmol/min; $H_2S(g)$ = 0.3; 0.5; 0.8l/min [T01 – T03] 81
Figure 33: Pseudo-kinetic modelling of nickel precipitation from synthetic $NiSO_4$ when $H_2S(g)$ = 0.1L/min NaOH = 2.23mmol/min [T04] 83
Figure 34: The precipitation of Ni using only NaOH = 1.20mmol/min for 0 - 4.5 minutes and $H_2S(g)$ = 0.3L/min for 4.5 – 8 minutes 83
Figure 35: Semi-batch precipitation of nickel using $H_2S(g)$ = 0.3L/min and NaOH = 1.20, 1.75 and 2.23mmol/min [T03, T07 and T09] 84
Figure 36: Sulphide usage efficiency threshold; comparing experimental and modelled regions of $H_2S(g)$ mass transfer resistance [T01 – T11] 85
Figure 37: Higbie's penetration theory applied nickel sulphide precipitation from a synthetic nickel sulphate solution using $H_2S(g)$ promoted by alkalinity addition $\ln(18.18 + C[NiSO_4])/(18.18 + C^0[NiSO_4])$ vs time for different $H_2S(g)$ flowrates when NaOH = 2.23mmol/min [T01 – T04] 86
Figure 38: Higbie's penetration theory applied nickel sulphide precipitation from a synthetic nickel sulphate solution using $H_2S(g)$ promoted by alkalinity addition $\ln(18.18 + C[NiSO_4])/(18.18 + C^0[NiSO_4])$ vs time for the same $H_2S(g)$ flowrate = 0.3L/min [T03, T07 and T09] 87
Figure 39: Repeat PSDs measured using the Beckman Coulter® Counter t minutes after complete reaction when NaOH = 1.75mmol/min, $H_2S(g)$ = 0.3L/min [T07] 89
Figure 40: Repeat PSDs measured using the Malvern Mastersizer® t1 minutes after complete reaction when NaOH = 1.75mmol/min, $H_2S(g)$ = 0.3L/min [T07] 90
Figure 41: Sulphide precipitation of nickel and cobalt from RES using $H_2S(g)$ without alkalinity addition [RES01] 92
Figure 42: Amount of acid needed to facilitate pH change in the diluted RES solution to quantify buffering capacity using alkalinity (equivalent mg of $CaCO_3$/L) 93
Figure 43: Sulphide precipitation of nickel and cobalt from RES using $H_2S(g)$ (0.3L/min) with alkalinity addition NaOH = 1.20mmol/min [RES02] 94
Figure 44: Comparison of sulphide in the NaOH trap for semi-batch precipitation of Ni^{2+} and Co^{2+} from diluted RES without NaOH input where NaOH = 1.20mmol/min 94
Figure 45: Comparison of the precipitation of nickel and cobalt from diluted RES and nickel from synthetic $NiSO_4$, NaOH = 1.2mmol/L $H_2S(g)$ = 0.3L/min 96

List of tables

Table 1: Aggregation kernels after Bramley et al (1996) 21
Table 2: Solubility product expressions and values for some metal sulphides (Jackson, 1986) 25
Table 3: Summary of stability constants for proposed nickel sulphide complexes and the methods used (Rickard and Luther, 2006) 32
Table 4: Details of batch experiments with aqueous sulphide to determine the effect of individual sulphide species on nickel removal 52
Table 5: Details of batch experiments to determine the effect of metal to sulphide ratio on nickel removal by batch aqueous sulphide 53
Table 6: Details of experiments to determine the effect of using low NaOH flowrates on removal of Ni^{2+} by semi-batch gaseous sulphide precipitation 54
Table 7: Details of experiments using higher NaOH flowrates to determine effect on removal of Ni^{2+} by semi-batch gaseous sulphide precipitation 55
Table 8: Details of semi-batch gaseous experiments using RES diluted by 1 in 6-6.5 56
Table 9: Values of $H_2S(g)$ and NaOH input for pseudo-kinetic thermodynamic modelling of the precipitation of nickel sulphide when $H_2S(g)$ = 0.8L/min and NaOH = 2.23 mmol/min carried out in OLI Stream Analyzer 57
Table 10: Comparison of experimental and OLI modelled percentage decrease in Ni^{2+} ions and pH after reaction for nickel sulphide precipitation reactions carried out at different pHi values 66
Table 11: pH after batch precipitation of nickel from $NiSO_4$ using Na_2S for various ratios of Ni:S 72
Table 12: Initial Zeta potential values of precipitates formed with varying molar ratios of Ni:S (B01, B04 – B06) 75
Table 13: Time taken for complete reaction for experiments run with high alkalinity input at various $H_2S(g)$ flowrates 78
Table 14: Supersaturations at time, t = 0.01s, using HS- for experiments T01, T02, T03, T07 and T09 88

List of symbols

S = supersaturation
C = actual concentration
C* = concentration at equilibrium
$\Delta\mu$ = change in chemical potential
μ_2 = chemical potential of the crystal (state 2)
μ_1 = chemical potential of a supersaturated solution (state 1)
ΔG = change in Gibbs' Free Energy
ϕ = reaction affinity
μ_i = chemical potential of solution i
μ_i° = chemical potential of a solution I at its standard state
a_i = activity of solution i
T = temperature in K
R = universal gas constant
γ_i = activity coefficient of species i
C_i = concentration of species i
τ = number of moles of positive and negative ions in 1 mole of solute
IAP = Ionic Activity Product
K_{SP} = solubility product
a_i, $a_{i,eq}$ = activity of species i at actual and equilibrium states
$\gamma_{i,1}$, $\gamma_{i,2}$ = activity coefficients of species i at states 1 and 2
$C_{i,1}$, $C_{i,2}$ = concentrations of species i at states 1 and 2
$a_{i,1}$, $a_{i,2}$ = activities of species i at states 1 and 2
γ_{HS^-} = activity coefficient of the HS^- ion
$\gamma_{Ni^{2+}}$ = activity coefficient of Ni^{2+} ion
$[Ni^{2+}]$ = concentration of the nickel ion
$[HS^-]$ = concentration of the bisulphide ion
$K_{SP,NiS}$ = solubility product of NiS
B_0 = rate of nucleus formation
A = pre-exponential factor
K = Boltzmann's constant
ΔG_{cr} = critical free energy for nucleation
ΔG = free energy change
ΔG_s = free energy change for the formation of a nucleus surface
ΔG_v = free energy change for phase transformation
σ = surface or interfacial tension
β = shape factor
α = volume factor
r_c = critical cluster radius
c = the concentration of clusters of size r
c^* = equilibrium concentration of clusters of size r
r = cluster size
ϑ = wetting angle
ΔG_{hom} = change in Gibbs' Free Energy for homogeneous nucleation

ΔG_{het} = change in Gibbs' Free Energy for heterogeneous nucleation

$r_{agg}(L, \lambda)$ = rate at which particles aggregate

L, λ = sizes of particles which aggregate

$\beta(L, \lambda)$ = rate constant for aggregation, aggregation kernel

$f(L, \lambda)$ = function of particle size reflecting the mechanism of aggregation

$S(l,s)$ = breakage selection rate constant

k_{break} = breakage constant

l = size of fragment of particle that breaks

$a^m_{M^{z+}}$ = activity of metal ion with charge z+

$a^n_{P^{y-}}$ = activity of anion with charge y-

$a_{M^{z+}P^{y-}}$ = the activity of a pure condensed solid

$\left[M^{z+}\right]^m$ = concentration of metal ion

$\left[S^{2-}\right]^n$ = concentration of sulphide ion

u = the settling velocity of the particles

d = diameter of settling particles

ρ = density of settling particles

μ = viscosity of the aqueous medium in which the particles are settling

ρ_o = density of the aqueous medium in which the particles are settling

g = acceleration due to gravity

pK_1 = -log of the equilibrium constant for speciation of $H_2S(aq)$ into HS^-

pK_2 = -log of the equilibrium constant for speciation of HS^- into S^{2-}

K_1 = the equilibrium constant for speciation of $H_2S(aq)$ into HS^-

K_2 = the equilibrium constant for speciation of HS^- into S^{2-}

$[S]_{total}$ = total concentration of free sulphides in solution

$[H_2S]$ = concentration of aqueous H_2S in solution

$[HS^-]$ = concentration of bisulphide ions in solution

$[H^+]$ = concentration of hydrogen ions in solution

$[S^{2-}]$ = concentration of sulphide ions in solution

I = ionic strength of solution

logK = conditional stability constant valid only for the stated conditions

B = species through which species A diffuses

A = diffusing species

A = cross sectional area through which diffusion occurs

D_{AB} = diffusivity of A through B (or reverse)

n_A = molar flux of species A

$A\Delta z$ = differential area through which species A dissolves

c_A = concentration of species A

c_B = concentration of species B

c = total concentration of species A and B

Δz, = film through which species A diffuses

Δc_A = change in concentration of species A

k_C = mass transfer coefficient

p_A = partial pressure of species A
c_{Ai} = concentration of species A at the interface
c_{Ab} = concentration of species A in the bulk fluid
c_B = concentration of well-mixed bulk region
t_c = contact time of bubble with fluid pocket
$2R_B$ = bubble diameter
V_B = rising bubble velocity
A_b = the interfacial area
V = the volume of the liquid phase

$C^t_{MeSO_4}$ = the concentration of the metal sulphate with time during the reaction

$C^0_{H_2S}$ = interfacial concentration of H_2S (18.18kg/m^3)

n = the number of bubbles/s
h = height of the liquid phase

$\overline{R}$ = the rate of absorption of H_2S(g) into solution per unit interfacial area
t = the time taken for one bubble to travel the length of the bubble column

1. Introduction

One of the principle causes of water pollution is the industrial discharge of wastes and by-products. The pollution of surface and ground water by heavy metal species represents a significant environmental threat. The mining and mineral processing industries are seen as heavily polluting as they generate high volume wastewaters, often with significant concentrations of heavy metals. Acid Mine Drainage (AMD) is formed as a consequence of mining and contains large amounts of heavy metals. Exposure of mineral sulphides to water and oxygen through mining activities leads to the generation of AMD. The removal of such metals from waste streams is an environmental priority enforced by government legislation, while the recovery of valuable metals from waste streams could have economic benefits.

Several treatment techniques have been used to remove heavy metals from wastewater. These include ion-exchange, evaporation, reverse osmosis, carbon adsorption, complexation and chemical precipitation, which is the most commonly used method (McNally et al, 1984). Precipitation is the formation from solution of a solid product as a result of addition of a precipitating agent to the solution (Jackson, 1986). A controlled precipitation process allows for efficient removal of harmful heavy metals on an industrial scale.

Precipitation has long been used as both a means of recovery and for the separation of metals from solution. It is the favoured method used as a scavenging process in the recovery of heavy metals present in solution in low concentrations prior to such solutions going to waste (Jackson, 1986). For example, both hydroxide and carbonate precipitation are used for effective treatment of AMD (Pulles et al., 1996).

Precipitation may also be used to separate a metal or a group of metals from others, either for the removal of impurities or minor metallic constituents, or for recovery from solution of the major metal (Jackson, 1986). The Sherritt-Gordon ammonia leach process for the treatment of nickel rich concentrates uses sulphide precipitation early in the process in order to remove copper from the leach solution. Later in the process cobalt and the remaining nickel are stripped from solution as sulphides using precipitation.

An important practical aspect of precipitation is the subsequent separation of the solid precipitate from solution. This is usually achieved through thickening and/or filtration (Jackson, 1986; Coulson and Richardson, 2002). Separation is most effective if the precipitate is dense, crystalline and above a certain size. Precipitates that are too small are

difficult to separate from solution on an industrial scale. A particle size of at least 10μm is necessary for retention by a "fine filter" (Jackson, 1986).

Supersaturation is the thermodynamic driving force for the precipitation process and is one of the key variables in determining the size of particles. The supersaturation is the difference in the theoretical solubility of the precipitating substance and the activities of its ions in solution. Because of the low solubilities and resulting high supersaturations generated in precipitating systems, control of the process is difficult. Sparingly soluble compounds such as nickel sulphide have extremely low solubilities, where $K_{SP} = 3.98 \times 10^{-20}$.

In order to control product characteristics in precipitation processes, solution supersaturation and the nucleation rate must be controlled. Therefore a sound mechanistic background is necessary in order to understand and implement control in the precipitating system.

1.1. Metal sulphide precipitation

Metal recovery and reuse, attractive for economic and environmental reasons, can be achieved by means of precipitation with sulphide. This is convenient as many metal-refining operations are equipped to deal with sulphides as they are designed for processing sulphide ores (Esposito et al., 2006). The high reactivity of the sulphide ion reduces the retention time required in the reaction tank (Bhattacharyya et al., 1981). Metals recovered as sulphides can be processed in existing smelters for pure metal recovery, leading to financial benefits (Bhattacharyya et al., 1981 in Hammack et al., 1993).

The formation of Ni(s) in the hydrogen reduction autoclave of the modified Sherritt-Gordon Leach Process used at Impala Platinum Refineries produces an aqueous Reduction End Solution (RES) containing significant amounts of Ni (1.0-1.5g/l) and Co (0.2-0.3g/l). The removal of Ni and Co from this stream is desirable since they are impurities that contaminate the $(NH_4)_2SO_4$, which is subsequently recovered for reuse in the process. For process efficiency and economic gain nickel and cobalt must be removed to low concentrations from the RES (Lewis and Butler, 2001).

Sulphide precipitation to remove Ni and Co from the RES is attractive owing to the low solubilities of metal sulphides over a broad pH range and the rapid precipitation kinetics (Bhattacharyya et al., 1981). However, the combination of these factors may be

disadvantageous to the sulphide precipitation process as they lead to rapid generation of extremely high supersaturation, resulting in difficulty in the control of the precipitation process and the formation of fine particles.

The use of a gaseous sulphide source to decrease the rate of generation of supersaturation has been proposed (Hammack et al., 1993, 1994). The mass transfer of sulphide from gaseous to aqueous phase reduces the rate at which aqueous sulphide is made available for reaction and therefore the supersaturation is reduced.

pH dependent speciation has been exploited to control the precipitation rate, since at acidic pH values spontaneous nickel sulphide precipitation does not occur (Kolthoff and Moltzau, 1935; Simons, 1963). At acidic pH values the sulphide species present is predominantly $H_2S(aq)$, as shown in the pH dependent speciation equations of $H_2S(aq)$ below

$$H_2S(aq) \rightleftharpoons HS^- + H^+ \quad pK_1 = 6.99 \text{ (Jackson, 1986)} \qquad (1\text{-}1)$$

$$HS^- \rightleftharpoons S^{2-} + H^+ \quad pK_2 = 17.4 \text{ (Midgisov et al., 2001)} \qquad (1\text{-}2)$$

This suggests that the $H_2S(aq)$ species is not able to react with Ni^{2+} to form nickel sulphide. In a continuous or semi-batch system, by controlling the pH, the bisulphide ion availability can be exploited to dictate the rate of the sulphide precipitation reaction.

The second inference of equations 1-1 and 1-2 is that S^{2-} does not occur at significant concentrations within the limits of the real pH scale and thus does not contribute significantly to the precipitation of nickel sulphide. Kolthoff and Moltzau (1935), support this by stating that the bisulphide ion (HS^-) is responsible for the precipitation of metal sulphides through the formation of intermediary hydrosulphides of the metal.

1.2. Objectives

The first objective of this research was to confirm experimentally that the $H_2S(aq)$ species is not able to precipitate nickel. These tests were carried out in a batch reactor using an aqueous sulphide source.

The second objective was to investigate the effect on nickel precipitation of manipulating supersaturation by controlling HS^- availability. This was achieved by manipulating gas flowrates and alkaline addition. Supersaturation control, such that metal removal was

complete and rapid with efficient utilisation of sulphide was desired. In addition, the nature of the precipitate should facilitate easy solid/liquid separation.

Finally, once the reaction mechanisms were characterised using the model, synthetic nickel sulphide system, the removal of Ni and Co from RES was investigated.

1.3. Thesis overview

The main experimental work presented in this thesis focuses on precipitation of NiS from a synthetic aqueous stream in both batch and semi-batch systems, using aqueous and gaseous sulphide sources, respectively.

Supersaturation and particle rate processes such as nucleation, aggregation and growth are discussed in detail in Chapter 2. These are important aspects to consider in attempts to control the formation of particles large enough to facilitate the separation of solid precipitates from the aqueous phase post-precipitation. The generation of supersaturation results from the availability of the correct sulphide species in solution. Sulphide speciation and associated aspects of sulphide precipitation are discussed in Chapter 3. Chapter 4 discusses methods used to control the generation of supersaturation in precipitating systems. Chapter 5 expands on the use of a gaseous sulphide source to control the precipitation reaction as the diffusion of gaseous sulphide into solution from a gaseous bubble is rate limiting. The materials and experimental methodology are described in Chapter 6. Chapter 7 discusses results from the aqueous batch system and the gaseous semi-batch system and Chapter 8 draws conclusions of this work and recommendations for further work on metal sulphide precipitation.

2. Precipitation theory

This chapter describes important aspects of precipitation theory, showing the differences between crystallisation and precipitation processes. The concept of supersaturation as the driving force behind precipitation reactions is defined. The effect of supersaturation on predominant mechanisms involved in particle formation is discussed from colloid formation at high supersaturations and primary and secondary nucleation at lower supersaturation values. Primary nucleation and birth of nuclei is discussed after which induced nucleation including possible sources for secondary nuclei in the precipitating system is presented. The most relevant post-nucleation particle enlarging mechanisms are then described.

Crystallisation is used in industry as one of the cheapest and most effective methods for production, purification and recovery of pure solids from impure solutions (Mullin, 2001). In addition, crystallisation produces an end product, the crystals, with many favourable characteristics such as good flow and handling properties. Crystallisation occurs when the concentration of a solute is raised above its solubility limit (Mullin, 1972). Thus, crystals are obtained from solution through (a) cooling, (b) increasing the concentration of the solute through solvent evaporation, (c) a combination of (a) and (b) when solvent evaporation is used for both cooling and evaporation, and (d) by salting or drowning-out with the use of a co-solvent. Crystallisation is usually a slow process leading to the formation of uniform, well-ordered, highly crystalline solids.

Precipitation is the crystallisation of sparingly soluble substances (Söhnel and Garside, 1992). Precipitation is known as reactive crystallisation because the thermodynamic driving force for crystal formation, which is supersaturation (S), does not result from action on physical properties of the solution. The supersaturation is generated from the reaction of two soluble components leading to the formation of a sparingly soluble precipitate. Precipitation is a rapid process due to the high supersaturations generated by the low solubilities of the precipitated products. Precipitation processes can produce amorphous and compound phases as well as various polymorphs, hydrates or other solvates. Usually only one specific form is acceptable to ensure formation of the desired product (Söhnel and Garside, 1992).

It is well established that high supersaturations induce high nucleation rates (Jackson, 1986) and a large number of precipitate particles are formed, thus limiting the average size to which precipitates grow. If precipitates are sufficiently small, secondary processes such as agglomeration may occur resulting in a significant increase in particle size (Söhnel

and Garside, 1992). Thus, a fundamental approach is necessary to understand the mechanisms of the precipitation process.

The removal of nickel from solution using sulphide as the precipitating agent is an efficient precipitation system due to the sparingly soluble nature of NiS. As a result, sulphide precipitation is the chosen means of scavenging Ni and Co present in the RES prior to the ammonium sulphate solution being recycled for reuse in the Sherrit-Gordon Leach process (Jackson, 1986). The solubilities of both NiS and CoS are sufficiently low ensuring essentially complete removal of these heavy metals.

2.1 Supersaturation

Supersaturation is the key variable in any precipitation process and it governs nucleation, growth and aggregation (Söhnel and Garside, 1992) and thus the particle size of precipitates (Jackson, 1986). A saturated solution having a concentration of C* is in thermodynamic equilibrium with the solid phase. A supersaturated solution has a concentration greater than the thermodynamic supersaturation concentration (C*). Crystallisation processes can only take place in supersaturated phases.

Supersaturation can be simply defined as the difference in concentration between the actual (C) and equilibrium (C*) concentrations or as a relative supersaturation:

$$S = \frac{C}{C^*} \qquad (2\text{-}1)$$

This definition of supersaturation assumes an ideal solution with an activity coefficient equivalent to 1 (Myerson, 2002). In an ideal solution where components do not influence each other the activities of the components are equal to their concentrations (Söhnel and Garside, 1992). However, in a real solution, the activities and concentrations of the components are not equal to due to interactions between the aqueous components. Thus, in real solutions, activities are expressed as a product of the concentration and the activity coefficient, which is a term representing the deviation from ideality. A more general definition of the supersaturation, in which the activity coefficients are not taken as unity, is derived below.

Supersaturation is alternatively defined as the difference in the chemical potential of the crystallizing compound in a supersaturated solution (state 1) and the crystal (state 2), which is the free energy change in the precipitating system (Söhnel and Garside, 1992)

$$\Delta\mu = \mu_2 - \mu_1 = \Delta G \tag{2-2}$$

In a spontaneously crystallising system the change in Gibbs' free energy is negative. The driving force for crystallisation is typically presented as a positive value thus the reaction affinity, ϕ , is defined as (Söhnel and Garside, 1992)

$$\phi = -\Delta\mu \tag{2-3}$$

The chemical potential of a solution is defined as

$$\mu_i = \mu_i^\circ + RT\, ln\, a_i \tag{2-4}$$

Where a_i is the activity of species I, R is the universal gas constant and T is the temperature of the solution in Kelvin. The activity of species i in solution can be expressed as the product of the concentration of species i in solution, C_i, and the activity coefficient γ_i,

$$a_i = \gamma_i C_i \tag{2-5}$$

Combining the above equations produces (Söhnel and Garside, 1992)

$$\frac{\phi}{RT} = \upsilon \ln \frac{a_{i,1}}{a_{i,2}} = \upsilon \ln \frac{\gamma_{i,1} C_{i,1}}{\gamma_{i,2} C_{i,2}} \tag{2-6}$$

where υ is the number of moles of positive and negative ions in 1 mole of solute.

The supersaturation of a solution is defined as the difference in activities between states 1 and 2, as defined above

$$S = \frac{a_i}{a_{i,eq}} = \frac{a_{i,1}}{a_{i,2}} = \frac{\gamma_{i,1} C_{i,1}}{\gamma_{i,2} C_{i,2}} \tag{2-7}$$

Mullin (2001) defines the supersaturation of a sparingly soluble electrolyte as the ratio of the ion activity product and the solubility product. The ion activity product is the activity of the electrolyte at state 1 and the solubility product is the product of activities at equilibrium (state 2).

$$S = IAP/K_{SP} \qquad (2\text{-}8)$$

The definition of supersaturation according to Mullin (2001) was applied to the precipitation of NiS to quantify supersaturation in both the batch and gaseous systems. Thus the supersaturation expression was described as

$$S = \frac{\gamma_{Ni^{2+}}[Ni^{2+}]\gamma_{HS^-}[HS^-]}{K_{SP,NiS}} \qquad (2\text{-}9)$$

Combining equations 2-6 and 2-7,

$$\frac{\phi}{RT} = \nu \ln S \qquad (2\text{-}10)$$

which incorporated the supersaturation term as the driving force behind precipitation processes.

The degree of supersaturation determines the rate and the mechanism by which crystallisation occurs. Supersaturated solutions are metastable i.e. not at equilibrium (Myerson, 2002). Two types of phase transition have been postulated to relieve supersaturation. The first type consists of large fluctuations in concentration, infinitesimal in spatial extent and the second infinitesimal in degree and large in extent. The classic nucleation theory is based on the former postulate and also requires that a sharp interface exists between the nucleating (stable) and supersaturated (unstable) phases. Spinodal decomposition is based on the latter postulate and differs in that a diffuse interface may exist between the stable and unstable phases (Mullin, 2001). For a supersaturated solution within the metastable region, which is below the metastable limit and above the solubility limit, the phase separation mechanisms are nucleation and crystal growth. Within the metastable zone nucleation is necessary to effect phase change (Mullin, 2001). The metastable limit or spinodal curve is the highest supersaturation concentration after which phase separation occurs by spinodal decomposition (Myerson, 2002). Above the metastable limit within the spinodal region any phase separation can lower the free energy of the system and no nucleation step is required (Mullin, 2001).

Crystallisation of precipitates is the result of nucleation and growth and then secondary processes such as aggregation and breakage (Söhnel and Garside, 1992).

Figure 1 shows the position of various crystallisation regions within the metastable limit. Zone 1 is outside the metastable limit and is thus undersaturated. The boundary of Zone

1 is the solubility of the AB compound. For sparingly soluble substances, this boundary lies very close to the axes.

At very high supersaturations colloid and gel formation occur (Zones 5 and 6). Colloids and gels have very poor dewatering capabilities and are therefore difficult to handle in downstream phase separation and can be considered as undesirable products. Zone 4 is the region of homogeneous nucleation which produces small precipitates that have poor settling properties. Zones 2 and 3 are the preferred regions of operation. These are the areas of lowest supersaturation and thus the regions in which control of the precipitation process is possible. In both zones precipitation is facilitated by the presence of catalysing particles. Zone 2 is the region of secondary nucleation where nucleation is catalysed by the presence of nuclei formed by homogeneous nucleation and Zone 3 is the area of heterogeneous nucleation in which foreign particles facilitate precipitation.

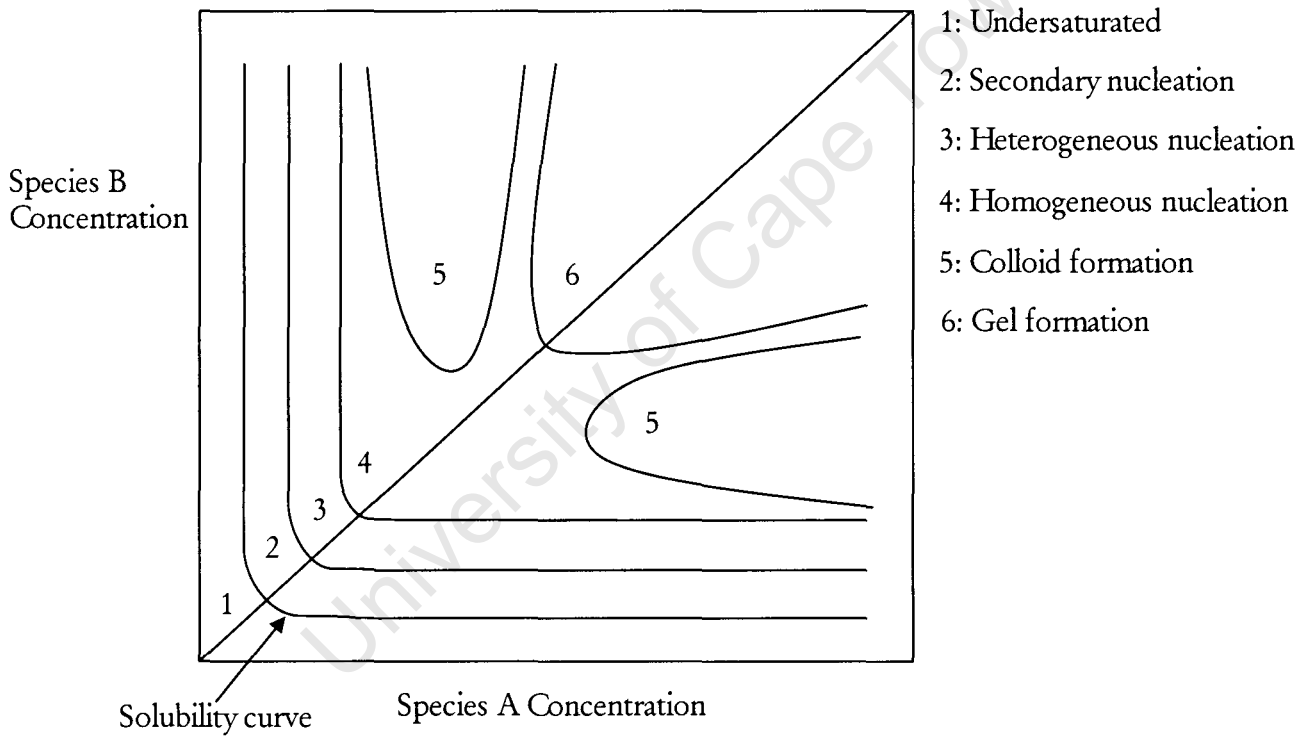

Figure 1: Various regions of supersaturation and predominant particle formation mechanisms (Gosele and Kind, 1991)

In this study control of the precipitation reaction, such that primarily particle enlarging processes such as growth and aggregation occur after controlled nucleation, is attempted. It is not certain which post-nucleation particle enlarging process will predominate and thus both are discussed in detail below. Further evidence such as PSD data will provide evidence as to which mechanism is most significant. The "slug" dose manner of reagent

addition in the batch system generates very high supersaturations and thus nucleation is the dominant particle formation process. In the semi-batch gaseous system the generation of supersaturation is controlled, thereby limiting nucleation and encouraging subsequent growth and/or aggregation of precipitates.

2.2 Nucleation

In order to relieve supersaturation and move towards equilibrium, a supersaturated solution will crystallise and nuclei are formed (Myerson, 2002). Nucleation is the initial formation of the smallest thermodynamically stable solid phase from a supersaturated solution (Jones, 2002).

There are various mechanisms for the formation or birth of nuclei (nucleation) as shown below

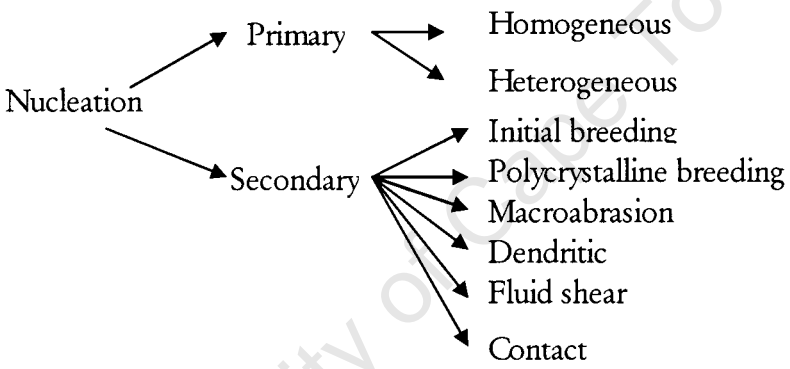

Figure 2: Different mechanisms of nucleation (Söhnel and Garside, 1992)

2.2.1 Homogeneous nucleation

Homogeneous nucleation is the formation of a solid phase not initiated by the presence of any solid phase (Söhnel and Garside, 1992). It is spontaneous nucleation from a clear solution (Jones, 2002).

The classical theory of nucleation (Nielsen, 1964) assumes that clusters are formed by a sequence of bimolecular additions until the critical size is reached.

$$A + A \rightleftharpoons A_2$$

$$A_2 + A \rightleftharpoons A_3$$

$$A_{n-1} + A \rightleftharpoons A_n \text{ (critical cluster)}$$

Further molecular additions to the critical cluster would result in nucleation and subsequent growth of the nucleus. The construction of clusters, which occurs very rapidly, can only occur and continue in regions of very high supersaturation and many of the embryos or 'sub-nuclei' fail to reach maturity. These redissolve because they are too unstable. If, however, the nucleus grows to a certain size, as explained below, it becomes stable under the average conditions of supersaturation present in the bulk of the fluid (Mullin, 2001).

The rate of nucleus formation, B_0, by this mechanism is given below

$$B_0 = A\exp\left(-\frac{\Delta G_{cr}}{kT}\right) \qquad (2\text{-}11)$$

Where the pre-exponential factor A has a theoretical value of 10^{30} nuclei/cm^{3}s, ΔG_{cr} is the critical free energy for nucleation, k is Boltzman's constant and T is temperature (Myerson, 2002).

The classical theory of nucleation is based on the condensation of a vapour to a liquid, and this treatment may be extended to the crystallisation from solutions (Mullin, 2001). The free energy change (ΔG) for the formation of this new phase through homogeneous nucleation is the combination of the free energy change for the formation of the nucleus surface (a positive value), ΔG_s, and the free energy change for the phase transformation (a negative value), ΔG_v (Myerson, 2002).

$$\Delta G = \Delta G_s + \Delta G_v = \beta L^2\sigma + \alpha L^3 \Delta G_v \qquad (2\text{-}12)$$

σ is the surface or interfacial tension, β and α are the shape and volume factors respectively, based on the characteristic length, L. Various shape and volume factors for different shaped particles can be found in numerous texts. For spherical nuclei $\beta = \pi$ and $\alpha = \pi/6$ and the characteristic length L on which these are based is the diameter, d. Thus, equation 2-12 becomes:

$$\Delta G = 4\pi r^2\sigma + \frac{4}{3}\pi r^3 \Delta G_v \qquad (2\text{-}13)$$

The free energy changes as a result of surface formation (ΔG_s), which is the excess free energy between the surface of the particle and the bulk of the particle, and phase

transformation (ΔG_v) and their resulting overall free energy change (ΔG) are shown in Figure 3 below.

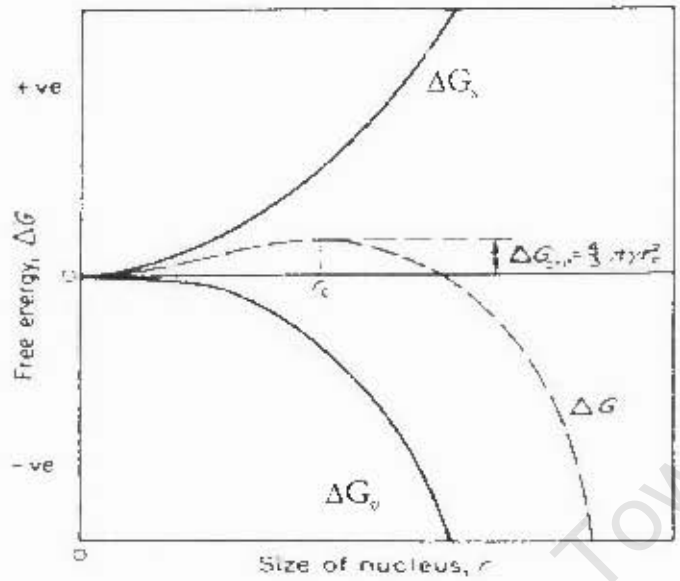

Figure 3: Free energy diagram for nucleation explaining the existence of a 'critical nucleus', free energy vs cluster size (Mullin, 1972)

In a supersaturated solution the free energy required to form a new phase (ΔG_v) is a negative quantity as the system is not in equilibrium and wishes to attain a more stable state by undergoing nucleation. The free energy required to form a surface (ΔG_s) increases with increasing nucleus size. The overall excess free energy resulting from a combination of these two energies is the critical energy barrier (ΔG_c) that must be overcome in order to form a critical cluster of radius (r_c).

The critical cluster size (r_c) can be found by minimising the free energy function with respect to the radius.

$$\frac{d(\Delta G)}{dr} = 8\pi r_c \sigma + 4\pi r_c^2 \Delta G_v = 0 \qquad (2\text{-}14)$$

Thus the critical cluster radius is

$$r_c = -\frac{2\sigma}{\Delta G_v} \qquad (2\text{-}15)$$

and the critical free energy change is

$$\Delta G_{\sigma} = \frac{4\pi r_c^2 \sigma}{3} \tag{2-16}$$

The newly formed crystalline lattice structure in a supersaturated solution may either redissolve or grow, depending on its size, but the process it undergoes should always result in the decrease of free energy of the particle. The critical radius size, r_c, represents the minimum size of a stable particle.

The Gibbs-Thompson equation governs the growth of clusters

$$\ln\left(\frac{c}{c^*}\right) = \ln S = \frac{2\sigma v}{kTr} \tag{2-17}$$

where c is the concentration of clusters of size r. Thus smaller clusters dissolve and larger clusters grow until they reach the critical size r_c and a new phase is formed. Substituting r_c from equation 15 into equation 14

$$\Delta G_{cr} = \frac{16\pi\sigma^3 v^3}{(3kT\ln S)^2} \tag{2-18}$$

The nucleation rate, equation 2-11, becomes

$$B_0 = A\exp\left(\frac{-16\pi\sigma^3 v^3}{3k^3T^3(\ln S)^2}\right) \tag{2-19}$$

From equation 2-19 it can be seen that the nucleation rate increases with increasing supersaturation and temperature, and decreases with an increase in interfacial tension, or surface energy, because there is more tendency for nuclei to not form or to dissolve if the surface energy is large.

Homogeneous nucleation forms the basis of several nucleation theories but rarely occurs in practice due to the presence of dissolved impurities and physical features such as reactor walls, stirrers and baffles.

2.2.2 Heterogeneous Nucleation

Heterogeneous nucleation is the formation of a new solid phase catalysed by the presence of a foreign solid (Söhnel and Garside, 1992; Jones, 2002).

Heterogeneous nucleation occurs at a lower supersaturation than homogeneous nucleation because the free energy barrier is lowered by the presence of a foreign substance, which reduces the energy required for nucleation. The decrease in free energy results from the wetting or contact angle, ϑ, of the solid phase. The wetting angle is the contact angle between the foreign catalyzing solid and the precipitate nucleus formed on its surface, as illustrated below (Figure 4). The wetting angle serves to reduce the free energy required for nucleation.

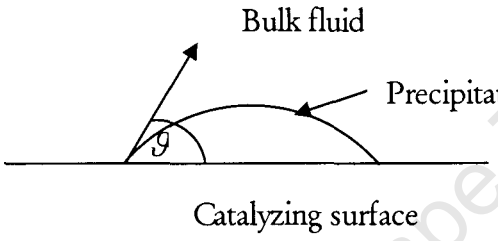

Figure 4: Heterogeneous nucleation; precipitate deposit on a catalyzing foreign surface illustrating the wetting angle

If the wetting angle, $\vartheta = 180°$, then the overall energy of nucleation is the same as that required for homogenous or spontaneous nucleation. When there is partial affinity between the solid surface and the precipitate ($0 < \vartheta < 180°$), nucleation is easier to achieve because the overall excess free energy required is less than that for homogeneous nucleation. When there is complete wetting ($\vartheta = 0°$) the free energy of nucleation is zero. This case corresponds to the seeding of a supersaturation solution with crystals of the required crystalline product, so no nuclei have to be formed in the solution (Mullin, 2001).

Thus,

$$\Delta G_{\text{hom}} = \phi \Delta G_{het} \qquad (2\text{-}20)$$

Where the factor ϕ is less than unity and is expressed in terms of the wetting angle as

$$\phi = \frac{1}{4}(2 + \cos\vartheta)(1 - \cos\vartheta)^2 \qquad (2\text{-}21)$$

Thus a lower supersaturation can facilitate nucleation in a heterogeneous system.

In sulphide precipitation of nickel the dominant particle forming mechanism is primary nucleation.

2.2.3 Secondary Nucleation

Secondary nucleation results from the presence of pre-existing precipitates in the supersaturated solution. These parent crystals have a catalysing effect on the nucleation process and thus nucleation takes place at a lower supersaturation than that required for spontaneous nucleation. (Jackson, 1986)

There are several theories which have been proposed to explain secondary nucleation. The origin of secondary nuclei may be traced back to parent crystals as in initial or dust breeding; needle breeding; and collision breeding. The secondary nuclei may also result from solute in the liquid phase such as impurity concentration gradient breeding and nucleation due to fluid shear (Myerson, 2002). The various theories of secondary nucleation propose that the secondary nuclei either originate from the parent crystals or the boundary layer of the growing crystals.

The rate of secondary nucleation is a result of three processes:
1. The generation of secondary nuclei on or near the parent crystal
2. Removal of the clusters
3. Growth to form a new solid phase

The degree of supersaturation is a critical parameter controlling the rate of nucleation and affects it in three different ways. At higher supersaturation the adsorbed layer around a crystal is thicker and thus results in a large number of nuclei. The size of the critical nucleus decreases with increasing supersaturation. As the supersaturation increases, the micro-roughness of the surface of the crystal increases, resulting in a larger nuclei population. (Myerson, 2002)

2.3 Growth

Crystal growth is the crystallisation process by which nuclei grow larger by the addition of solute molecules from the supersaturated solution (Myerson, 2002).

Crystal growth and nucleation, as well as secondary processes such as aggregation and breakage, work in combination to control the final particle size distribution (PSD) of the system. The conditions and rate of crystal growth impact significantly on the product purity and the crystal habit and are thus important parameters in the development of industrial crystallisation processes.

The "linear growth rate" of a crystal is the linear growth of a face of the crystal in a direction normal to that face. Face growth rates, however, are not normally used to describe the overall growth of a crystal. A more useful definition of growth of a crystal is the rate of increase of some characteristic dimension of the crystal. If the crystal was a sphere the characteristic dimension is the diameter, but if the crystal is another shape the characteristic shape is usually the second longest dimension.

2.3.1 Crystal growth theories

Crystals are thought to grow in a layer by layer fashion. Molecules must desolvate and absorb on the crystal surface. The general mechanism by which a molecule is incorporated into a crystal face is its adsorption onto a face followed by its diffusion along the face to an energetically favourable step (site B) or kink site (C) for its incorporation. The difference between step and kink sites is shown in Figure 5 below. Energetically site B is more favourable than A and C more favourable than B. It is easier for molecules to bond to an existing step or kink than to spread over a surface to form a new step and thus crystals grow layer by layer.

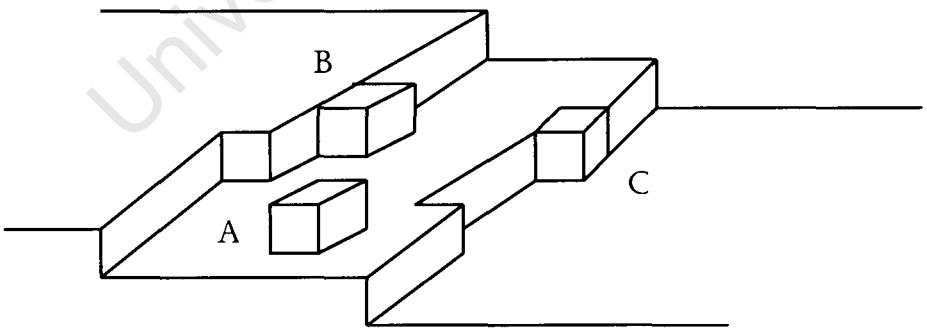

Figure 5: Surface structure of a growing crystal (Ohara and Reid, 1973)

This explains the method of crystal growth but neither the formation of the steps nor the controlling factor for the rate of growth of steps.

2.3.1.1 Two-Dimensional Growth Theories

This theory describes the birth of a step, which is analogous to the formation of nuclei clusters, but in only two dimensions. The step can be seen as the formation of a circular nucleus on a flat surface, effectively cancelling out one dimension. Molecules will continually adsorb, surface diffuse and desorb onto the surface and also collide and form two-dimensional aggregates.

Once the surface nuclei are formed, the manner in which they spread and form a complete layer is encompassed by the mononuclear model, the polynuclear model or the birth and spread model (Myerson, 2002).

Mononuclear model: The simplest crystal growth theory predicts the spread of the surface nucleus across the surface at an infinite velocity. The rate determining step in this model is the formation of the surface nucleus and the growth rate of a face is proportional to the area of that face. Thus larger faces grow faster than smaller faces, which is contradictory to the observed fact that the fastest growing faces have the smallest areas, while larger faces have slower growing areas. This eliminates the usefulness of the mononuclear model. (Myerson, 2002)

Polynuclear model: This theory predicts the formation of a layer is not due to the spread of nuclei but is composed of enough two dimensional nuclei of critical size to cover the layer. The polynuclear model predicts that the growth rate will increase with increasing nucleation rate but that the growth rate will decrease with the decreasing nuclei size. The critical nuclei size decreases with increasing supersaturation. The polynuclear growth rate does not predict a continuous increase in crystal growth rate with increasing supersaturation; instead it predicts that at some supersaturation, growth is a maximum that will decline if the supersaturation is increased or decreased. This prediction has not been observed, and is unlikely (Myerson, 2002).

Birth and spread model: Between the extremes of the mononuclear and the polynuclear models, in which the spread velocities are infinite and zero respectively, is the birth and spread model. The birth and spread model allows the spreading of nuclei at a finite velocity and assumes that the rate of spread is independent of size. (Myerson, 2002)

Each of these models fails at low supersaturations due to dependence on two-dimensional nucleation, unless a very low surface energy is used. Therefore these models are not suitable for predictive purposes but are illustrative with regards to crystal growth mechanisms.

2.3.1.2 BCF (Burton-Cabrera-Frank) surface diffusion Model

The previous models are unsatisfactory because they make crystal growth a non-continuous process with the rate determining step being the formation of a critical two-dimensional surface nucleus (Myerson, 2002). Frank (1949) put forward a theory in which steps are self-perpetuating and stem from dislocations in the crystal surface known as "screw dislocations" thus providing a way in which steps and therefore crystals grow continuously. These dislocations arise because crystals growing layer-by-layer often have imperfections (Mullin, 2001).

Molecules adsorbed onto the crystal surface migrate to the higher of the two planes of the screw dislocation, thus forming a spiral staircase (left- or right-hand). The dislocation is still present after the layer is complete, so further molecules can absorb, migrate and form layers. The screw dislocation (a) from which the staircase grows follows a spiral radius (b) which is limited by the supersaturation, and thus a completely smooth face is not possible under spiral growth conditions as seen from the side view (c) (Figure 6).

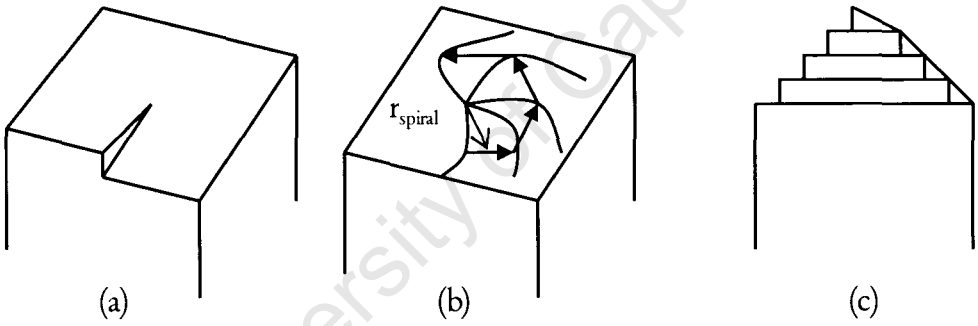

Figure 6: Development of a growth spiral from the screw dislocation (Mullin, 2002)

Surface nucleation is not required for growth and growth can occur at a finite rate at low supersaturations in this model.

2.3.1.3 The Diffusion Layer Model

Boundary layer thickness and diffusion of the solute through the boundary layer can be significant factors in controlling the growth of a crystal (Myerson, 2002). The diffusion layer model focuses on the diffusion of the solute through the boundary layer.

As a crystal grows, solute molecules migrate from the supersaturated solution and are incorporated into the crystal face, thus depleting the solute in the region of the crystal-

liquid interface. Solute will diffuse from the bulk solution (high concentration) to the crystal-liquid interface which is at a significantly lower concentration. The region in which the concentration of solute is changing is known as the "concentration boundary layer". The distance from the crystal surface to where the concentration is equal to the bulk concentration is known as the boundary layer thickness, δ.

There are two stages of mass deposition of the solute molecules onto the crystal surface (Figure 7); a diffusion process where solute molecules travel to the crystal surface from the bulk, followed by a first order "reaction" when the solute molecules arrange themselves into the crystal lattice. (Mullin, 2001)

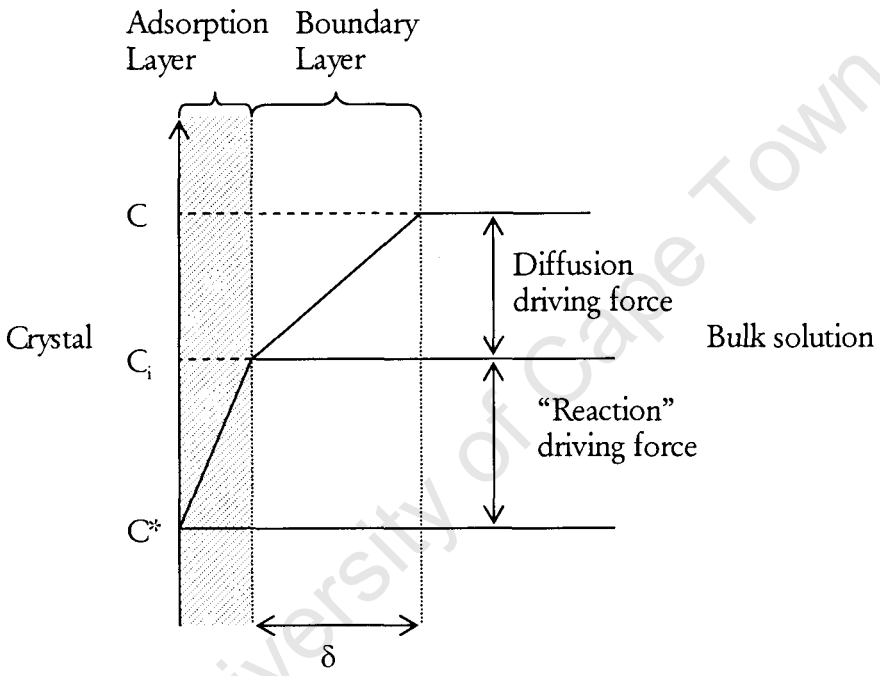

Figure 7: Concentration profile and concentration driving forces in crystallisation from solution according to the simple diffusion-reaction model (Mullin, 2001; Myerson, 2002)

2.4 Aggregation

Aggregation is the adherence of primary particles that are cemented afterwards by a crystalline bridge between two or more crystals (Mersmann and Braun, 2001). The bridge is as a result of crystal growth for which supersaturation is necessary.

Aggregation occurs when small particles collide and form a permanent attachment if the van der Waals forces are stronger than the gravitational forces. The rate of particle

agglomeration is dependent on the frequency of collisions and the efficiency of particle contact (Mullin, 2001).

Aggregation consists of three steps illustrated diagrammatically in Figure 8 below (Franke and Mersmann, 1995)

1. The collision of particles
2. the "staying together" of particles
3. the formation of crystalline bridges between these particles (cementation)

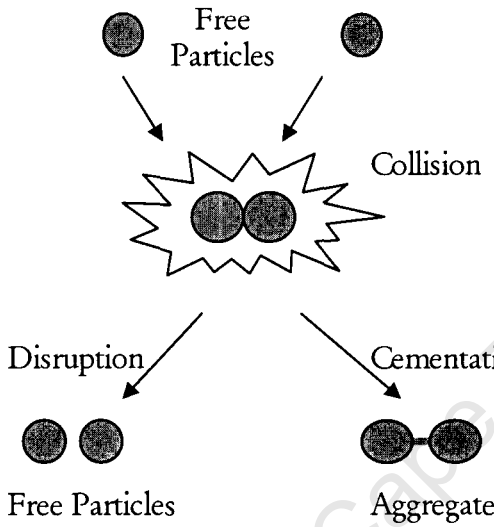

Figure 8: Formation of an aggregate - free particles collide and either disrupt and remain as free particles or cement together via growth of a crystalline bridge between the particles and form an aggregate

The rate of bridge formation is directly linked to the growth rate of the precipitate in the space between the touching particles. Both electrostatic stabilisation (via repulsion of electric double layers) and steric stabilisation (via polymeric or macromolecular adsorbents to impart colloidal stability) are considered in the formation of aggregates (Myerson, 2002).

The rate $r_{agg}(L, \lambda)$ at which particles of size $[L, L + dL]$ aggregate with particles of size $[\lambda, \lambda + d\lambda]$ is proportional to the product of the number of particles in these respective size ranges. The rate of aggregation is characterised by a rate constant $\beta(L, \lambda)$, termed the aggregation kernel. The rate of aggregation is thus expressed as

$$r_{agg}(L, \lambda) = \beta(L, \lambda) dN_L dN_\lambda \qquad (2\text{-}23)$$

The aggregation kernel is a measure of the frequency with which a particle of size L aggregates with one of size λ. The assumption is that all particle collisions are binary and it is thus implied that particle concentrations are sufficiently low. Kernels are thus a product of two factors

$$\beta(L, \lambda) = \beta_o \times f(L, \lambda) \qquad (2\text{-}24)$$

where β_o depends on operating conditions such as the local fluid velocity and the chemical environment and is independent of size. $f(L, \lambda)$ is a function of particle size and often reflects the mechanism of aggregation. The table below summarizes some aggregation kernels formulated in this way. (Bramley et al., 1996)

Table 1: Aggregation kernels after Bramley et al (1996)

Mechanism	**Kernel $\beta(L, \lambda)$**
Size independent	β_o
Brownian motion (Smoluchowski, 1917)	$\beta_o(L + \lambda)(L^{-1} + \lambda^{-1})$
Gravitational (Berry, 1967)	$\beta_o(L + \lambda)^2 \lvert L - \lambda \rvert$
Shear (Smoluchowski, 1917; Low, 1972)	$\beta_o(L + \lambda)^3$
Particle inertia (Drake, 1972)	$\beta_o(L + \lambda)^2 \lvert L^2 - \lambda^2 \rvert$
Thompson kernel, empirical (Thompson, 1968)	$\beta_o(L^3 - \lambda^3)^2 / (L^3 + \lambda^3)$

The formation of these aggregation kernels can be classified into two broad categories

i. Perikinetic collision - where particles are present in a stagnant fluid and come into contact via Brownian motion and thus is usually only valid for small particles ($<1\mu m$). These collisions are also influenced by the zeta potential of the particles.
ii. Orthokinetic collision - if particles are sufficiently large or the fluid shear rate high, thus in agitated dispersions, where the relative motion of velocity gradients exceeds that caused by Brownian effects.

The disruption of aggregates takes place by the same collision mechanisms.

Aggregation can play an important role in increasing particle sizes due to the small particle sizes and high particle concentrations in precipitation systems (Myerson, 2002). Properties of precipitates are strongly dependent on the extent to which secondary processes such as agglomeration have modified the initial suspension (Söhnel and Mullin, 1987). Aggregation occurs alongside crystal growth and is responsible for rapid enlargement of particle size. Aggregation and particle growth are both strongly dependent on supersaturation and solution composition (Hounslow et al, 2001), and a high level of supersaturation will favour aggregation of particles over crystal growth.

2.5 Breakage

Breakage occurs when the combined effect of the fluid shear rate and the mass (density) of the particles causes a large enough force to break apart large colliding particles into smaller particles. Breakage usually occurs only after particles have grown to a certain size and are subject to a sufficiently turbulent environment.

Hounslow et al (2005) use a breakage function for which there is an analytical solution. The breakage selection rate constant, $S(l,s)$, is the rate at which a fragment of a particle size l will be selected to break. The selection rate was taken to increase with the size cubed and the binary breakage function is formulated as one that gives uniform probability of all fragment sizes on a volume scale, that is

$$S(l,s) = k_{break} l^n \qquad (2\text{-}42)$$

where S is the breakage selection rate (s^{-1}), k_{break} is the breakage rate constant ($s^{-1}.m^{-3}$), l is the particle size (m), and

$$b(l,x,s) = \frac{6x^2}{l^3} \qquad (2\text{-}43)$$

This is just one example of the two expressions for breakage considered by Hounslow et al (2005) in developing a model framework for the crystallisation of a single solid species in a well-mixed compartment at steady state.

Supersaturation as the driving force behind precipitation processes was described. A detailed description of particle forming mechanisms, such as nucleation, aggregation and breakage, which dictate particle size, was presented in this chapter.

3. Sulphide Precipitation

This chapter focuses specifically on the precipitation of metal sulphides. The potential advantages and disadvantages of using sulphide as the precipitating agent are listed. The reactive nature of sulphide is highlighted, which leads to the low solubility products of metal sulphides. The relationship between solubility and pH is discussed including how pH can be manipulated to facilitate selective precipitation of different metal sulphides. Practical challenges such as controlling precipitate formation and properties arising from low solubilities are discussed. Hydrogen sulphide speciation is explained. Discussion of the formation of polysulphide clusters as intermediates during precipitate formation and as products of metal sulphide dissolution.

Many hydrometallurgical industries exploit sulphide precipitation using $H_2S(g)$. The Kokkola cobalt plant of the Outokumpu Company of Finland uses selective sulphide precipitation to achieve solution purification (Jackson, 1986).

This process exploits several advantageous aspects of sulphide precipitation, shown in the list below;

- Good metal removal efficiency is possible due to the sparingly soluble nature of metal sulphide precipitates (Bhattacharrya, 1981)
- Selective metal recovery is feasible (Veeken et al., 2003)
- Metal removal is possible over a wide pH range (Mishra and Das, 1992)
- Low residence time required in the reaction tank because of the high reactivities (rapid kinetics) of metal sulphides (Veeken et al., 2003)
- Sulphide will precipitate metals complexed with most complexing agents (Mishra and Das, 1992)
- Sludge volumes of metal sulphide precipitates are relatively low compared to when using other precipitating agents such as carbonates or hydroxides (Bhagat et al., 2004)
- Sulphide precipitates can be processed by existing smelters for metal recovery (Bhattacharrya, 1981)

However, there are disadvantages associated with sulphide precipitation as well;

- The rapid reaction kinetics means that effective control of the precipitation process is required for selective precipitation of metals (Jandová et al., 2005)
- High reactivities and the sparingly soluble nature of metal sulphides form very small particle sizes (colloids) making phase separation after filtration difficult (Jandová et al., 2005)

- The formation of $H_2S(g)$ at low pH values presents a gas odour and safety problem (Hammack et al., 1994)

Thus, in order to operate effective sulphide precipitation processes control is necessary to prevent or alleviate difficulties inherent in the process as a result of the sparingly soluble nature of sulphide precipitates and their rapid reaction rates.

The following sections highlight some aspects of metal sulphide precipitation to be considered in order to facilitate efficient metal removal using a sulphide precipitating agent.

3.1. Metal sulphide solubilities

A sparingly soluble salt, such as a metal sulphide, undergoes partial dissolution with dissociation into ions when in equilibrium with a limited amount of water. The equilibrium established for a salt M_mP_n is

$$M_mP_n \rightleftharpoons mM^{z+} + nP^{y-} \qquad (3\text{-}1)$$

And the thermodynamic equilibrium constant, in terms of activities, is

$$K_{SP} = \frac{a_{M^{z+}}^{m} \times a_{P^{y-}}^{n}}{a_{M^{z+}P^{y-}}} \qquad (3\text{-}2)$$

The activity of a pure condensed solid ($a_{M^{z+}P^{y-}}$) is taken as unity and thus the equation becomes

$$K_{SP} = a_{M^{z+}}^{m} \times a_{P^{y-}}^{n} \qquad (3\text{-}3)$$

This thermodynamic equilibrium constant, K_{SP}, is known as the solubility product. Metal sulphides are sparingly soluble and, hence, have very low solubility product values. Thus the ion activity coefficient will be close to unity and the solubility product may be expressed in terms of concentrations. For metal sulphides $a_{P^{y-}}^{n} = a_{S^{2-}}^{n}$ and so the solubility product becomes

$$K_{SP} = \left[M^{z+}\right]^{m} \times \left[S^{2-}\right]^{n} \qquad (3\text{-}4)$$

Solubility product values of several metal sulphides as well as solubility product expressions with respect to activities are displayed in Table 2.

Table 2: Solubility product expressions and values for some metal sulphides (Jackson, 1986)

Metal sulphide	Solubility product at 25°C		
	expression	K_{SP}	$\log K_{SP}$
CdS	$a_{Cd^{2+}} \times a_{S^{2-}}$	$= 1.58 \times 10^{-26}$	-25.8
CoS	$a_{Co^{2+}} \times a_{S^{2-}}$	$= 5.01 \times 10^{-22}$	-21.3
CuS	$a_{Cu^{2+}} \times a_{S^{2-}}$	$= 7.94 \times 10^{-37}$	-36.1
FeS	$a_{Fe^{2+}} \times a_{S^{2-}}$	$= 7.94 \times 10^{-19}$	-18.1
HgS	$a_{Hg^{2+}} \times a_{S^{2-}}$	$= 2.00 \times 10^{-53}$	-52.7
MnS	$a_{Mn^{2+}} \times a_{S^{2-}}$	$= 3.16 \times 10^{-11}$	-10.5
NiS	$a_{Ni^{2+}} \times a_{S^{2-}}$	$= 3.98 \times 10^{-20}$	-19.4
PbS	$a_{Pb^{2+}} \times a_{S^{2-}}$	$= 3.16 \times 10^{-28}$	-27.5
ZnS	$a_{Zn^{2+}} \times a_{S^{2-}}$	$= 2.00 \times 10^{-25}$	-24.7

This table quantifies the sparingly soluble nature of several metal sulphide compounds.

Solubility data may be conveniently presented in a graphic form by rearranging equation 3-3 to give

$$a_{M^{z+}}^{m} = \frac{K_{SP}}{a_{S^{2-}}^{n}} \qquad (3\text{-}5)$$

taking the log of both sides of the equation yields a straight line graph of the log of the sulphide ion activity with respect to the metal ion activity, with the solubility product as the gradient of the line, since m = n = 1 for all metal sulphides in question

$$\log a_{M^{z+}}^{m} = \frac{\log K_{SP}}{m} - \frac{n \log a_{S^{2-}}^{n}}{m} \qquad (3\text{-}6)$$

The expression is the basis of the curves shown on the sulphide precipitation diagram in Figure 9.

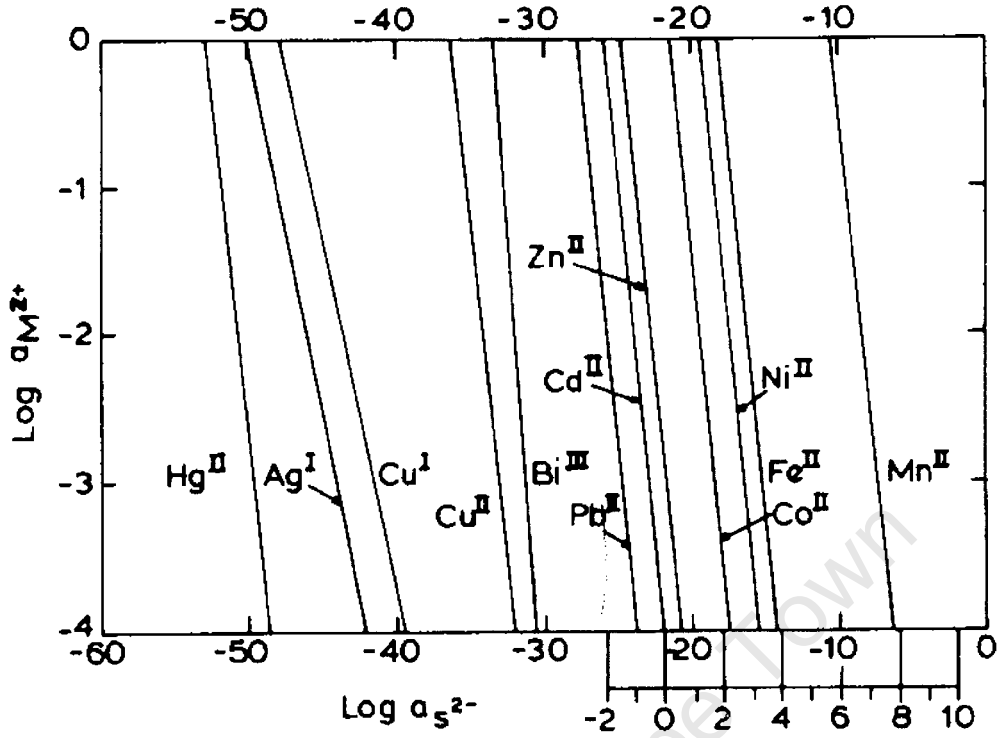

Figure 9: Metal sulphide precipitation diagram [25°C and 1 atm for $H_2S(g)$] (Jackson, 1986)

This diagram illustrates the dissolution concentrations of various metal sulphides. The sulphide activity on the x axis represents the total sulphide concentration upon dissociation of the metal sulphide. The point on a curve for a given metal activity of a particular metal sulphide will yield a sulphide activity on the x axis, below which precipitation of the metal sulphide will not occur. Figure 9 gives an indication of the order of metal sulphide precipitation as the sulphide activity is increased. Superimposed on the log sulphide activity scale are corresponding pH values for standard conditions, which allows for direct assessment of the thermodynamic tendency for precipitation to occur in terms of the pH of the solution (Jackson, 1986).

Metal sulphide solubility is closely linked with pH (section 3.2) and therefore this must be considered for metal sulphide precipitation. For example, NiS solubility is amphoteric as shown in the following graph of pH dependent solubility of nickel sulphide (Figure 10).

The very low solubility of nickel sulphide coupled with the high reactivity facilitates almost complete removal of heavy metal ions in solution between pH values of 3 – 14.

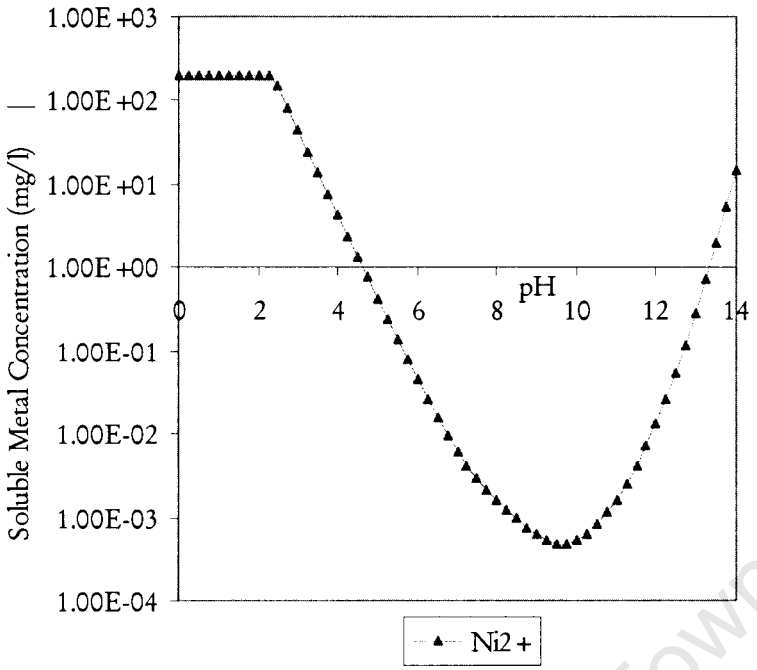

Figure 10: Solubility of nickel sulphide in solution generated using the OLI Stream Analyzer software (25 July 2005)

The disadvantages associated with sparingly soluble metal sulphide precipitation stem from the very same low K_{SP} values and high reactivities. The supersaturation is generated instantaneously and the precipitation reaction is thus difficult to control.

At the high supersaturations generated in sparingly soluble systems, nucleation governs particle rate processes rather than growth. This produces many small particles (nm - μm). The removal of precipitates by filtration is then entirely dependent on the smallest filter size available.

Precipitates may also be removed by settling under gravity, which is based on the terminal velocity of the particles. The terminal velocity is a combination of the gravitational downward force provided by the weight of the particle and the resisting buoyant force on the particle. The time taken for settling to occur is a combination of these two forces. Assuming a spherical particle, the smaller the particle radius the longer it takes to settle because of the decreased surface area to weight ratio and thus gravitational force. Therefore, the settling tank must be longer to provide more time for settling in order to efficiently separate the solid and aqueous phases. Very fine particles in the sub-micron range ($< 1\mu m$) are very readily affected by natural convection currents in the fluid and their behaviour is also affected by Brownian motion. The settling particles are bombarded with molecules of the fluid in a random manner thus the net resultant

force acting at any instant may be large enough to cause change in its direction of motion, leading to inefficient settling (Coulson and Richardson, 2002). Thus, small particles do not settle well based on the sedimentation velocity expressed in the equation below

$$u = \frac{d^2 g(\rho - \rho_o)}{18\mu} \qquad (3\text{-}7)$$

where u is the settling velocity of the particles, d their diameter and ρ their density. μ and ρ_o are the viscosity and the density of the aqueous medium in which the particles are settling and g the acceleration due to gravity.

Reducing the supersaturation of the precipitating system will encourage larger precipitate particle sizes through growth and/or aggregation rather than the principle particle rate process being nucleation. Therefore, if the particles formed are larger, there will be increased phase separation efficiency through both filtration and settling.

3.2 Sulphide Speciation

Hydrogen sulphide is a gas which dissolves in water and, as a weak dibasic acid, undergoes dissociation in two stages prior to reaction with metal to form the metal sulphide (Jackson, 1986). The speciation of aqueous H_2S is the pH dependent equilibria between the sulphide species (H_2S, HS^-, S^{2-}) and is expressed in the ionic dissociation equations 3-8 and 3-9

$$H_2S \rightleftharpoons HS^- + H^+ \qquad pK_1 = 6.99 \text{ (Jackson, 1986)} \qquad (1\text{-}1)$$

$$HS^- \rightleftharpoons S^{2-} + H^+ \qquad pK_2 = 17.40 \text{ (Midgisov et al., 2001)} \qquad (1\text{-}2)$$

The diagrammatic representation of these equations is shown in Figure 11

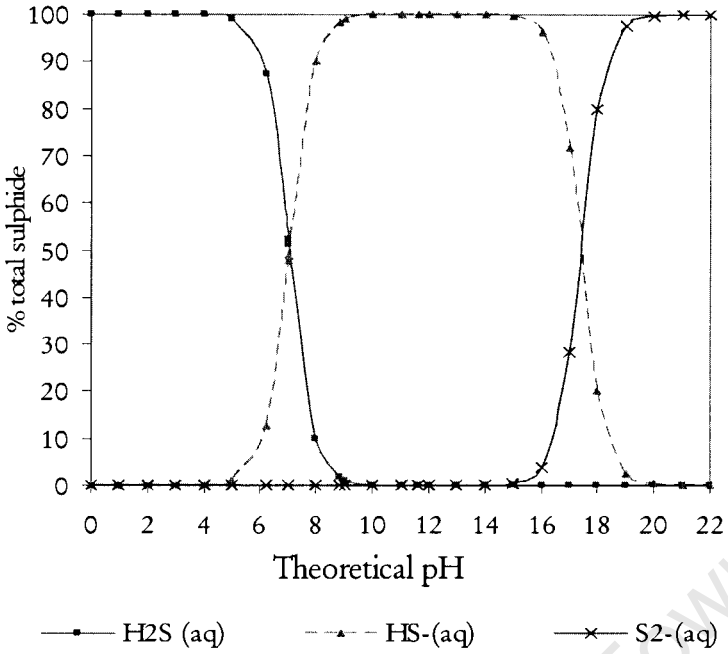

Figure 11: The pH dependent speciation dissociation of free sulphides

The equilibrium concentrations of the sulphide species used to construct the above graph (Figure 11) are quantified by the following equilibrium concentration expressions (Stumm and Morgan, 1996)

$$[H_2S] = \frac{[S]_{total}}{1 + \frac{K_1}{[H^+]} + \frac{K_1K_2}{[H^+]^2}} \quad (3\text{-}8)$$

$$[HS^-] = \frac{[S]_{total}}{\frac{[H^+]}{K_1} + 1 + \frac{K_2}{[H^+]}} \quad (3\text{-}9)$$

$$[S^{2-}] = \frac{[S]_{total}}{\frac{[H^+]^2}{K_1K_2} + \frac{[H^+]}{K_2} + 1} \quad (3\text{-}10)$$

There is a discrepancy relating to the value of the second dissociation constant (pK_2). Stumm and Morgan (1996) state that the second dissociation constant is between 13 and 19 but that more recent, spetrophotometrically determined, constants are between 17 and 19. The most recent value found is 17.4 ± 0.3 (Migdisov, 2001) which has been used in the graph and equations above. These high values imply that S^{2-} rarely occurs at significant concentrations in aqueous solution (Licht, 1988; Stumm and Morgan, 1996).

In a study by Kolthoff and Moltzau (1935) it was proposed that sulphide precipitation involves the reaction of bisulphide ions to give first a metal hydrosulphide complex of the metal which, by secondary loss of hydrogen sulphide, results in the formation of the metal sulphide itself. More recently van Hille et al. (2005) have also suggested that the principle sulphide species participating in the sulphide precipitation reaction was the bisulphide ion. Thus, the main reaction expected for sulphide precipitation becomes

$$Me^{2+} + HS^- \rightarrow MeS + H^+ \qquad (3\text{-}11)$$

3.3 Formation of aqueous polysulphide complexes/clusters

In metal sulphide precipitation, the formation of aqueous polysulphide complexes or clusters is either an intermediary step before formation of the solid precipitate, or a means by which solid precipitates dissolve after precipitation. Indeed, both processes may occur. Thus, consideration of polysulphide complexes and clusters is important to provide insight to the mechanism of formation of metal sulphide precipitates and also their mechanism of dissolution.

The formation of polysulphide complexes or clusters results from the presence of stoichiometrically excess sulphide and is caused by either the addition of excess sulphide or local sulphide excesses present in the precipitating system. Local excesses are formed as a result of inefficient mixing owing to rapid reaction kinetics in the precipitating system and can occur despite the addition of stoichiometric or below stoichiometric concentrations of metal and sulphide to the reactor.

There are two possible consequences of stoichiometrically excess sulphide reagent present in a metal precipitating system;

- the formation of soluble polysulphide complexes (Luther et al., 1999; van Hille et al., 2005)
- the formation of aqueous clusters (Luther et al., 1999; Luther et al., 2002)

Complexes are simply defined as coordination compounds, where a central atom or ion, M, unites with one or more ligands, L, to form a species of the form $ML_iL_jL_k$ (Cotton et al., 1999). The metal and ligands may all be charged. Further, these complexes:

a should contain a central metal ion capable of significant existence, and
b should exist for a substantial period of time under reaction conditions

A cluster is defined as a polynuclear complex. There is an electrochemical operational continuum between metal sulphide clusters and complexes and the first condensed solid (Rickard and Luther, 2006). Both complexes and clusters are possible when the metal ion is copper.

A study carried out by van Hille et al. (2005) investigated the precipitation of copper sulphide in a seeded fluidised bed reactor. In an attempt to improve the removal of Cu^{2+} ions from solution an excess of sulphide was introduced to the system. It was found that even under significant stoichiometric excess the free aqueous sulphide (S^{2-}, HS^-, and H_2S (aq)) concentration did not exceed 1ppm.

It was concluded that the system was complicated by the formation of stable, soluble copper polysulphide complexes as shown below (van Hille, 2005).

$$Cu^{2+} + 3HS^- \Leftrightarrow CuS(HS)_2^{2-} + H^+ \qquad (3\text{-}12)$$

$$Cu^{2+} + 4HS^- \Leftrightarrow CuS(HS)_3^{3-} + H^+ \qquad (3\text{-}13)$$

An alternative explanation is the formation of aqueous clusters which was investigated in a copper system by Luther et al, 2002. The process involves the formation of Cu_3S_3, 6-membered rings in solution and these trinuclear Cu rings are the building blocks for the aqueous CuS cluster, which result in CuS precipitation. The Cu_3S_3 reacts with and without aqueous sulphide (specifically bisulphide) to form Cu_4S_6 and Cu_4S_5 aqueous clusters respectively as shown below (Luther et al., 2002)

$$2Cu_3S_3(H_2O)_6 \rightarrow Cu_4S_5(H_2O)_4^{4-} + Cu_2S^{2+} + 2H_2O \qquad (3\text{-}14)$$

$$2Cu_3S_3(H_2O)_6 + HS^- \rightarrow Cu_4S_6(H_2O)_4^{4-} + 3Cu_2S^{2+} + H^+ + 2H_2O \qquad (3\text{-}15)$$

Luther et al. (1999) also investigated zinc sulphide precipitation and found very similar results. Aqueous zinc reacts with aqueous sulphide to form a Zn_3S_3 aqueous cluster, which then reacts further with aqueous sulphide to form a $[Zn_4S_6^{4-}]$ polysulphide ion. The ion condenses with Zn_3S_3 (aq) to form solid ZnS, and the kinetics of this final step are relatively slow.

A study performed by Rickard and Luther (2006) has identified a number of possible nickel sulphide complexes which may form when an excess amount of sulphide is present in the precipitating solution. The table below shows the likely nickel sulphide complexes with their stability constants and the method in which they were formed.

Table 3: Summary of stability constants for proposed nickel sulphide complexes and the methods used (Rickard and Luther, 2006)

Species	logK	*I*	Method	Reference
	4.77	0.7	Ligand competition	Al-Farawati and van den Berg (1999)
$[Ni(HS)]^+$	5.3	0.7	Sulphide titration	Zhang and Millero (1994)
	4.97	0.7	Sulphide titration	Luther et al. (1996)
$[Ni(HS)_2]^0$	10.47	0.7	Ligand competition	Al-Farawati and van den Berg (1999)
$[Ni_2(HS)]^{3+}$	9.99	0.7	Sulphide titration	Luther et al. (1996)
$[Ni_3(HS)]^{5+}$	15.90	0.7	Sulphide titration	Luther et al. (1996)
$[Ni(S_4)]$	5.72	0.55	Sulphide titration	Chadwell et al. (2001)
$[Ni_2(S_4)]^{2+}$	11.01	0.55	Sulphide titration	Chadwell et al. (2001)
$[Ni(S_5)]$	5.53	0.55	Sulphide titration	Chadwell et al. (1999)
$[Ni_2(S_5)]^{2+}$	11.06	0.55	Sulphide titration	Chadwell et al. (1999)

where *I* is the ionic strength and logK the conditional stability constant valid only for the stated conditions i.e. for the ionic strength shown. The ionic strength directly influences the activity coefficients for the complexes formed by affecting the activity of either the metal or the ligand.

There are two instances when polysulphide ions may be encountered in the precipitation of metal sulphides (Luther et al., 1996);

i. during precipitation as intermediates in the formation of solid metal sulphides, or
ii. post precipitation as a means in which solid metal sulphide dissolution occurs

Any excess sulphide present will react with precipitated nickel sulphide to form polysulphide complexes or aqueous polysulphide clusters, thereby providing a way in which metal ions remain in solution (Luther et al, 1999; 2002). Thus, efficient sulphide precipitation requires stoichiometric amounts of sulphide and metal ions and effective control mechanisms to maintain the stoichiometric ratio during operation.

This chapter discussed the various aspects to be considered in the practical application of metal sulphide precipitation technology and a significant number of application-specific publications were cited.

4. Methods of reducing local supersaturation

This chapter highlights high supersaturation as a particularly important phenomenon which needs to be addressed in order to improve process conditions. High supersaturation can be both a global or local phenomenon, with local supersaturation being particularly important in applications where the reactivity between the reagents is high, such as the metal sulphide system. In this case supersaturation around reagent inlet points can be extremely high, despite the globally calculated value being acceptable. The chapter identifies three potential methods to reduce local supersaturation: Improved mixing, modifications to reactor design and employing a gaseous sulphide source.

Control of the precipitating environment is desired in order to avoid unfavourable reactions, and the subsequent formation of unwanted products. This can be achieved through lowering the local supersaturation and reducing the spatial inhomogeneity of the supersaturation. Even if the global stoichiometry of the system is controlled, control of the local supersaturation is necessary due to the rapid kinetics of the precipitation reaction.

There are various ways of reducing local supersaturation in order to promote control of the particle rate processes and decrease the chance of formation of polysulphide complexes and clusters. This can be best achieved by controlling the local reagent concentrations.

Mixing of reagents plays an important role in the generation of supersaturation as it is the means by which the concentrations of reagents are dispersed in the solution and thus directly affects the formation of local supersaturations.

The fluidised bed reactor (FBR) highlights two methods in which supersaturation can be lowered in this reactor configuration for the formation of sparingly soluble precipitates; increasing the number of reagent inlet points and introducing a recycle stream to the reactor.

The use of a gaseous precipitating reagent will decrease the rate at which the active reagent enters solution due to mass transfer constraints. The supersaturation is therefore limited, which in turn limits the rate of precipitation. Thus, by using a gaseous sulphide precipitating agent it is possible to slow the rate of formation of metal sulphides by harnessing the mass transfer rate.

4.1 Mixing

The size and morphology of crystals obtained by precipitation are greatly affected by hydrodynamic conditions within a precipitation reaction (Myerson, 2002) because the mixing of the system directly affects the distribution of the reagents in the system, thus the local supersaturation. Good mixing of the reactant feed stream with the bulk solution of the precipitation vessel is essential to achieve good overall mixing in the system and to smooth out any supersaturation peaks in local regions (Mullin, 2001).

The importance of mixing is illustrated in Figure 12.

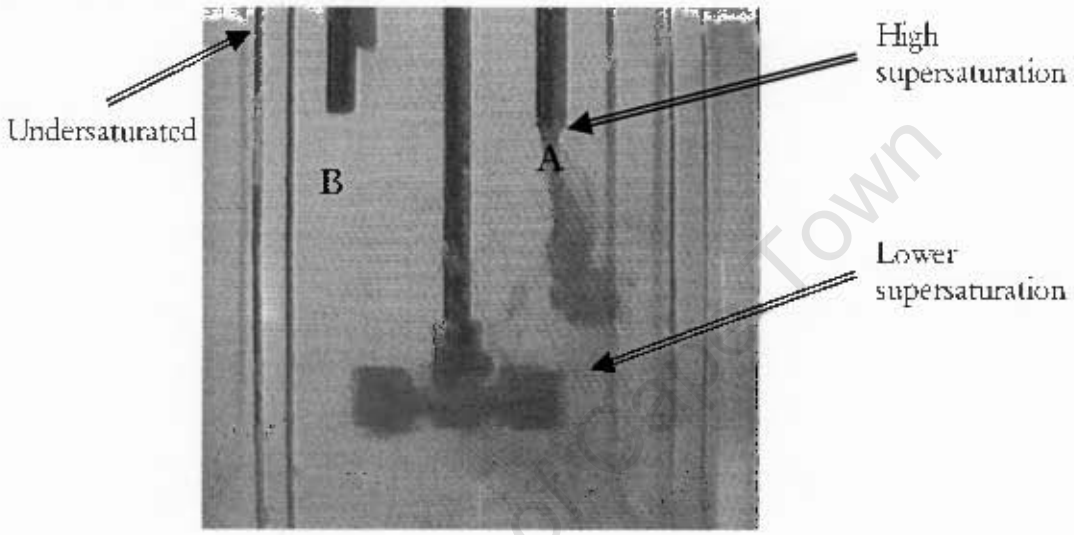

Figure 12: Introduction of a reagent feed stream into a stirred, baffled batch reactor showing variations in concentration with spatial position (Vicum et al., 2004)

Precipitating reagent A is introduced into a bulk solution of B in a fed batch system. The plume of reagent is clearly visible, indicating inefficient mixing. The supersaturation along the boundary of the feed plume close to the entry point is extremely high as the concentration of feed reagent is highest. Around the impeller the supersaturation is decreased because the concentration of the feed reagent is distributed by agitation. At the extremities of the reactor, where the effects of mixing are not yet significant, the region is undersaturated.

Meso-mixing is illustrated in Figure 12. It is the turbulent dispersion of an incoming fresh feed plume within a precipitator. Macro-mixing is concerned with bulk fluid movement and blending and is influenced by precipitator related variables such as agitator speed and vessel geometry. Micromixing is mixing on or near a molecular level and is influenced by fluid physical properties and local conditions.

Various configurations of batch precipitating systems have been proposed in order to lower the high local supersaturation effect of which two are discussed (Lewis et al., 2005).

i. Both reagents, A and B, can be continuously fed into a bulk carrier solution which serves to dilute their concentrations. The probability of A and B molecules interacting in large concentrations is decreased and thus the supersaturation (an equilibrium normalised concentration product of the two reagents) of the system is decreased.
ii. A T mixer in which reagents A and B are mixed in small proportions prior to discharge into the bulk reaction solution provides a means of control over the supersaturation created. The small amounts of reagent solutions allowed by the scale of the T mixer allow this control. Also, very efficient mixing is possible at this small scale. When one of the reagent streams is diluted with a recycle stream from the bulk reactor then the supersaturation is lowered as well as controlled.

Heavy metal precipitation using an aqueous source of sulphide requires very fine control to ensure that high local supersaturations, along with associated negative effects such as colloid formation, do not occur in the bulk of the solution. Therefore, control of precipitation processes employing an aqueous sulphide source is usually not robust enough to be applicable on an industrial scale. This is inferred from large scale processes such as the Sherrit-Gordon process which use $H_2S(g)$ as the precipitating agent (Jackson, 1986).

Figure 12 illustrates the importance of the local supersaturation when considering precipitation in a sparingly soluble system. The global supersaturation calculation provides an insufficient description of the system due to local supersaturation gradients. Efficient mixing is difficult to achieve in sparingly soluble precipitation systems because of their rapid kinetics, leading to local gradients in supersaturation (Myerson, 2002). Local supersaturation gradients impact the sparingly soluble precipitation process significantly because mixing time, even on a molecular scale (micromixing), is much slower than the rate of reaction (Baldyga and Bourne, 1989). For example, the reaction between copper and sulphide falls into the instantaneous regime (Söhnel and Garside, 1992), which is characterised by the nucleation rate being much faster than the micromixing time. Therefore the formation of solid takes place while mixing is still imperfect.

4.2 Fluidised Bed Reactor (FBR)

This reactor configuration is used in an attempt to decrease local supersaturation using an aqueous reagent source. It has been used effectively in the softening of water by precipitation of $CaCO_3$ (Schöller et al., 1987) and more recently in the precipitation of nickel hydroxyl-carbonate for removal of heavy metals from solution (Costodes et al., 2006). Van Hille et al., 2005, attempted copper sulphide precipitation in a FBR.

In FBRs radial mixing is highly efficient although there is no axial mixing thus there is, theoretically, a uniform concentration in every part of the bed (Costodes et al., 2006). In reality the flow pattern in an FBR bed is intermediate between perfectly mixed and plug-flow and therefore it is difficult to achieve complete distribution of supersaturation in all parts of the bed.

The FBR reactor has highlighted ways of reducing the local supersaturation of sparingly soluble systems. Fines production in an FBR must be minimised or eliminated in order to prevent elutriation of precipitates from the reactor and, hence, a decrease in process efficiency. Figure 13 shows a schematic of an FBR and methods used to decrease supersaturation (Costodes et al., 2006).

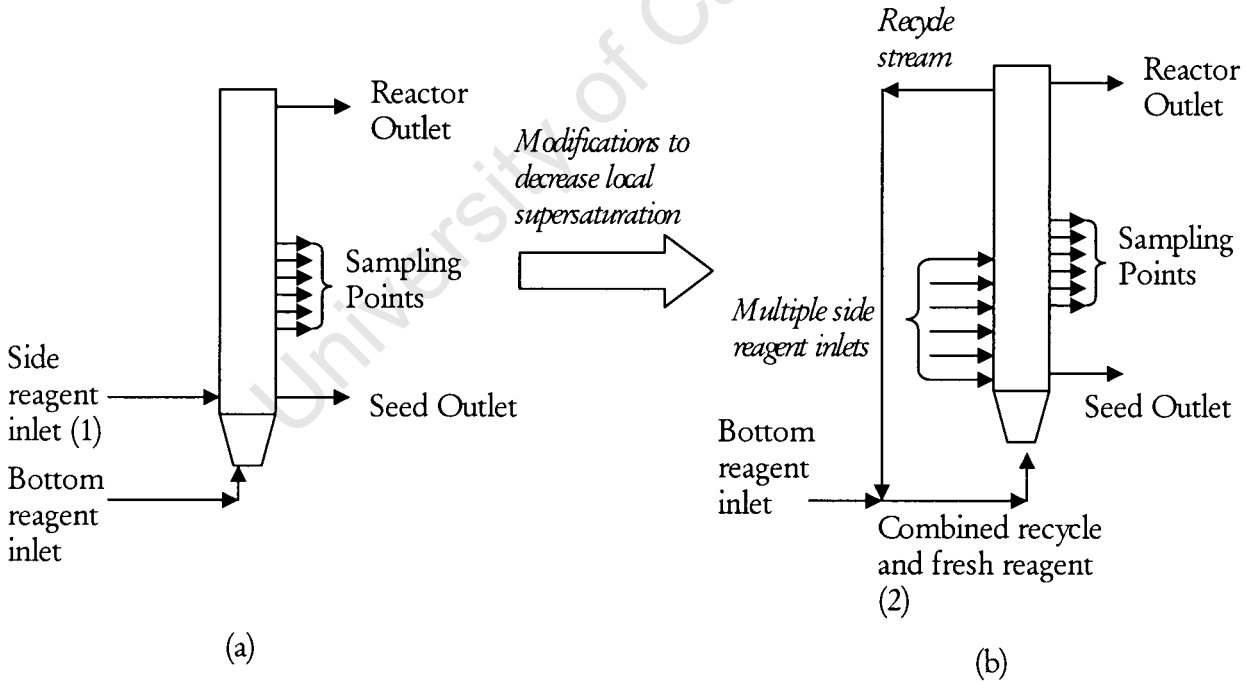

Figure 13: Schematic of an FBR and methods used to decrease local supersaturation (van Hille, 2005; Guillard, 2001)

Van Hille (2005) used the FBR configuration shown above to precipitate copper sulphide and Guillard (2001) and Costodes (2006) used it to precipitate nickel hydroxy-carbonate. For both precipitation systems, the solution containing the metal ion was pumped vertically upwards into the bed and the precipitating agent was injected horizontally into the bed.

Fines production in the FBR is due to (Guillard, 2001, Costodes, 2006)

i. High local supersaturations at the side reagent inlet point
ii. Attrition of precipitates as a result of collisions in the bed

The high local supersaturations generated at the side reagent inlet point (1) result in rapid production of many fine particles by primary nucleation. By reducing the local supersaturation at the side reagent inlet point of the reactor it is possible to promote heterogeneous nucleation and thus encourage precipitate to deposit only on the sand particles.

The high local supersaturation at the side reagent inlet point is caused by the high reagent concentration introduced to the FBR. Therefore, decreasing the reagent concentration at the side inlet and splitting the feed concentration along a section of the reactor length will result in lower local supersaturations (Costodes et al., 2006).

The application of multiple side reagent inlet points while decreasing the feed concentration to FBRs has resulted in a significant decrease in fines production by effectively reducing the local supersaturation in the side inlet region thus enhancing process efficiency (Costodes et al., 2006). Multiplying the side reagent inlets has resulted in decreased fluctuations in the supersaturation levels, therefore better control of supersaturation in the system which also contributes to increased process efficiency. Successful applications of this approach have been carried out in a nickel hydroxy-carbonate system by Guillard (2001) and Costodes et al. (2006). However, in the copper sulphide precipitation system it was necessary to not only split the multiply the feed stream and reduce its concentrations, but to also add acid, thus manipulating the speciation of the aqueous sulphide stream in order to reduce local supersaturations (van Hille et al., 2005).

Another means of reducing the reagent concentration entering the FBR, and thus reducing the local supersaturation at feed inlet points, is by introducing a recycle stream. This dilutes the reagent stream coming in at the base of the reactor (2), and contributes to the decrease in local supersaturation at the side inlet feed points (Costodes et al., 2006). In the sulphide system the effect of diluting the incoming stream increases the

likelihood of local stoichiometric excess of sulphide in the inlets and therefore is not effective (van Hille, 2005).

The recycle stream is also useful because fluidisation of the bed is mainly achieved through the recirculation flowrate (Guillard, 2001). The mixing intensity caused by the recirculation stream is sufficient to break up agglomerates of pellets when supersaturations are low.

The precipitates in the FBR copper sulphide system did not form on the surface of the sand particles and exited with the treated solution from the top reactor outlet. Only when the sand was pretreated did the copper sulphide precipitate directly onto the sand particles. However, the insoluble nature of CuS, even at acidic pH values, precluded the recovery of the precipitated copper off the seed particles. Therefore, this reactor configuration appears to have limited potential for the recovery of valuable metals as metal sulphides.

4.3 Gaseous precipitating reagent

A method which can be used to decrease the rate of generation of supersaturation in the precipitating system is to supply the precipitating reagent in a gaseous form. Copper has efficiently been removed from mixed effluent streams using hydrogen sulphide gas (Hammack et al., 1993, 1994). By using a gaseous sulphide source the rate at which the sulphide enters solution is limited by the rate of dissolution of $H_2S(g)$. Thus the high local supersaturations are avoided by the mass transfer constraint. In addition the gas bubbles move up through the reactor so the diffusion zone is dynamic rather than static. Therefore, the aqueous sulphide species are diffused throughout most of the reactor volume, limiting regions of high local supersaturation and the formation of a product with unfavourable characteristics.

The use of a gaseous precipitating reagent is rate limiting for the precipitation process due to the mass transfer limitation.

In this chapter methods of reducing local supersaturation were discussed and it was found that

- Improving mixing was discounted as a practical solution due to the nucleation rate being more rapid than the micromixing time
- Fluidised bed reactors were only successful in systems where the K_{SP} of the products were significantly higher than those for metal sulphides and attempts to utilise the fluidised bed for copper sulphide were less successful

- The use of a gaseous sulphide reagent, which has been successfully employed to precipitate base metal sulphides, was identified as the most promising option and its advantages are discussed in greater detail in Chapter 5

5. Gaseous dissolution and reaction of $H_2S(g)$

The chapter describes dissolution and subsequent speciation of $H_2S(g)$ in an aqueous medium. It begins with the derivation of Higbie's Penetration Theory and continues with the application of this model to the dissolution of $H_2S(g)$ and subsequent precipitation of metal sulphides.

Mass transfer across an interface between a gas and a liquid or between two liquid phases is important in separation processes such as distillation (Seader and Henley, 1998) and is applicable in precipitation when using a gaseous precipitating agent. Fluid-fluid mass transfer is used to describe the dissolution of a substance from a gas bubble into the surrounding solution. Oktaybas et al. (1994) investigated the precipitation of copper with $H_2S(g)$ using Higbie's penetration theory to determine the mass transfer coefficient and thus quantify the rate of dissolution of the sulphide precipitating agent.

The fundamental diffusion equations on which Higbie's theory is based are those which describe simple one dimensional unsteady state molecular diffusion, which are derived below. In addition, Higbie's penetration theory uses mass transfer coefficients to model more simply the complex diffusion and reaction of metal sulphides.

5.1 One dimensional unsteady state molecular diffusion (Seader and Henley, 1998)

Fick's first law of ordinary molecular diffusion relates the molar flow flux through species B of diffusing species A, across a given cross-sectional area, A, to the diffusivity, D_{AB}, and the concentration gradient of the area A.

$$n_A = -D_{AB} A \left(\frac{dc_A}{dz} \right) \qquad (5\text{-}1)$$

Equation 5-1 is applied to unsteady state molecular diffusion by considering the accumulation or depletion of a species with time in a unit volume through which the species is diffusing. Figure 14 shows diffusion of species A through species B through a differential volume in only the z direction.

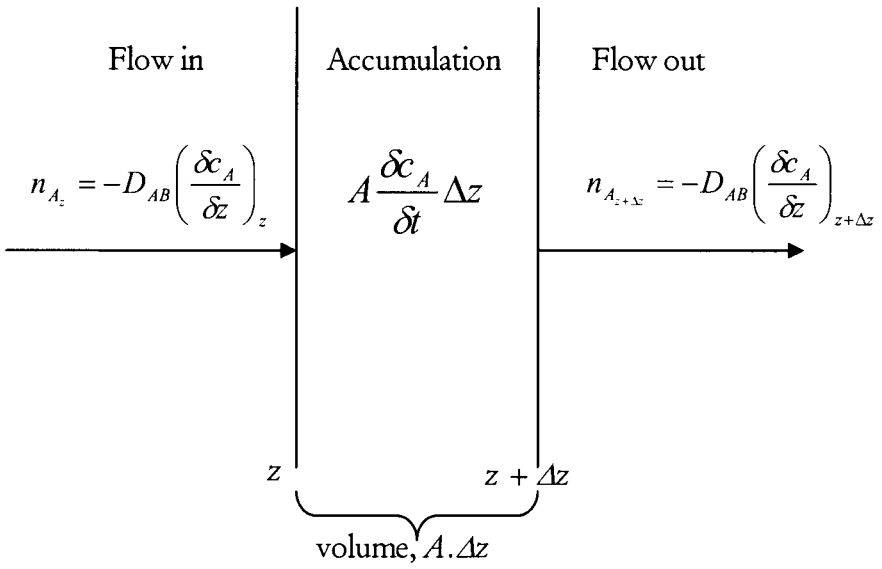

Figure 14: Unsteady state diffusion through a differential volume $A\Delta z$ (Seader and Henley, 1998)

Assuming a constant total concentration, $c = c_A + c_B$, constant diffusivity, and negligible bulk flow, the molar flowrate of species A by diffusion at the plane z =z is given by

$$n_{A_z} = -D_{AB}\left(\frac{\delta c_A}{\delta z}\right)_z \tag{5-2}$$

And at the plane $z + \Delta z$, the diffusion rate is

$$n_{A_{z+\Delta z}} = -D_{AB}\left(\frac{\delta c_A}{\delta z}\right)_{z+\Delta z} \tag{5-3}$$

The accumulation of species A in the control volume is

$$A\frac{\delta c_A}{\delta t}\Delta z \tag{5-4}$$

Applying rate in – rate out = accumulation,

$$n_{A_z} = -D_{AB}\left(\frac{\delta c_A}{\delta z}\right)_z + n_{A_{z+\Delta z}} = -D_{AB}\left(\frac{\delta c_A}{\delta z}\right)_{z+\Delta z} = A\frac{\delta c_A}{\delta t}\Delta z \tag{5-5}$$

Rearranging and simplifying,

$$D_{AB} = \left[\frac{(\delta c_A / \delta z)_{z+\Delta z} - (\delta c_A / \delta z)_z}{\Delta z} \right] = \frac{\delta c_A}{\delta t} \tag{5-6}$$

Taking the limit as $\Delta z \rightarrow 0$,

$$\frac{\delta c_A}{\delta t} = D_{AB} \frac{\delta^2 c_A}{\delta z^2} \tag{5-7}$$

This is Fick's second law for one dimensional diffusion. For diffusion in the radial direction only in spherical co-ordinates, Fick's second law becomes,

$$\frac{\delta c_A}{\delta t} = \frac{D_{AB}}{r^2} \frac{\delta}{\delta r} \left(r^2 \frac{\delta c_A}{\delta r} \right) \tag{5-8}$$

Analytical solutions to these partial differential equations are available for a number of boundary conditions, discussed in Seader and Henley (1998).

Mass transfer problems are mostly solved using mass transfer coefficients (Seader and Henley, 1998). As concentration is defined in many different ways, different mass transfer coefficients are defined. If Δc_A is selected as the driving force for mass transfer, then the mass transfer coefficient, k_c (mol/time-area-driving force) is defined as shown below,

$$n_A = k_c A \Delta c_A \tag{5-9}$$

Higbie's penetration theory has been developed to describe mass transfer from a fluid to the fluid-fluid interface by determining the mass transfer coefficient, that is, the area normal rate of mass transfer for fluid-fluid diffusion (Seader and Henley, 1998).

Higbie's penetration theory offers a realistic physical model of mass transfer across a gas-liquid interface into a bulk liquid stream, shown in Figure 15.

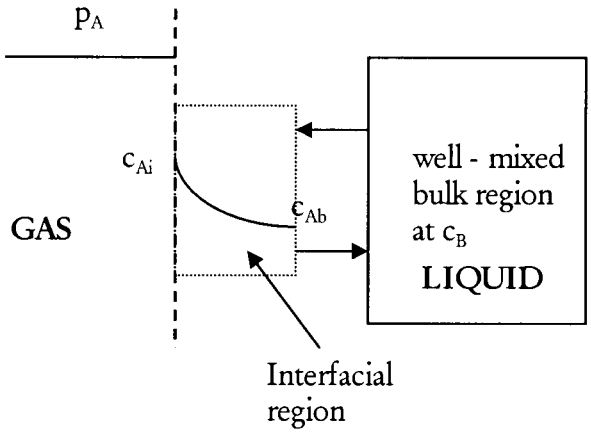

Figure 15: Penetration and surface renewal theory for the mass transfer from a fluid-fluid interface into a liquid (Seader and Henley, 1998)

Within the interfacial region Boussinesq eddies occur that, during a cycle

1. move from the bulk to the interface,
2. stay at the interface for a short, fixed period of time during which they remain static so that molecular diffusion takes place normal to the interface; and
3. leave the interface to mix with the bulk stream.

When one eddy moves to the interface, it replaces another static eddy. Thus, eddies are both stagnant and moving, and turbulence extends to the surface.

In the penetration theory, unsteady-state diffusion takes place when the eddy is static. This process is governed by Fick's second law, equation 5-7 derived above. The boundary conditions are

$$c_A = C_{Ab} \text{ at } t = 0 \text{ for } 0 \leq z \leq \infty;$$

$$c_A = c_{Ai} \text{ at } z = 0 \text{ for } t > 0;$$

$$\text{and } c_A = c_{Ab} \text{ at } z = \infty \text{ for } t > 0$$

Thus the average mass transfer flux of A in the absence of bulk flow is,

$$N_A = 2\sqrt{D_{AB}/\pi t_c}\,(c_{Ai} - c_{Ab}) \qquad (5\text{-}10)$$

In which the mass transfer coefficient is, as defined by the penetration theory

$$k_c = 2\sqrt{D_{AB}/\pi t_c} \qquad (5\text{-}11)$$

For bubbles, the contact time, t_c, is defined as the ratio of the bubble diameter, $2R_B$, over the rising bubble velocity, V_B.

5.2 Higbie's penetration theory applied to metal sulphide precipitation

Higbie's theory has been applied to precipitation of metal from sulphate solutions by $H_2S(g)$ (Mishra and Kapoor, 1978 and Oktaybas et al., 1994). The overall metal sulphide precipitation reaction,

$$MeSO_4(aq) + H_2S(g) \rightarrow MeS(s) + H_2SO_4 \qquad (5\text{-}12)$$

consists of the following steps

1. absorption of H_2S by the gas-liquid interface
2. diffusion of H_2S to the reaction zone
3. diffusion of the metal ion to the reaction zone
4. reaction at the reaction zone
5. precipitation of reaction products from the reaction zone

It has been found that the diffusion steps (2 and 3) are rate limiting (Mishra and Kapoor, 1978). Thus, Higbie's penetration theory for the rate of metal sulphide precipitation can be expressed as

$$\frac{dC^t_{MeSO_4}}{dt} = -\frac{A_b}{V} k_c \left(C^t_{MeSO_4} + C^0_{H_2S}\right) \qquad (5\text{-}13)$$

where A_b is the interfacial area, V is the volume of the liquid phase, $C^t_{MeSO_4}$ is the concentration of the metal sulphate with time during the reaction and $C^0_{H_2S}$ the interfacial concentration of H_2S ($18.18 kg/m^3$) (Oktaybas et al., 1994). Thus, by integrating we obtain

$$\ln\left(\frac{18.18 + C^t_{MeSO_4}}{18.18 + C^0_{MeSO_4}}\right) = \frac{A_b}{V} k_c t_c \qquad (5\text{-}14)$$

The slope, k, of the graph drawn with $\ln\left(\frac{18.18+C^{t}_{MeSO_4}}{18.18+C^{0}_{MeSO_4}}\right)$ vs time, t, yields

$$k = \frac{A_b}{V} k_c \tag{5-15}$$

where

$$A_b = \frac{\pi n R_B^2 h}{V_B} \tag{5-16}$$

where n is the number of bubbles/s, R_B the radius of the bubble and V_B its rising velocity, and h the height of the liquid phase. The rising bubble velocity is,

$$V_B = 1.02\sqrt{gR_B} \tag{5-17}$$

with g being acceleration due to gravity.

The contact time, t_c, of the volume of liquid that the bubble is exposed to before being renewed by a new volume of liquid from the bulk solution, according to the surface renewal theory, is

$$t_c = \frac{2R_B}{V_B} \tag{5-18}$$

Substituting the expressions for V_B and t_c into equation 5-11 yields

$$k_c = 0.82\sqrt{D_{H_2S}}\left(\frac{g}{R_B}\right)^{1/4} \tag{5-19}$$

In this study gaseous sulphide will be used to precipitate nickel from a sulphate solution. Figure 16 shows the dissolution and speciation of $H_2S(g)$ and the subsequent almost instantaneous reaction of the bisulphide ion with the nickel ion in solution.

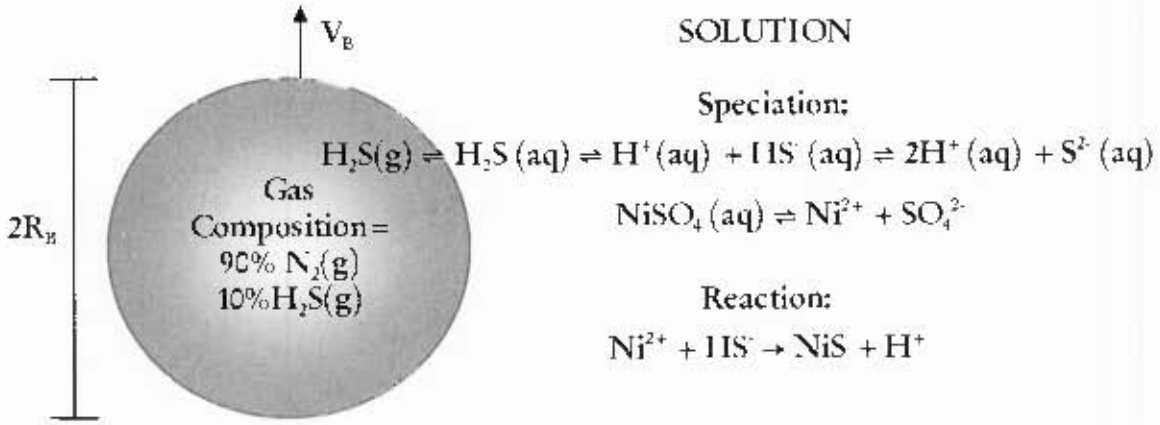

Figure 16: Schematic of the diffusion of gaseous hydrogen sulphide into solution, followed by speciation of $H_2S(g)$ and reaction with Ni^{2+}

In this study Higbie's theory is applied to metal sulphide precipitation and used to determine k_c and thus quantify the rate of diffusion of $H_2S(g)$ into solution through the following equation

$$\overline{R} = \frac{N_A}{t} = k_c(c_{Ai} - c_{Ab}) \qquad (5\text{-}20)$$

where $\overline{R}$ is the rate of absorption of $H_2S(g)$ into solution per unit interfacial area and t is the time taken for one bubble to travel the length of the bubble column.

As nickel sulphide precipitates, protons are released according to reaction 5-21

$$Ni^{2+} + HS^- \rightarrow NiS + H^+ \qquad (5\text{-}21)$$

after absorption and speciation as shown in Figure 16 above. Thus the solution becomes more acidic as the reaction progresses. The sulphide species is predominantly $H_2S(aq)$ at low pH values and therefore reaction is no longer possible. Alkalinity (NaOH) is supplied as a tool to drive sulphide speciation towards the formation of HS^- ions so that the reaction continues. The hydroxide ions consume protons generated by the precipitation reaction (5-21) and those released by dissociation of H_2S, allowing more sulphide to enter solution and speciate to form HS^-, which can react with nickel.

Al-Tarazi et al (2004) modelled the precipitation of metal sulphides using gaseous hydrogen sulphide and presented results for the simultaneous precipitation of Cu and Zn. The rate of $H_2S(g)$ gas flux from the bubble into solution was modelled using Higbie's Penetration Theory. The mathematical model showed that the rate of

precipitation of the metals was fully controlled by the mass transfer of $H_2S(g)$. The model does not predict a threshold pH below which precipitation does not occur for nickel, as demonstrated in this work. Although the model predicted higher precipitation rates at higher pH values, the information supplied does not encompass the discontinuation of precipitation of Ni from solution at pH values below 3 and therefore is not applicable to this system.

This chapter described the theory and presented detailed equations behind the gas-liquid precipitation of Ni in solution using $H_2S(g)$. It emphasised the use of Higbie's Penetration Theory to determine the flux of $H_2S(g)$ from the bubble into the reaction solution, which can then be used to calculate the rate of supersaturation generation. The release of protons by the speciation of aqueous H_2S and the reaction of HS^- with metal ions was highlighted in this chapter and this leads to the assumption that an alkaline source may be required to maintain the correct balance of bisulphide ions.

6. Materials and Methods

This chapter describes the solutions prepared and the analytical techniques used, the experimental apparatus for both batch aqueous and semi-batch gaseous runs and the details of experiments carried out for each reactor set-up. Experiments were carried out in the gaseous semi-batch column using a synthetic nickel sulphate solution and a reduction end solution obtained from industry. The details of modelling of the reaction system carried out using OLI Stream System Analyzer 2.0 are presented.

6.1 Solutions

All reagents ($NiSO_4.6H_2O$, NaOH, $Na_2S.9H_2O$) used in this investigation were analytical grade Merck chemicals.

Nickel sulphate ($NiSO_4.6H_2O$) and sodium sulphide ($Na_2S.9H_2O$) stock solutions were prepared to concentrations of 2g/L Ni^{2+} and 0.5mol/L Na_2S with oxygen free water. The oxygen free water was prepared by boiling distilled water for 20 minutes and then sparging with N_2 for a further 20 minutes during cooling to exclude any O_2 dissolved in the water.

NaOH solutions of various concentrations were made up using distilled water.

The reduction end solution (RES) was obtained from Impala Platinum Refineries and contained 1.5g/L Ni^{2+} and 200mg/L Co^{2+}. The heavy metals were present as ammonium sulphate complexes e.g. $Ni(NH_3)_nSO_4$.

For determining the sulphide concentration in the reactor the following specialised reagents were required. Zinc acetate solution was prepared to a concentration of 10.4g/L using deionised H_2O. Ferric chloride and *N,N*-dimethyl-*p*-phenylene diamine hydrochloride (DMPD) were made up to concentrations of 16g/L and 4g/L respectively in 6 molar HCl, using oxygen free water and 32% HCl.

6.2 Analytical Techniques

Total free sulphide ($H_2S(aq)$, HS^-, S^{2-}) in solution was determined using an spectrophotometric method based on the reaction of sulphide with *p*- phenylene diamine (Methylene blue method). The assay is only accurate to concentrations of 1.50mg/L; therefore dilutions of samples were made. A volume of sample, usually 15 - 50µL, was

transferred to a test tube containing 200μL of zinc acetate. The zinc acetate reacted with any sulphide species present in the sample to form zinc sulphide. The volume was made up to 5mL by addition of oxygen free distilled water. 500μL of DMPD solution followed by 500μL of ferric chloride solution were added to the sample. The sample was mixed and allowed to react completely, about 5 minutes. The addition of the two highly acidic reagents caused dissolution of the zinc sulphide. The low pH of the sample ensured that all sulphide liberated from the zinc sulphide was present as $H_2S(aq)$ which reacted with DMPD to form the thiazine dye (methylene blue). The reaction is catalysed with ferric chloride. The concentration of sulphide was determined using a Spectroquant® Nova 60.

pH was measured with a Hanna pH 211 microprocessor and a HI 1332 pH probe.

Aqueous metal concentrations were determined using the Varian SpectrAA-30 atomic absorption spectrophotometer (AAS). Prior to AAS analysis, the liquid sample was filtered through 0.45μm nylon filters (Millipore).

Particle size distributions PSDs were measured using the Malvern Mastersizer® and the Beckman Coulter® Counter.

Zeta potentials were measured using the Malvern ZetaSizer® .

Settling efficiency was measured using Imhoff settling cones.

6.3 Reactors

6.3.1 Batch Reactor

The batch reactor configuration is shown in Figure 17. The reactor was a 1L closed glass vessel kept as airtight as possible using vacuum grease to seal any potential leaks where $H_2S(g)$ evolved during reaction could escape to the outside air, thus ensuring that the $H_2S(g)$ was captured in the NaOH sulphide trap. It was filled to a volume of 750ml for experimental runs to prevent overflow of solution during mixing. The mixing was effected by a Rushton impeller, 0.045m in diameter, suspended approximately one third of the reactor length above the bottom of the reactor. The impeller speed was kept constant for all experiments at 330rpm and the impeller diameter was 0.04m. The pH meter was suspended as close to the impeller as possible in order to record the pH of the well-mixed solution. Samples were taken from as close to the impeller as possible.

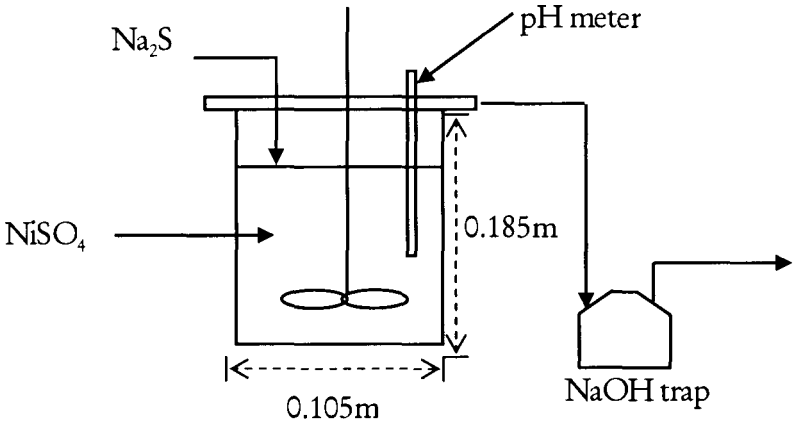

Figure 17: Batch reactor using aqueous sulphide to precipitate Ni^{2+}

6.3.2 Bubble Column

A schematic diagram of the experimental apparatus used to test the effects of a gaseous sulphide source and various NaOH concentrations on the precipitation process is shown in Figure 18. The reactor was charged with 750ml $NiSO_4$ solution with a concentration equivalent to 200ppm Ni^{2+}. NaOH was pumped in at a constant rate of 4.46ml/minute using a Watson Marlow 505S pump, through Norprene® MasterFlex® 6402-16 tubing. An aquarium airstone with a diameter of 0.025m was used to sparge the $H_2S(g)$ into the reactor. The reactor was sealed, and therefore any unreacted $H_2S(g)$ was collected in the NaOH sulphide trap. The flowrate of the $H_2S(g)$ was adjusted using a TIV Tokyo Keiso rotameter with a range from 0 to 1.0L/min. ⅛" steel tubing was used to convey the $H_2S(g)$ gas from the supply tank to the reactor in order to fulfil safety obligations. The flux values of the $H_2S(g)$ entering the reaction solution were between 8.38-1.05 x 10^{-10} m/s. pH was recorded at the top and bottom of the bubble column. Samples were taken at the top of the column.

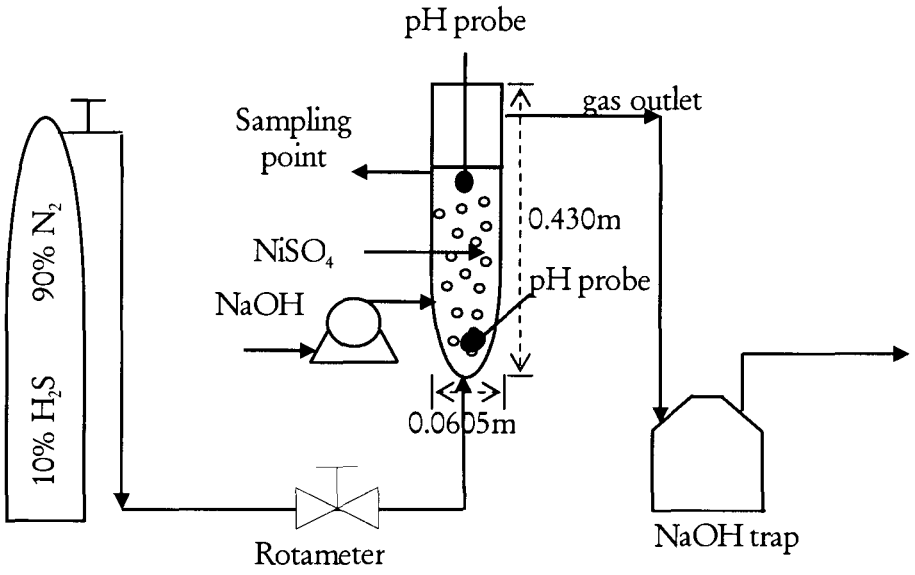

Figure 18: Semi-batch bubble column using $H_2S(g)$ to precipitate Ni^{2+}

6.4 Experimental Design

6.4.1 Batch Aqueous Experiments

The desired initial concentration of metal reagent was 200ppm Ni^{2+} for all experiments. This concentration was obtained by adding a volume of stock $NiSO_4$ solution to distilled water to make up 750ml of reagent. Prior to all reactions the actual concentration (ppm) of Ni^{2+} in solution used for the experimental run was determined by AAS.

In the batch system the sulphide source was provided as aqueous Na_2S. From the stock solution of 0.5M Na_2S specific volumes of the aqueous sulphide reagent were extracted to react with Ni^{2+} at the molar ratios of Ni: S displayed in Tables 4 and 5.

The batch reactor was charged with 750ml $NiSO_4$ solution with a concentration equivalent to ±200 ppm Ni^{2+} to which the sulphide reagent was "slug-dosed" using an "Eppendorf" pipette according to the desired Ni:S ratio. Thus, a single dose of sulphide was injected as fast as possible to the reactor at the start of the run only and then sealed.

The mixing rate was kept constant at 330rpm for the duration of the experimental run. Samples (5ml) were withdrawn at 30s, 2, 5, 10, 15 and 20 minutes after the sulphide addition and immediately filtered through a 0.45μm nylon membrane filter. pH readings

and samples for sulphide analysis were taken at these times. Filtered samples were sent for AAS analysis to determine Ni^{2+} concentrations.

Two cases were tested in the batch reactor using an aqueous sulphide reagent - the effect of individual sulphide species, specifically $H_2S(aq)$ and HS^-, and the effect of varying the ratio of sulphide to metal on the precipitation reaction. Experiments were repeated in triplicate to decrease the experimental error.

6.4.1.1. Control of the sulphide species available for reaction

In these batch experiments the initial pH of the sulphide reagent added to the reactor was adjusted such that only a single sulphide species was present at each pH tested (Table 4). The concentration of sulphide reagent was measured after pH adjustment to determine any loss of $H_2S(g)$ and if so the volume of sulphide added was adjusted to maintain the desired stoichiometry. These experiments were based on the pH dependent sulphide speciation equations (1-1 and 1-2), discussed in Chapter 3, and their respective reaction constants*.

Table 4: Details of batch experiments with aqueous sulphide to determine the effect of individual sulphide species on nickel removal

Run	pH_i (Initial pH of $Na_2S(aq)$)	$H_2S(aq)$, HS^-, S^{2-} * (theoretical sulphide species available for reaction)	$[Ni^{2+}]$: [Sulphide] (ratio of reagents)	$[Ni^{2+}]$ (mg/L)
B01	11.95 (unadjusted)	HS^-	1: 1	201.10
B02	9.88	HS^-	1: 1	215.45
B03	4.24	$H_2S(aq)$	1: 1	238.95

* based on pK_1 = 6.99 (Jackson, 1986) pK_2 = 17.4 (Midgisov et al., 2001)

6.4.1.2. Molar ratio of Ni:S

Various Ni:S molar ratios were tested (Table 5) to ascertain the effect of excess or limiting sulphide reagent on the precipitation reaction because during batch experimentation with low alkalinity flowrates, a dissolution phenomenon was encountered when excess sulphide was present in solution. These batch experiments with varying sulphide dosage were designed to further study the dissolution effect.

The stoichiometric ratio of nickel to sulphide was used for comparison with the non-stoichiometric reagent ratios.

Table 5: Details of batch experiments to determine the effect of metal to sulphide ratio on nickel removal by batch aqueous sulphide

Run	$[Ni^{2+}]$: [Sulphide] (ratio of reagents)	$[Ni^{2+}]$ (mg/L)
B04	1: 0.5	198.2
B01	1: 1.0	201.1
B05	1: 1.5	206.8
B06	1: 2.0	179.8

6.4.2 Semi-batch gaseous experiments

Bubble column experiments were conducted to study the efficiency of Ni^{2+} removal with varying alkalinity by adjusting the NaOH and $H_2S(g)$ flowrates to the reactor.

The bubble column reactor was charged with 750ml $NiSO_4$ (200ppm Ni^{2+}) through which the gaseous sulphide reagent as a 90: 10% mixture of $N_2/H_2S(g)$ was bubbled. Thus precipitation was carried out in a semi-batch manner. The $N_2/H_2S(g)$ mixture was bubbled into the reactor through a gas disperser fitted to its bottom. Samples (5ml) were taken at 0, 1, 2 minutes and every two minutes afterwards for the 40 minute duration of the run. The samples of reaction solution were filtered and sent for AAS analysis to determine the nickel ion concentration during reaction (Table 6 and Table 7). pH readings and duplicate or triplicate sulphide samples were taken at these times as well. The concentration of sulphide in the NaOH sulphide trap was monitored throughout the run to quantify unreacted and thus wasted sulphide reagent.

Fresh NaOH solutions were made up for each run in the bubble column. NaOH(aq) of various concentrations were made up using distilled water. These concentrations were determined from the desired rate of NaOH(aq) addition to the gaseous column, which varied between 0.100 and 2.23 mmol/min as shown in Table 6 and Table 7.

6.4.2.1. Low alkalinity (NaOH) concentrations

Experiments were run to determine the effect of a continuous supply of low concentrations of alkalinity on the removal of nickel when a gaseous sulphide source was employed for NiS precipitation. The molar flowrates of $H_2S(g)$ were at least an order of magnitude greater than those of NaOH. The experiments that were run are listed in Table 6.

Table 6: Details of experiments to determine the effect of using low NaOH flowrates on removal of Ni^{2+} by semi-batch gaseous sulphide precipitation

Run	**NaOH** (mmol/min)	**$N_2/H_2S(g)$ mixture** [10% $H_2S(g)$; 90%N_2] (L/min)	**$[H_2S(g)]$** (mmol/min)	**$[Ni^{2+}]$** (mg/L)	**[NaOH]: [Sulphide]** (ratio of reagents)
L01	0.100	0.2	0.893	206.9	0.11: 1
L02	0.100	0.6	2.68	195.7	0.037: 1
L03	0.200	0.8	3.57	210.1	0.056: 1
L04	0.150	0.8	3.57	196.8	0.042:1
L05	0.100	0.8	3.57	210.4	0.028:1
L06	0	0.8	3.57	210.6	-

Experiment L05 was repeated in triplicate to determine the experimental error representative of this section of experiments (Appendix B).

6.4.2.2. Higher alkalinity (NaOH) concentrations

Higher concentrations of alkalinity were employed thus the ratios of molar flowrates of NaOH to $H_2S(g)$ are of the same order of magnitude or one order less but not any lower.

Table 7: Details of experiments using higher NaOH flowrates to determine effect on removal of Ni^{2+} by semi-batch gaseous sulphide precipitation

Run	NaOH	$N_2/H_2S(g)$ [10% $H_2S(g)$; 90%N_2]	$[H_2S(g)]$	$[Ni^{2+}]$	[NaOH]: [Sulphide]
	(mmol/min)	(L/min)	(mmol/min)	(mg/L)	(ratio of reagents)
T01	2.23	0.8	3.57	215.5	0.62:1
T02	2.23	0.5	2.23	217.4	1.0:1
T03	2.23	0.3	1.34	210.5	1.7:1
T04	2.23	0.1	0.446	208.9	5.0:1
T05	1.75	0.8	3.57	182.6	0.49:1
T06	1.75	0.5	2.23	183.2	0.78:1
T07	1.75	0.3	1.34	217.0	1.3:1
T08	1.75	0.1	0.446	199.7	3.9:1
T09	1.20	0.3	1.34	197.7	0.90:1
T10	1.20	0.2	0.893	217.4	1.3:1
T11	1.20	0.1	0.446	217.1	2.7:1

Experiment T05 was repeated in duplicate to determine the experimental error representative of this section of experiments (Appendix B).

6.4.2.3. RES experiments

Semi-batch experiments were run in the bubble column using RES obtained from a nickel refinery. The sampling and analyses were the same as for the previous set of experiments.

This solution varied significantly from the synthetic nickel reagent used in previous bubble column experiments. RES is an nickel ammonium sulphate solution, $Ni(NH_3)_nSO_4$ thus the alkaline source was complexed with the nickel. The ammonium ion acts as a buffer to the pH drop that occurs upon precipitation of NiS. The precipitation of nickel from RES was modelled in OLI (15 April 2007) and the final pH was 4.85 whereas that of the synthetic $NiSO_4$ solution was pH 2.29. The higher final pH of the RES after complete precipitation of nickel compared with the synthetic solution final pH indicates that the system was buffered.

The RES also differed because the concentration of Ni^{2+} (1.5g/L) was much higher and due to the presence of a significant amount of Co^{2+} (0.5g/L). Thus experiments involved

diluting the RES so that the nickel concentration was similar to that used in previous experiments (200ppm). The dilution factor was between 6 and 6.5.

These experiments tested what was shown in the synthetic system; that NaOH is necessary to facilitate reaction despite the alkalinity provided as the ammonium complex of the RES.

Table 8: Details of semi-batch gaseous experiments using RES diluted by 1 in 6-6.5

Run	$N_2/H_2S(g)$ [10% $H_2S(g)$; 90%N_2] (L/min)	$[H_2S(g)]$ (mmol/min)	$[Ni^{2+}]$ (mg/L)	$[Co^{2+}]$ (mg/L)	[NaOH] (mmol/min)
RES01	0.3	1.34	225.6	25.40	0
RES02	0.3	1.34	252.2	24.35	1.20

Alkalinity measurements to determine the buffering capacity of the diluted RES were carried out by titrating with 0.02N H_2SO_4 and measuring the pH change with the volume of acid added. The calculation to determine the alkalinity, as $CaCO_3$ equivalents, is shown below

Alkalinity = (volume of 0.02 N H_2SO_4) × 10 × (100/ dil. RES sample volume) (6-1)

6.4.3 Modelling

Modelling was carried out using the OLI Stream System Analyzer 2.0 (OLI© 2006) for the batch and a selection of semi-batch experiments in order to compare the purely thermodynamic model results with those obtained experimentally, when kinetic parameters were significant. The OLI modelling software has an extensive database containing all possible reactions. From this the most likely thermodynamically occurring reactions are selected. No specification of reactions occurring is necessary by the user.

OLI utilises a thermodynamic formulation to calculate Gibbs Free Energy, enthalpy, entropy, heat capacity and volume based on the calculation of the standard state terms (G^o,H^o, S^o, C_p^o and V^o) using the framework of Helgeson and co-workers, and the frameworks of Bromley, Zemaitis, Pitzer and Debye-Huckel to calculate the excess terms (G^E,H^E, S^E, C_p^E and V^E) (http://support.olisystems.com/Documents/Manuals/).

$$G_i = G_i^o + G_i^E \quad (6\text{-}2)$$

$$H = H^o + H^E \quad (6\text{-}3)$$

$$S = S^{o} + S^{E} \quad (6\text{-}4)$$

$$C_P = C_P{}^{o} + C_P{}^{E} \quad (6\text{-}5)$$

$$V = V^{o} + V^{E} \quad (6\text{-}6)$$

OLI, through the Helgeson thermodynamic framework can predict individual G^{o} for any species, i, in water and thus predict any equilibrium constant. In addition, OLI can consider, simultaneously, the formation of any solids that might precipitate, the formation of a gas phase and a second, non-aqueous liquid phase. Thus, OLI was useful in modelling the precipitation of NiS using both aqueous (Na_2S) and gaseous sulphide sources ($H_2S(g)$) and considered the thermodynamic possibility of other precipitates such as $Ni(OH)_2$.

Nickel precipitation efficiency, determined by Ni^{2+} remaining in solution, and the final pH values for the slug-dosed batch experiments were simply modelled in OLI by inputting the initial concentrations of $NiSO_4$ and Na_2S reagents experimentally used.

Pseudo-kinetic modelling was carried out in OLI for the semi-batch experiments using a high NaOH concentration (2.23mmol/min), to facilitate precipitation, at varying $H_2S(g)$ flowrates (0.1; 0.3; 0.5; 0.8l/min) (Table 9). The concentrations of NaOH and $H_2S(g)$ were input at 20s intervals, based on their flowrates, until the nickel ions in solution were depleted. The entire initial 200ppm Ni^{2+} as $NiSO_4$ solution was input initially and updated at every 20s time interval. Thus, the % nickel removal and pH after every 20s of reaction was determined.

Table 9: Values of $H_2S(g)$ and NaOH input for pseudo-kinetic thermodynamic modelling of the precipitation of nickel sulphide when $H_2S(g)$ = 0.8L/min and NaOH = 2.23 mmol/min carried out in OLI Stream Analyzer

time		NaOH	$H_2S(g)$
(min)	(seconds)	mmol	mmol
0	0	0	0
0.33	20	1.32	2.12
0.67	40	2.64	4.23
1.00	60	3.96	6.35
1.33	80	5.28	8.47
1.67	100	6.60	10.6
2.00	120	7.93	12.7
2.33	140	9.25	14.8
2.67	160	10.6	16.9
3.00	180	11.9	19.0
3.33	200	13.2	21.2

This chapter provided a comprehensive description of batch and bubble column reactors. The initial batch experiments were designed to confirm that $H_2S(aq)$ ion was not capable of precipitating nickel. This was achieved by manipulating the pH of the sulphide reagent to control speciation. The effect of changes to the molar ratio of Ni:S was tested in the batch system, to test the phenomenon of formation of the polysulphide complex formation in the presence of excel bisulphide, which was observed in the bubble column. The semi-batch bubble column was operated under three sets of conditions; in the absence of added alkalinity and with the addition of a dilute or more concentrated NaOH stream at a constant flow rate. In addition, under both conditions the $H_2S(g)$ flowrate was varied between 0.1 – 0.8 L/min. After these experiments, the precipitation of nickel from diluted RES was tested in order to ascertain the applicability of laboratory data to real world process stream. OLI modeling of the synthetic $NiSO_4$ system is used to compare thermodynamic modeled values and experimentally determined kinetics results.

7. Experimental results and discussion

7.1. Batch results

The pH probe was placed and samples were taken in the well-mixed region, in close proximity to the impeller, to ensure that the reaction was monitored in a region where concentration gradients were reduced. Thus, the sample was representative of a region where active precipitation was occurring. Figure 19 shows turbulent dissipation energy in a batch reactor with two feed streams placed close to the Rushton impeller. There is very high turbulent dissipation energy near the impeller indicating that there is good mixing in this region. Thus, the concentration gradients in this region are minimised and the local supersaturation would be approximately constant within the sample volume, with respect to distance at time t. Since the sulphide reagent was introduced to the batch reactor close to the impeller the sulphide concentrations would be the highest in this region and thus local supersaturations would be high.

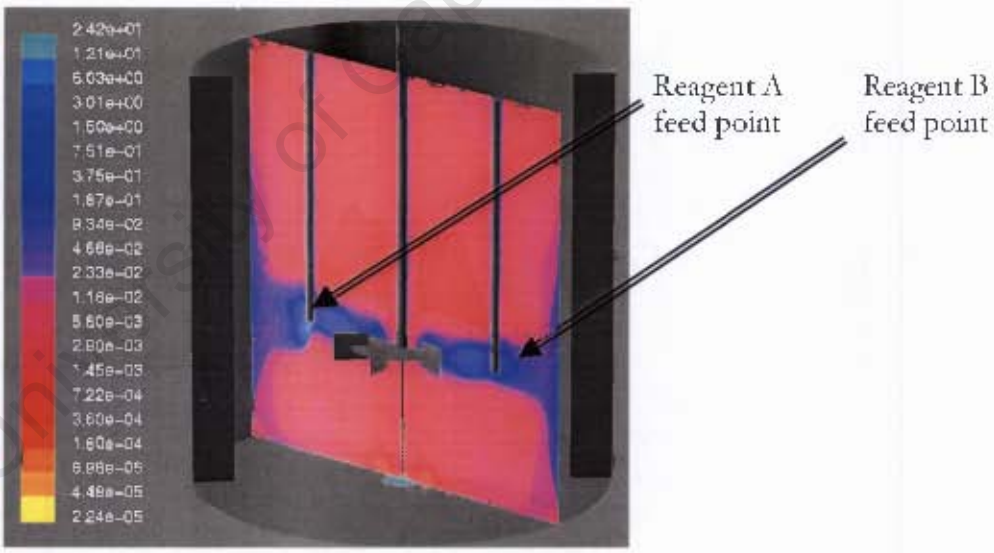

Figure 19: Showing the high turbulent dissipation in the vicinity of the impeller in a batch reactor. Three dimensional computational fluid dynamics (CFD) model using the k-ε model in FLUENT 6.1 (Fluent Inc., Lebanon, USA) (Vicum et al., 2004)

7.1.1 Varying pHi

The initial pH displayed on all graphs represents the pH of the starting $NiSO_4$ solution (200ppm Ni^{2+}).

pHi represents the pH of the sulphide precipitating agent added to the $NiSO_4$ solution. The sulphide solution pH values were adjusted such that predominantly one sulphide species was present at each pHi tested. The second dissociation constant which governs the pH at which HS^- equilibrates with S^{2-} or pK_2 is 17.4 (Midgisov et al., 2001), which is the most recent value reported. Thus, the major sulphide species present in the unadjusted sulphide solution (pH 11.95) was the bisulphide ion (HS^-). At pHi = 9.88, the same species was in the largest concentration (99.86% HS^-) within the sulphide solution. When pHi was adjusted to 4.24, the HS^- ion was no longer the prevalent sulphide species (HS^- = 0.24%) since pK_1 = 6.99 (Jackson, 1986) and therefore the $H_2S(aq)$ species was almost exclusively ($H_2S(aq)$ = 99.76%) present in solution.

For B01 (pHi = 11.95) and B02 (pHi = 9.88) ± 5ml of sulphide solution was added to the $NiSO_4$ to make up 750ml of reacting solution. When pHi was adjusted to a value of 4.24 (B03) with H_2SO_4, sulphide from the Na_2S solution was lost as $H_2S(g)$ and as a result approximately 60ml of sulphide reagent was required in order to achieve the desired molar ratio of Ni:S. The volume of the nickel sulphate solution was decreased accordingly, maintaining the same concentration (200ppm Ni^{2+}), so that the total volume of B03 remained at 750ml.

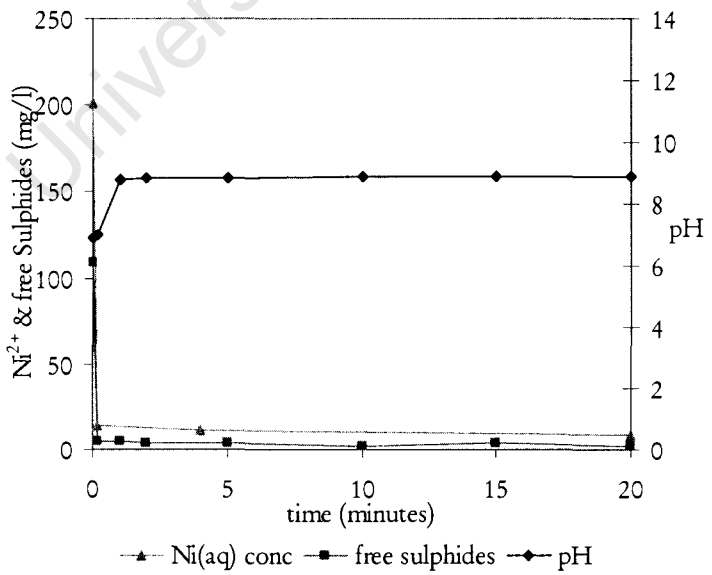

Figure 20: Nickel sulphide precipitation pHi = 11.59 (unadjusted) showing concentrations of nickel ions and free sulphides in solution and solution pH [B01]

The precipitation reaction occurred instantaneously, converting the nickel and sulphide ions into solid NiS precipitate. Figure 20 shows that after the first sample was taken at 10s, the nickel and sulphide present in the reacting solution were simultaneously depleted by 94%. These concentrations do not change after 10s which was expected since no further sulphide reagent was added. There was ± 11ppm of nickel remaining in solution was due to the formation of polysulphide ions. The expected final pH after complete precipitation was 7.04 which is the pH of the mother liquor (Na_2SO_4). The final pH after reaction was higher (pH 8.80) than the expected neutral final pH because H^+ ions were bound within polysulphide ion complexes such as $Ni(HS)^+$,$Ni(HS)_2$, $Ni2(HS)_{2+}$ or $Ni_3(HS)^{5+}$.

The pH increased between the 10s and 1 minute readings although no further reaction occurred, as shown by the approximately constant concentrations of Ni^{2+} and free sulphides after 10s. The pH at 10s (7.02) was similar to that of the initial $NiSO_4$ (200ppm Ni^{2+}) solution (pH = 6.88), and significantly lower than the readings taken after this time, which were all similar varying slightly between pH 8.80 – 8.91. Therefore, the pH reading taken after 10s was most likely inaccurate due to the reaction time of the probe. Thus, the pH increase shown as a result of mixing and reaction of the sulphide and nickel sulphate solutions was from pH 6.88 to pH 8.80.

The pH as a result of reaction (pH 8.80) was due to the speciation of sulphide (equation 7-1) and the precipitation of NiS generating H^+ ions (equation5-21);

$$Na_2S + H_2O \rightarrow 2Na^+ + HS^- + OH^- \qquad (7\text{-}1)$$

$$Ni^{2+} + HS^- \rightarrow NiS(s) + H^+ \qquad (5\text{-}21)$$

and the subsequent reaction of the liberated protons with OH^- ions present in the initial sulphide solution (pHi = 11.95). The ± 11ppm Ni^{2+} ions which remained in the reaction solution account for the relatively high pH post precipitation compared with B02 (final pH = 3.95) and B03 (final pH = 4.79). The unreacted Ni^{2+} represents unliberated H^+ ions (according to equation 5-21) which represent a significant pH change since the system is unbuffered. Using the formula for pH (pH = - log[H^+]) the protons liberated from the reaction of 11ppm of Ni^{2+} will result in the pH decreasing from 8.80 to a value of 6.62, which is comparable to the final pH values obtained from experiments B02 and B03 (to follow) in that it is slightly acidic.

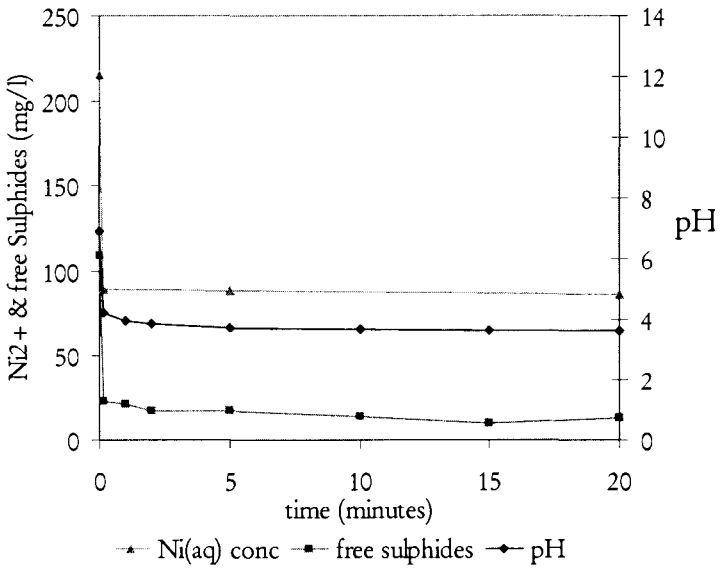

Figure 21: Nickel sulphide precipitation pHi = 9.88 showing concentrations of nickel ions and free sulphides in solution and solution pH [B02]

For run B02 (Figure 21), the initial concentration of OH ions in the sulphide solution was lower than the previous experiment (pHi = 11.95) since some acid was needed to reduce the pH to 9.88. Therefore, in this experiment (B02) there are fewer hydroxyl ions to neutralise the protons released from generation of NiS according to equation 7-1. Thus, the pH after reaction was more acidic for run B02. The pH decreased instantaneously as the reaction occurred. The pH value at 10s was neglected due to the time delay of the pH meter, thus the pH decrease was measured as 3.95 after 1 minute. The pH then remained acidic for the remainder of the run, decreasing from 3.95 to 3.63 with time.

When the pHi was lowered to 9.88 the initial sulphide species present in the sulphide solution was predominantly HS^- as in the previous experiment (B01), however, the nickel and sulphide concentrations in solution were not decreased to the same extent as when pHi = 11.95. The pH decrease to acidic values limited the reaction and thus total removal of nickel and sulphide was not possible. As protons were released by the precipitation reaction the sulphide speciation changed and $H_2S(aq)$ formed which does not appear to be able to react to form NiS. The nickel concentration decreased to 59% of the original 200ppm Ni^{2+} concentration indicating incomplete precipitation. The sulphide concentration in solution also decreased but this time by 78% due to the combined effects of reaction and the release of $H_2S(g)$. No further reaction occurred after the initial decrease in pH to an acidic value which was maintained for the duration of the run and thus the Ni^{2+} and sulphide concentrations remained at 88ppm and 24ppm, respectively. Jackson (1986) stated that in practice no precipitation of NiS is possible at

room temperature from a solution of pH3. Hammack et al (1993) state that the minimum pH at which precipitation of NiS occurs is 5.5 and that pH = 6.2 is the minimum pH necessary to lower the soluble metal concentration to below 0.1mg/L.

This suggests that no precipitation of nickel sulphide was possible with the $H_2S(aq)$ species. In order to test this, a further experiment was conducted in which the pHi was lowered to 4.24. The acidic pH value was chosen such that the sulphide species present was predominantly (99.76%) $H_2S(aq)$, based on pK_1 = 6.99 (Jackson, 1986), and was below the predicted pH at which NiS precipitation is possible according to Hammack (1993). The results of this experiment are shown in the Figure 22.

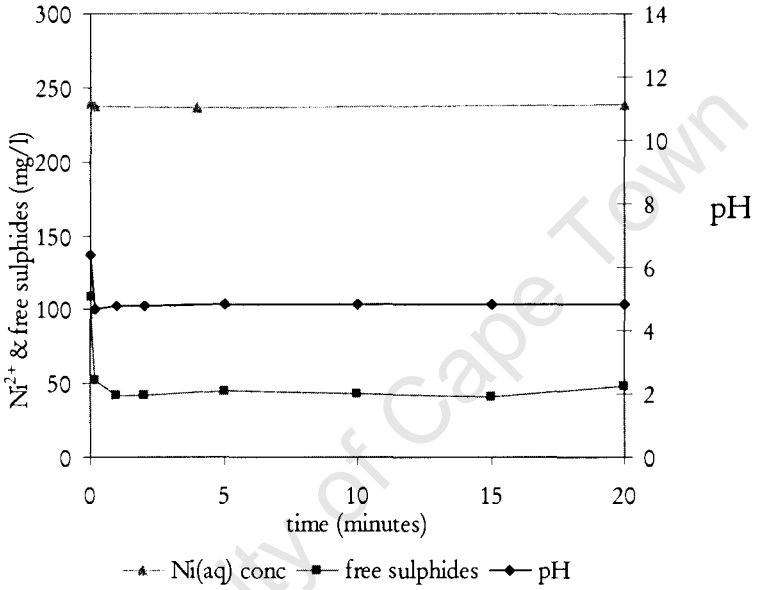

Figure 22: Nickel sulphide precipitation when pHi = 4.24 showing concentrations of nickel ions and free sulphides in solution and solution pH [B03]

The nickel ion concentration in solution remained constant throughout the run despite addition of sulphide reagent.

The pH measured after 1 minute was 4.79, and remained within the acidic region of the pH scale varying between pH values of 4.79 – 4.83. The decrease in pH from pH 6.41 – 4.79 was probably instantaneous and was caused by the mixing of the two reagent solutions since no significant precipitation of NiS occurred and negligible H^+ ions were generated.

The decrease in free sulphide concentration from 109 - 52mg/L was greater than the sulphide required for the formation of NiS since negligible reaction occurred. The addition of sulphide solution was accompanied the noticeable odour of $H_2S(g)$, and

therefore the majority of the sulphide added was lost to the environment as $H_2S(g)$ due to the acidic pH of the sulphide reagent and the combined reagent solutions. The agitation (330 rpm) of the reaction solution contributed significantly to the loss of sulphide.

The increase in pH of the sulphide solution from pHi = 4.24 to 4.79 upon addition to the $NiSO_4$ reagent solution was due to mixing of the sulphide solution at pH 4.24 and the NiSO4 solution at pH 6.41.

The low pH (< pH 5.5) prevented the reaction from occurring despite the presence of significant concentrations of free sulphide (52 mg/L) and nickel (220.1ppm) in solution since the $H_2S(aq)$ sulphide species that was present was unable to precipitate nickel. The pH of the reaction solution (pH = 4.79) is above the pH = 3 prediction of Jackson (1986) below which reaction of NiS cannot take place, but still the reaction did not occur.

The redox potential values are shown in Figure 23 below for the batch experiments varying the initial pH of the sulphide reagent.

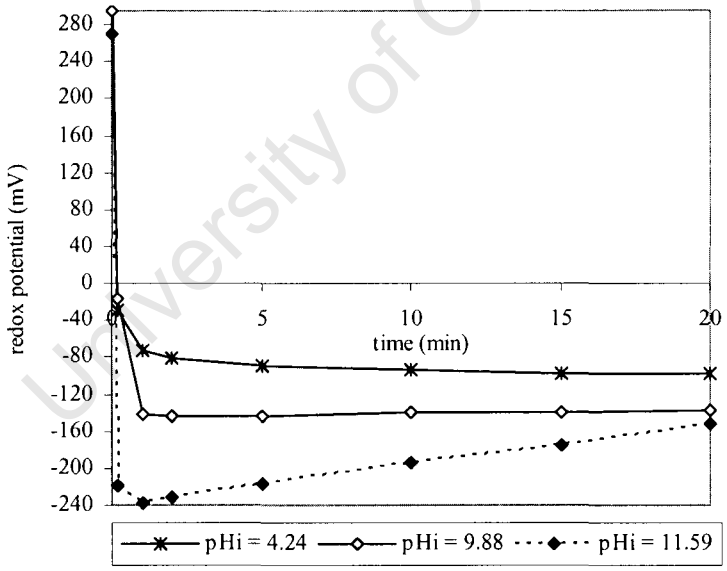

Figure 23: Redox potentials of batch experiments run varying the initial pH of the sulphide solution (B01, B02 and B03)

The oxidation of NiS precipitates was assumed negligible since the redox potentials were negative, indicating a reducing environment, for the duration of the batch experiments. The increasing redox potential for B03, where the pH of the sulphide solution was unadjusted, implies that oxidation occurred, but the negligible change in Ni^{2+}

concentration (Figure 20) indicates that this is insignificant for the NiS particle surfaces. Therefore, it can be assumed that the NiS precipitates do not oxidise and remain stable in the reducing environment which is maintained for the duration of the runs.

The following tables compare the experimental final pH values and percentage nickel removal to those modelled using OLI Stream System Analyzer 2.1.4 (November 2005). The experimental pH values after 1 minute were very similar to those taken after this time and thus were used for comparison. Similarly the nickel concentrations after 10s were used for comparative purposes. The final pH values experimentally determined were consistently lower than modelled pH values. The percentage nickel removal values were higher than those experimentally obtained, although the differences decreased with increased pHi. The modelled sulphide species available at each pHi tested (Appendix A) were similar to those experimentally determined except for the presence of the S^{2-} ion in the OLI modelled speciation at alkaline pH values due to the lower pK_2 value.

The OLI Stream System Analyzer 2.1.4 determined the pH and nickel concentrations at thermodynamic equilibrium using the initial experimental nickel and sulphide concentrations and sulphide solution pHi. The experimental results include the effect of kinetics on the precipitation reaction.

Experimentally, the pH decreased rapidly due to the release of protons from the NiS precipitation reaction (equation 5-21) for runs B02 (pHi = 9.88). The protons released were sufficient to consume OH^- ions introduced in the sulphide solution and present in the nickel sulphate reagent solution. When pHi was 11.95, the concentration of hydroxyl ions was much higher and the thus the hydrogen ions released do not decrease the pH to the extent exhibited by the other run.

Experimentally, at acidic pH values, i.e. below pH 5, the NiS precipitation reaction no longer occurred due to the predominance of the $H_2S(aq)$ species, as shown in previous batch experiments where pHi = 9.88 (B02) and 4.24 (B03). Therefore, no further protons were released because the reaction (equation 5-21) was halted by the deficiency of bisulphide ions, and the pH remained constant. At the acidic pH values there was a surplus of H^+ ions and thus no driving force to generate more HS^- ions since it would directly contribute to a stoichiometric increase in H^+ concentration.

The OLI model considered only the thermodynamic result and did not include the effect of kinetics on the reaction. Therefore, the final pH determined in OLI was much lower since infinite time was given to allow for the nickel to react with the small equilibrium concentrations of HS^- present in an acidic reacting environment. For example, at pH 4.79

there are 1.91×10^{-5} M HS^- ions present in solution. Thus, the nickel removal calculated from the OLI model were greater than the experimentally determined values (Table 10). The modelled final pH after reaction was lower than that experimentally obtained since the reaction occurred to a greater extent and thus more H^+ ions were generated decreasing the pH to below experimentally obtained values (Table 10).

Table 10: Comparison of experimental and OLI modelled percentage decrease in Ni^{2+} ions and pH after reaction for nickel sulphide precipitation reactions carried out at different pHi values

	Run	B01	B02	B03
	Initial pH	**pHi = 11.59**	**pHi = 9.88**	**pHi = 4.24**
Ni^{2+} removal	Experimental	93.1	42.8	7.3
	OLI model	100	74.9	48.4
Final pH	Experimental	8.80	4.07	4.70
	OLI model	7.21	2.93	2.64

7.2. Semi-batch results

The semi-batch experiments were all run with a synthetic $NiSO_4$ solution with a Ni^{2+} concentration of 200ppm.

pH measurements were taken from the reactor at the top, where samples were obtained to determine nickel and free sulphide concentrations in the solution, and side near the bottom, where the NaOH feed entered, and their comparison served as an indication of gradients in concentration that were present in the reacting solution. The minor differences in the pH values suggested that the solution was well-mixed and that the concentration differences of nickel ions and free sulphides were also negligible at the top and bottom of the reactor. Thus, a good approximation for the aqueous medium was that concentrations change with time and not with position in the reactor, similar to the continuously stirred tank reactor CSTR. However, the gaseous concentration of $H_2S(g)$ within the bubble decreased as the bubble travelled up the column as a result of diffusion of sulphide into solution. Thus, the gaseous flow through the reactor can be seen as plug flow, with the concentration changing with height in the reactor but not with time (Seader and Henley, 1998).

Figure 24 shows nickel and sulphide concentrations and pH changing with time during the run with no pH adjustment through alkalinity addition. It can be seen that when $H_2S(g)$ was bubbled through the nickel sulphate solution the pH dropped rapidly (within

1 minute) to an acidic value of 5.53 and then steadily continued decreasing from pH 5.02 – 4.00 between 2 and 30 minutes. At these acidic pH values the precipitation of nickel was negligible, with the nickel concentration decreasing by only 10ppm from 209.8 to 199.8ppm over the 30 minute duration of the experimental run. Jackson (1986) states that, kinetically, NiS precipitation at standard conditions does not occur below pH 3. Hammack et al (1993) state that the theoretical lower pH limit for precipitation of Ni^{2+} by gaseous sulphide is 5.8 and at pH 6.2 nickel can be removed to below 0.1ppm from solution. This supports data generated from the batch experiments (section 7.1) which indicates that $H_2S(aq)$ is unable to precipitate nickel.

The sulphide concentration increased rapidly between 0 and 6 minutes as the pH decreased from pH 7.43 – 4.62. After this, the sulphide concentration increased at a slower rate, approaching a saturation concentration at the constant pH = 4 attained in the solution. The abundance of protons present in solution at these acidic pH values prevented the speciation of the $H_2S(aq)$ into HS^- and thus NiS precipitation was not possible.

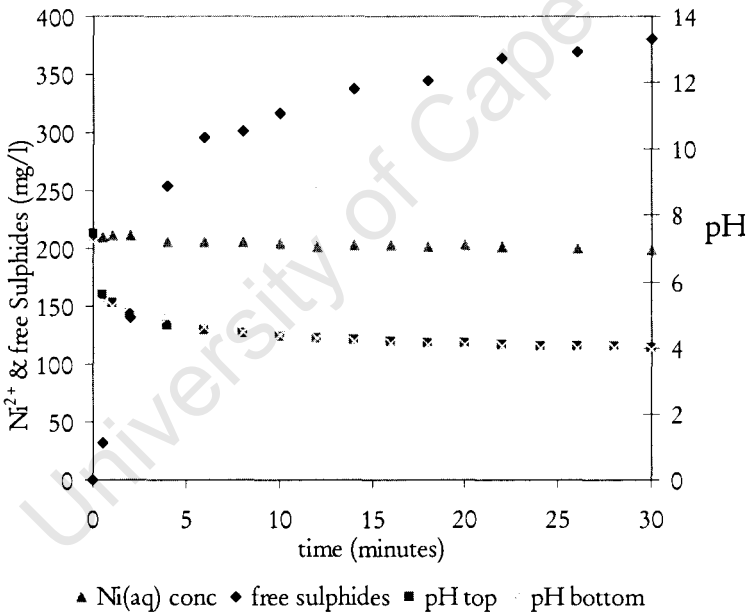

Figure 24: NiS precipitation in the semi-batch bubble column using $H_2S(g)$ (= 0.8L/min) with no addition of alkalinity [L06]

Therefore, in order to precipitate nickel from solution using $H_2S(g)$, the bisulphide ion must be made available. This was achieved by shifting the equilibrium speciation of $H_2S(aq)$ towards HS^- (equation 1-1) through manipulation of the pH.

$$H_2S \rightleftharpoons HS^- + H^+ \qquad pK_1 = 6.99 \text{ (Jackson, 1986)} \qquad (1\text{-}1)$$

Since the pH becomes acidic during reaction (Figure 24), an alkali source was added to facilitate the precipitation of NiS.

In most existing sulphide treatment systems, an alkaline agent such as lime is first added to raise the pH to between 6 and 8 after which the sulphide precipitating agent is introduced to the system (Hammack et al., 1994). Bhattacharyya (1981) investigated the combined effects of (a) sulphide-hydroxide precipitation and (b) sulphide followed by lime as precipitating agents. By the addition of lime or hydroxide ions (alkaline sources), pH manipulation was possible leading to the complete precipitation of all metals present, and further, selective precipitation of metals was possible at different pH values. Bryson and Bijsterveld (1991) utilised ammonium sulphide to precipitate manganese and cobalt, thus combining the alkali source with the sulphide precipitation agent. Esposito et al (2006) make use of independent addition of $NaHCO_3$ as well as sensitive sulphide control to precipitate ZnS using Na_2S and biogenic sulphide.

In this study, alkalinity, in the form of NaOH, was supplied to the reactor at a constant rate in order to promote the speciation of $H_2S(aq)$ towards HS^- (equation 1-1), and thus facilitate NiS precipitation. The alkali source was provided during, as opposed to prior to, the sulphide precipitation and independent of the sulphide source in order to harness the speciation of HS^- in a controlled manner. Therefore, the effect of various alkali feed rates on the rate of nickel removal, efficiency of sulphide usage and precipitate properties could be investigated.

7.2.1. Low alkalinity (NaOH) concentrations

Low NaOH concentrations were utilised to explore the effect of alkalinity addition on the precipitation process shown below in Figure 25. The relative error for experiment L05, representative of the error associated with the low alkalinity runs, is graphically shown in Appendix B.

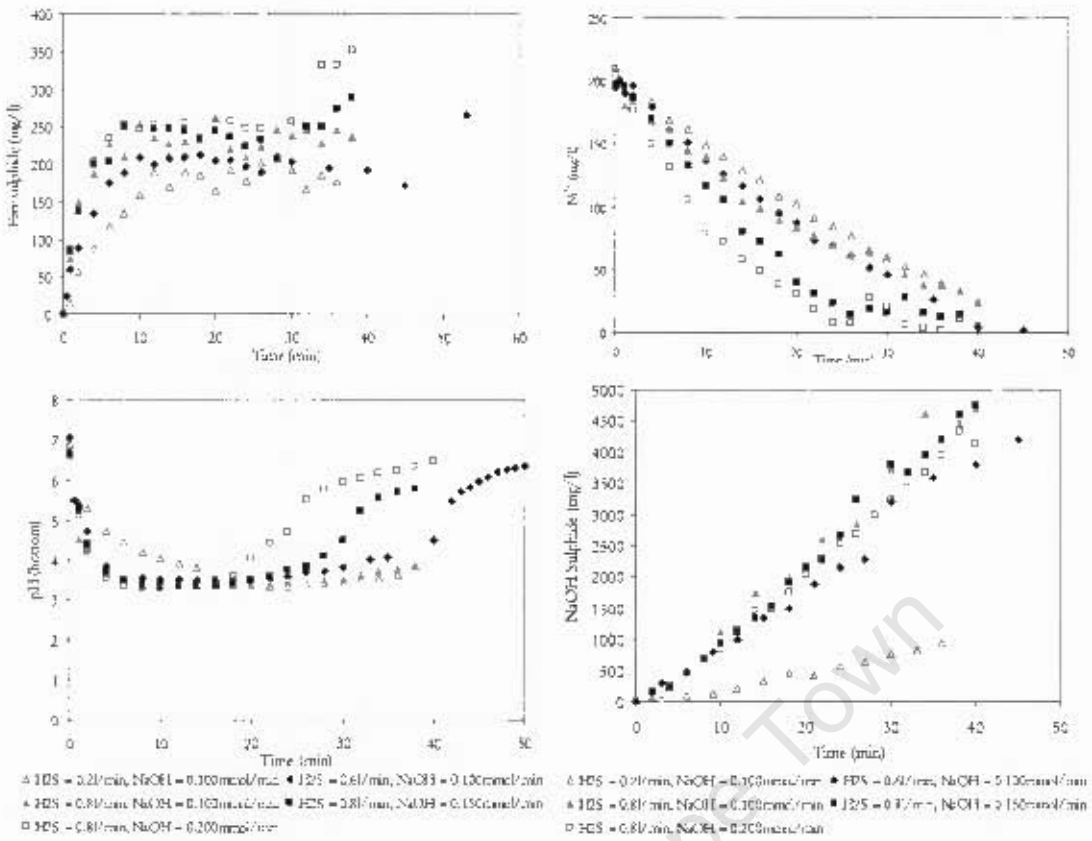

Figure 25: NiS precipitation using $H_2S(g)$ comparing low NaOH concentrations (0.100, 0.150 and 0.200mmol/min) used to facilitate reaction at different $H_2S(g)$ flowrates (0.2, 0.6 and 0.8L/min) [L01 – L05]

At the same NaOH concentration and varying $H_2S(g)$ flowrates (0.2; 0.6 and 0.8L/min) the rates of nickel removal from solution were very similar, and as the NaOH concentration increased (0.100; 0.150 and 0.200 mmol/min) the rates of nickel removal increased suggesting that the alkalinity is controlling the rate of precipitation. For the former set of experiments, where NaOH = 0.100mmol/min, 98.9% removal is achieved for $H_2S(g)$ = 0.6L/min which would be expected for $H_2S(g)$ = 0.2 and 0.8L/min at the same alkalinity rate.

However, complete removal of nickel from solution was not achieved for the runs $H_2S(g)$ = 0.8L/min and NaOH = 0.150 and 0.200 mmol/min. Figure 25 shows that after approximately 93% and 97% nickel removal at 24 and 26 minutes, respectively, the nickel concentrations in solution increased. The nickel concentrations peaked and then decreased, fluctuating, so that complete removal of nickel did not occur at the end of the run. The reintroduction of nickel into solution suggests that dissolution of precipitates occurred. The simultaneous, although slight, decreased sulphide concentration implies

that dissolution occurred by the formation of polysulphide complexes. However, the decreased sulphide concentrations were small compared to the concentrations present in solution since the sulphide flowrate was constant. The same phenomenon of redissolution of metal sulphide precipitates in the presence of excess sulphide was observed by van Hille et al (2005) when copper precipitation was carried out in a fluidised bed reactor using Na_2S. The concentration of free sulphides in solution decreased as the copper concentration increased, and, hence, removal of metal via sulphide precipitation was compromised.

The concentrations of sulphide in solution were very high during reaction, ranging between 150 – 275ppm as NaOH and $H_2S(g)$ flowrates increased, leading to wastage of sulphide reagent within the reaction solution. Associated disadvantages of excess sulphide within the mother liquor after precipitation include odour problems and recycling difficulties. Wastage of sulphide was also apparent in the large quantities of unabsorbed, unreacted sulphide present in the NaOH sulphide trap.

The sulphide concentrations increased rapidly and then remained constant, fluctuating slightly during nickel removal. A constant pH was maintained during reaction resulting from the equilibrium established between the rates of metal precipitation and NaOH addition. The sulphide concentration levelled off because the solution became saturated with $H_2S(aq)$ at the stable, acidic pH maintained during reaction, and thus no further sulphide accumulated in solution.

After the initial decrease in pH, the pH during the reaction was acidic pH (3.35 – 3.60). Around the region of the alkalinity entry point into the reactor local volume elements of higher pH occurred. However, since the rate of reaction was greater than the rate of macromixing, global acidic pH values were recorded and the pH values at the top and the bottom of the reactor were equivalent. When $H_2S(g)$ = 0.2L/min the decrease in pH was slower than for the higher $H_2S(g)$ flowrates since there were fewer protons generated by the precipitation reaction.

The constant acidic pH at which the reaction occurred allowed for only $H_2S(aq)$ species to persist in solution, with HS^- ions provided solely by the alkalinity supplied. The acidic pH shown was a global effect resulting from the instantaneous speciation of $H_2S(aq)$ to HS^- (equation 1-1), facilitated by the alkalinity, followed by the instantaneous reaction of Ni^{2+} and HS^- to form NiS, generating protons (equation 5-21) which reduced the pH. Thus, the alkalinity added to the reactor was insufficient to raise the pH above acidic values during reaction but did facilitate the reaction, by promoting speciation of a portion of sulphide to HS^-, which kept the pH acidic due to the generation of protons

from NiS precipitation. The alkalinity was used to neutralise the protons released by speciation and not those released during reaction. Jandová et al (2004) used slow, controlled addition of aqueous $(NH_4)_2S$ to enable efficient selective precipitation of copper at pH =1 and nickel and cobalt at pH = 3.0. Jandová et al (2004) supplied the bisulphide ions to the reactor and precipitation was faster than speciation of bisulphide into $H_2S(aq)$ which would have occurred since the reaction solution had an acidic pH. In this study, as described above, the sulphide was speciated to HS^- within the reactor due to addition of NaOH and not supplied as bisulphide ions as with Jandová et al. (2004).

An increased sulphide concentration was noted after nickel sulphide precipitation was complete, despite the dissolution of precipitates. The sulphide concentration in solution increased as a result of the increasing pH due to speciation of $H_2S(aq)$ to HS^- (equation 1-1). Thus, further sulphide accumulated in solution as the HS^- species since during reaction the solution was already saturated with $H_2S(aq)$.

7.2.2 Varying the Ni:S molar ratio

The following experimental results show the effect of varying the ratio of the nickel to sulphide ion concentrations, demonstrating the dissolution of NiS precipitates when excess sulphide ion was present in solution at neutral to alkaline pH values. Synthetic $NiSO_4$ solution was used with a concentration of 200ppm Ni^{2+} (Figure 26). The proposed mechanism for dissolution is the formation of aqueous polysulphide ions complexed to the NiS precipitate molecules. Luther et al (1996) reported on stable polysulphide complexes of various heavy metals including nickel. The proposed complexes of nickel are $NiS(HS)_3^{3-}$, $NiS(HS)_2^{2-}$ and $NiS(HS)_2^{2-}$ analogous to those of copper ($CuS(HS)_3^{3-}$ $CuS(HS)_2^{2-}$ $CuS(HS)^-$) and it follows that the mechanisms would then also be similar (Shea and Helz, 1988). The existence of these nickel polysulphide complexes has not been confirmed by molecular experimental data since species such as $MS(HS)_3^{3-}$ is indistinguishable from M_4S_6. The latter structure has been experimentally confirmed. The reaction stoichiometry suggests this type of complex may be forming, for which Ni_4S_6 may be a maturation product (Luther et al, 1996).

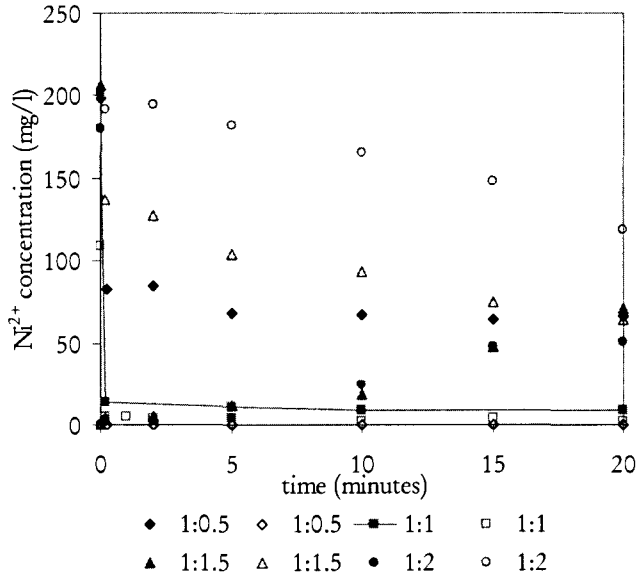

Figure 26: Nickel and sulphide concentrations (mg/L) for batch precipitation of nickel from $NiSO_4$ using Na_2S using varying ratios of Ni:S [B04, B01, B05 and B06] closed symbols = nickel, open symbols = sulphide

Table 11: pH after batch precipitation of nickel from $NiSO_4$ using Na_2S for various ratios of Ni:S

Run	Ratio Ni:S	Initial Ni^{2+} (ppm)	pH after reaction
B04	1:0.5	198.2	8.27 ± 0.02
B01	1:1.0	201.1	8.86 ± 0.05
B05	1:1.5	206.7	11.23 ± 0.05
B06	1:20	179.5	11.47 ± 0.04

When Ni:S = 1:1 (B01), the sulphide and nickel concentrations in solution were completely depleted owing to the formation of NiS precipitate. When the Ni:S was 1:0.5 (B04) the sulphide concentration was completely depleted upon reaction but nickel ions remained in solution because there was insufficient sulphide to precipitate the nickel ions completely. The final pH values obtained after reaction for experiments where NiS = 1:0.5 and 1:1 were approximately 8.27 and 8.86, respectively.

When the ratio of Ni:S was increased to 1:1.5 (B05) and 1:2 (B06), the sulphide concentrations were initially depleted to the stoichiometric requirement for the reacted nickel, but then, as the runs progressed, continued decreasing although no further reagents were added to the solutions. Initially, the nickel ions in solution for both regent ratios were completely precipitated as NiS and thus were no longer present in solution.

However, as the runs continued the nickel concentrations increased steadily up to 71 and 51 mg/L at 20 minutes for Ni:S = 1:1.5 and 1:2, respectively. This is equivalent to 34% and 28% of the initial nickel solution. The pH values for these runs were 11.23 and 11.47 for Ni:S = 1:1.5 and 1:2, respectively, which are more alkaline values than Ni:S = 0.5:1 (B04) and 1:1 (B01).

During runs B05 (Ni:S = 1:1.5) and B06 (Ni:S = 1:2) the nickel ions in solution increased while the sulphide ions in solution decreased with time. This evidence suggests that when there is excess bisulphide in solution there is dissolution of nickel sulphide precipitates by the formation of polysulphide complexes. The semi-batch data shows that $H_2S(aq)$ can be present at a concentration of 200ppm without affecting the stability of the NiS precipitate ie it will not dissolve in $H_2S(aq)$. The pH values of these solutions after reaction were above pH 7 and thus the formation of stable nickel polysulphide complexes with the bisulphide ion was possible (Luther et al., 1996).

Empirical evidence is supplied in Figure 27 and Figure 28, which show the filtrate after the reaction solution was filtered through a 0.22μm filter. The opacity of the filtrate increased with increasing time during the run for both B05 (Ni:S = 1:1.5) and B06 (Ni:S = 1:2), thus indicating that particle sizes decreased to at least below 0.22μm as the run progressed. The increase in filtrate opacity during the run also suggests that the polysulphide ions formed were black. The initial $NiSO_4$ synthetic solution before sulphide addition is represented by sample i.

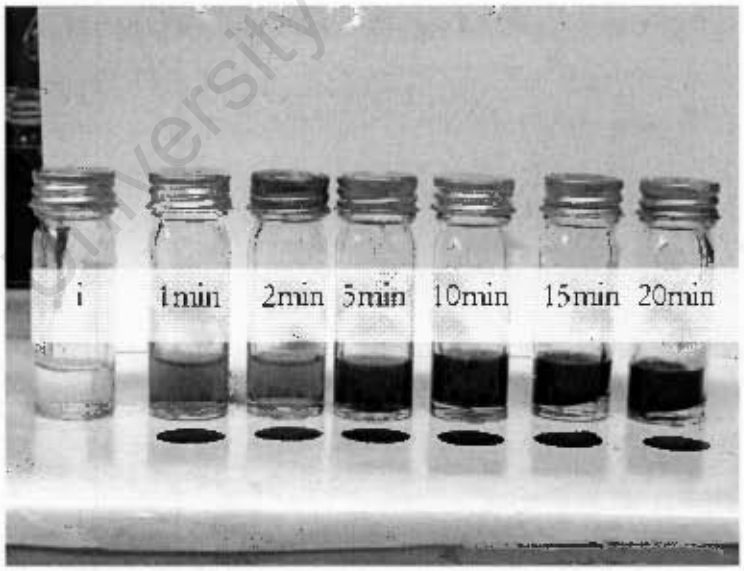

Figure 27: Ni:S = 1:1.5 [B05] showing the increasing filtrate opacity with time after initial addition of reagents

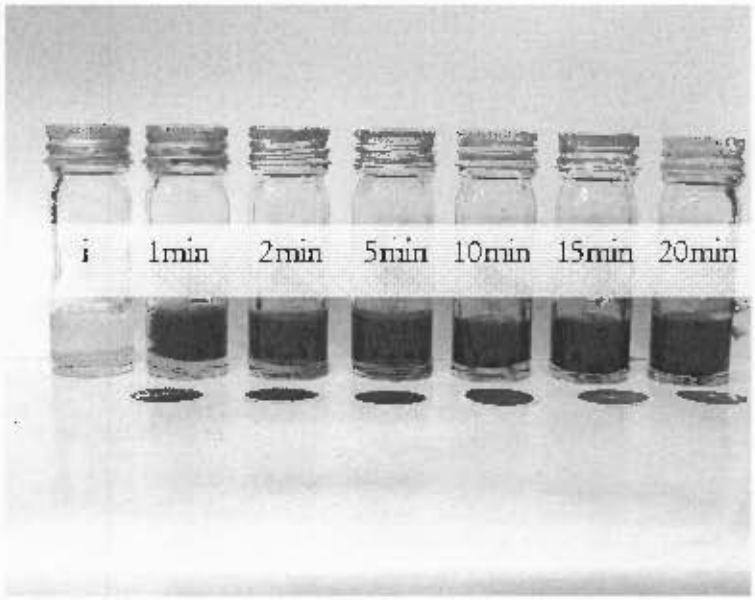

Figure 28: Ni:S = 1:2 [B06] showing the increasing filtrate opacity with time after initial addition of reagents

Metal sulphides usually form negatively charged lyophobic colloids (the charge on the dispersion is constant), termed sols (Jackson, 1986). Figure 29 shows settlability data of NiS precipitates formed as soon as possible after mixing (minimal contact time between the nickel and sulphide reagents). No settling was apparent for Ni:S = 1:1.5 (B05) and 1:2 (B06) up to 8 hours after 20 minutes of mixing. It may be that settling of a portion of the precipitates occurred before this time, but this could not be observed due to the opacity of the solution. Complete settling was visible after approximately 1 week. Thus, the presence of excess sulphides increased the settling time when the mixing time of the two reagents was long. When the sulphide was supplied in excess (B05 and B06), the supersaturation of the system increased resulting in the formation of precipitates of smaller sizes (Söhnel and Garside, 1992). As the contact time of sulphide and nickel reagents increased the precipitate sizes decreased further due to dissolution of precipitates and thus settling time was increased.

When the ratio of Ni:S was 1:1 (B01) settling occurred after ± 3 days, despite the short (30s) contact time and even though no dissolution of precipitates occurred, indicated by the relatively low, constant concentrations of nickel and sulphide after initial precipitation (Figure 26). Therefore, the colloidal suspension was stable, resisting flocculation thus indicating that the zeta potential of the precipitates was not close to the isoelectric point (Vergouw et al., 1998). It is unclear as to why precipitates formed when Ni:S = 1:1 do not settle well, even after a short agitation time.

When the ratio of Ni:S was not stoichiometric (Ni:S = 1:0.5 (B04) 1:1.5 (B05) and 1:2 (B06)) and mixing time was minimised (approximately 30s) the settling was complete after 6 minutes with very similar settling trends exhibited by all three runs. Settling occurred via the formation of flocculates, indicating that the zeta potential of the precipitates was close to zero (Vergouw et al., 1998). Flocculate formation was followed by rapid clearing of the Imhoff settling column. Flocculates were larger as the excess sulphide in solution decreased. Initial zeta potential measurements of precipitates formed in the above batch tests after a short contact time between Ni and S reagents are shown below in
Table 12.

Table 12: Initial Zeta potential values of precipitates formed with varying molar ratios of Ni:S (B01, B04 – B06)

Experiment	Ni:S Molar Ratio	Initial Zeta potential (mV)
B04	1:0.5	-9.47
B01	1:1	-38.9
B05	1:1.5	-39.5
B06	1:2	-40.3

These values provide no conclusive information linking the initial Zeta potential values to the settling trends shown or to flocculate formation.

The settling of B04 decreased to a lower value because the settled volume was smaller as there were fewer precipitates formed compared to the other runs. Thus, the presence of excess or limiting sulphides and the resulting increased or decreased supersaturation, respectively, did not adversely affect settling due to the formation of flocculates provided the contact time of the sulphide and nickel reagents is short (Milligan, 1995).

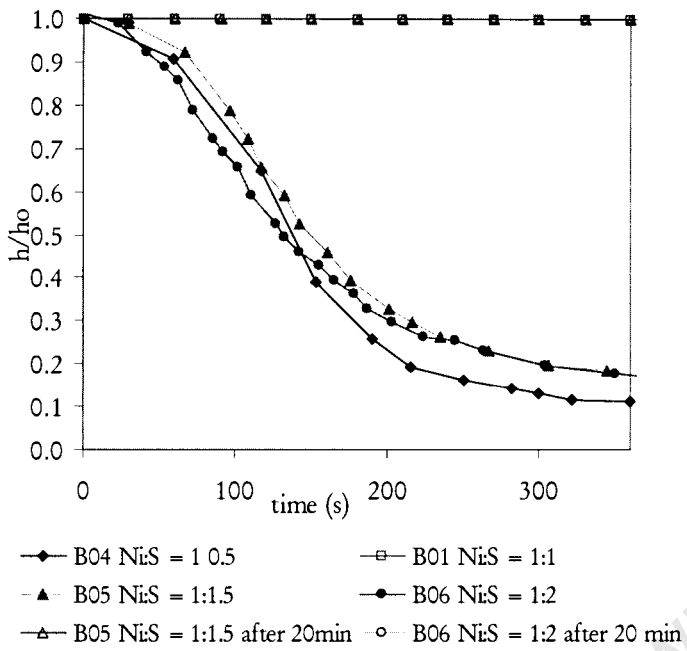

Figure 29: Settling data for the precipitation of NiS using from synthetic $NiSO_4$ (200ppm Ni^{2+}) Na_2S for various ratios of Ni:S

The following figure (Figure 30) shows the supersaturations based on initial global concentrations for each of the batch experiments run varying pHi and Ni:S molar ratio. Supersaturations were calculated using the HS^- ion concentrations as opposed to the total free sulphide concentrations in solution, based on the inability of $H_2S(aq)$ to precipitate nickel and the high pK_2 (17.4, Midgisov et al., 2001) value limiting the S^{2-} available for reaction for the extent of the real pH scale. Supersaturations were very similar for all experiments except when pHi = 4.24 (B03) because there was a negligible concentration of HS^- in the acidic sulphide solution compared to the alkaline ones.

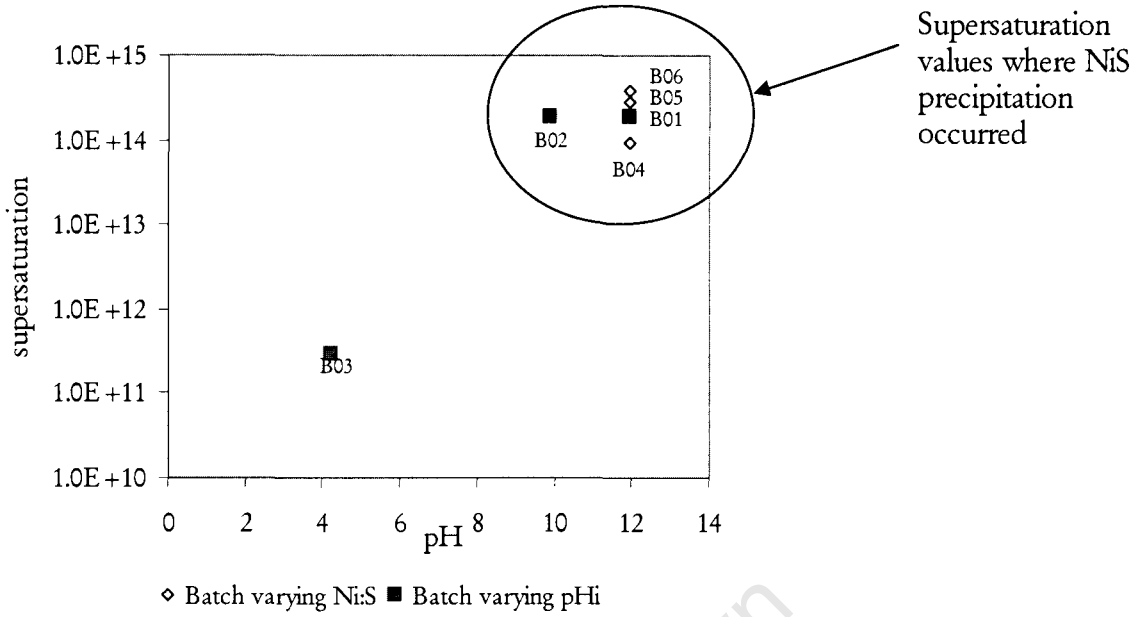

Figure 30: Supersaturations based on initial global concentrations for batch nickel precipitation experiments using Na_2S varying the initial pH (pHi) of the sulphide solution [B01, B02, B03] and varying the ratio of Ni:S [B04, B05, B06]

Despite the similarity in supersaturation values for all batch experiments where NiS precipitation occurred (Figure 30), the settling of precipitates formed from a stoichiometric molar ratio of Ni:S (B01) occurred much more slowly compared to the other molar ratios. Thus, the settling times and supersaturations, based on initial global concentrations, do not have an apparent connection. Higher supersaturations produce smaller particles because nucleation is the dominant particle rate process (Söhnel and Garside, 1992). Therefore, experiments generating lower supersaturations should produce larger particles which should theoretically settle faster than experiments with higher supersaturations, because the settling velocity of smaller particles is slower due to their decreased weight (equation 3-7). Although the supersaturations generated in the gaseous system were much lower (10^5 – 10^6) than those of the batch system (10^{12} – 10^{13}), the primary nucleation was still the dominant particle forming mechanism and therefore particle sizes generated remained too small to facilitate efficient settling for precipitates formed after an extended contact time between reagents. However, when contact time of the two reagents was minimised flocculation occurred and, as stated by Milligan (1995), flocculation produces high sediment flux of small particles which cannot be explained by simple Stokes' settling of single grains (equation 3-7). When the contact time of nickel and sulphide reagents was increased, flocculation was no longer apparent and thus Stoke's Law could be applied (equation 3-7). However, in this case, smaller particles and the presence of polysulphide species in solution increased solution opacity and thus hampered visibility and settling of larger particles, if any, could not be seen.

Due to the flocculation of precipitate particles immediately after mixing, settling data cannot be used to correlate the effects of supersaturation on particle size with varying Ni:S ratios. For increased contact time of the two reagents, flocculation did not occur and settling of larger precipitate particles was not observed due to the opacity imparted by the smaller particles in suspension and the polysulphide ions, the concentrations of which increased as dissolution of precipitates occurred. Therefore, settling was ineffective for rapid and efficient post precipitation phase separation.

7.2.3. High alkalinity (NaOH) flowrates

A series of experiments were performed as previously described, but with rates of alkali addition an order of magnitude greater. In all cases tested complete nickel removal was achieved in a relatively short time (Appendix C). The times taken for complete reaction for each of the flowrates of alkalinity and $H_2S(g)$ tested are shown below. The relative error for experiment T05, representative of the error associated with the high alkalinity runs, is graphically shown in Appendix B. Appendix C displays the actual values shown in Figure 31 in a tabular form.

Table 13: Time taken for complete reaction for experiments run with high alkalinity input at various $H_2S(g)$ flowrates

Run	NaOH	$H_2S(g)^{mix}$ [10% $H_2S(g)$; 90%N_2]	$[H_2S(g)]$	$[Ni^{2+}]$	Time for complete reaction
	(mmol/min)	(L/min)	(mmol/min)	(mg/l)	(minutes)
T01	2.23	0.8	3.57	215.5	2.5
T02	2.23	0.5	2.23	217.4	2.5
T03	2.23	0.3	1.34	210.5	2.5
T04	2.23	0.1	0.446	208.9	2.5
T05	1.75	0.8	3.57	182.6	3.5
T06	1.75	0.5	2.23	183.2	3.5
T07	1.75	0.3	1.34	217.0	3.5
T08	1.75	0.1	0.446	199.7	3.5
T09	1.20	0.3	1.34	197.7	4.5
T10	1.20	0.2	0.893	217.4	4.5
T11	1.20	0.1	0.446	217.1	4.5

The rates of nickel removal were found to be directly related to alkalinity.

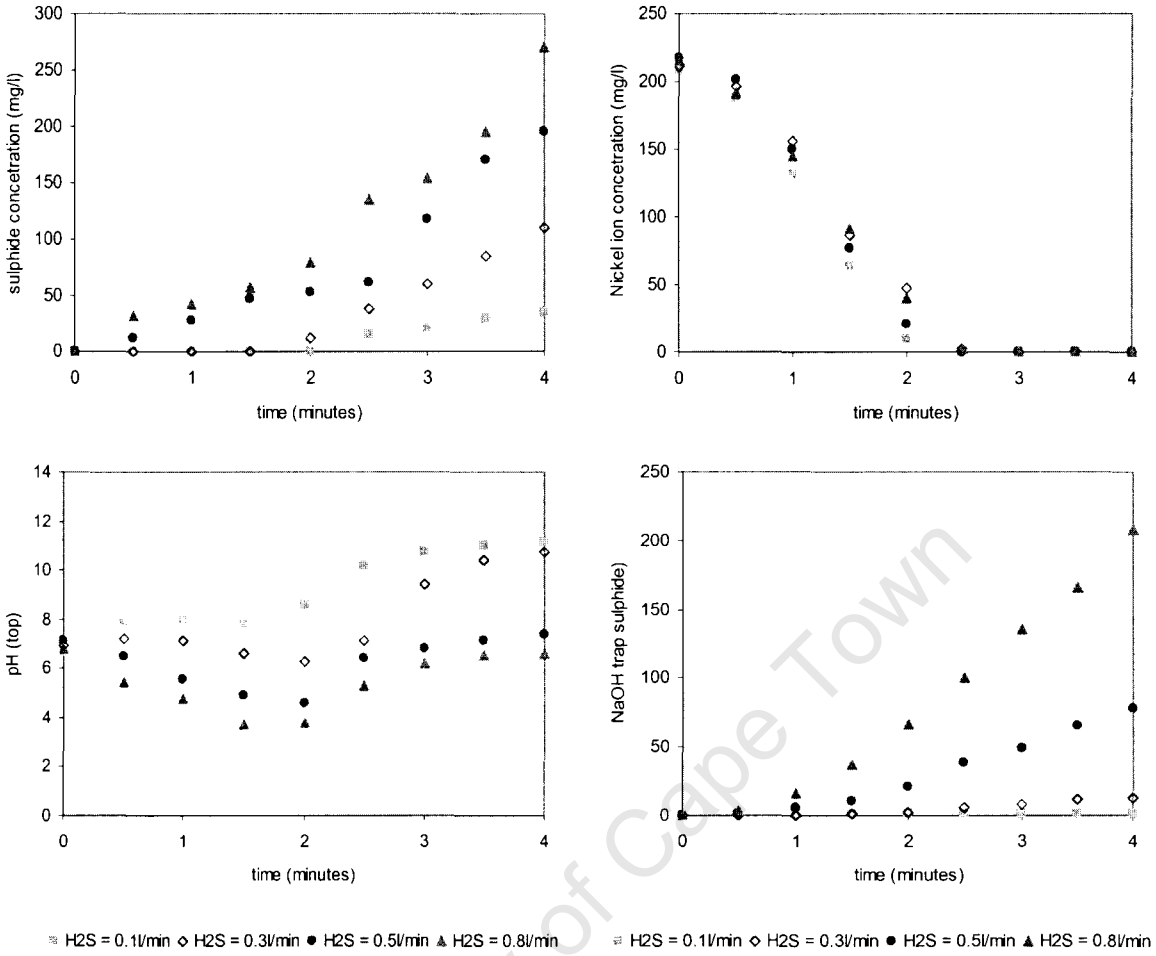

Figure 31: NiS precipitation using $H_2S(g)$ comparing different $H_2S(g)$ flowrates (0.1, 0.3, 0.5 and 0.8L/min) when NaOH = 2.23mmol/min [T01 – T04]

As seen in Figure 31, when NaOH = 2.23mmol/min, the nickel was completely removed after 2.5 minutes regardless of the $H_2S(g)$ flowrate supplied, which varied between 0.8 – 0.1L/min. Thus indicating that the rate at which the alkalinity was supplied controlled the rate of nickel sulphide precipitation. The combined effects of the nickel sulphide precipitation releasing protons and the alkaline effect of the NaOH supplied to the reactor were the same since the rates of alkaline added and NiS precipitation were the same for runs T01 – T04. The pH measured was the result of the speciation of the sulphide. At higher $H_2S(g)$ flowrates more sulphide diffused into solution and speciated releasing protons into solution, thus lowering the pH. Thus, the pH values range between acidic and alkaline values for the range of alkalinity flowrates tested.

The sulphide concentrations in solution increased with increasing $H_2S(g)$ flowrate and with increasing run time, since the $H_2S(g)$ input rate was constant throughout the run. When the $H_2S(g)$ flowrates were low i.e. $H_2S(g)$ = 0.1 and 0.3L/min, there was no

sulphide present in solution during the time taken for the nickel concentration in solution to be completely depleted. However, the rate of sulphide availability in solution did not limit the rate of the reaction since the time taken for complete removal remained at 2.5 minutes, as with all other $H_2S(g)$ flowrates tested. At low sulphide flowrates ($H_2S(g)$ = 0.1 and 0.3L/min), there was no detectable sulphide in solution and negligible sulphide in the NaOH sulphide trap. Since the flowrate of $H_2S(g)$ T04 (0.1L/min) was 3 times smaller than that of T03 (0.3L/min), and the rates of nickel removal were the same for T04 and T03 nickel hydroxide precipitation could have occurred in the former run. The alkalinity converted the sulphide in the reactor solution into HS^- upon entering the aqueous phase owing to the neutral and slightly basic pH values caused by the alkalinity addition and thus nickel sulphide precipitation occurred to an extent. However, since the rate of NaOH addition (2.23mmol/min) was greater than the rate of sulphide addition ($H_2S(g)$ = 0.1L/min), nickel hydroxide precipitation occurred to larger extent (T04).

When the $H_2S(g)$ flowrates were increased to 0.5 and 0.8L/min, there was sulphide present in solution throughout the run including during the reaction, which occurred simultaneously for the first two minutes. The rate at which sulphide was consumed by the nickel sulphide precipitation reaction was slower than the rate of sulphide addition because the alkalinity supplied was not sufficient to raise the pH sufficiently during reaction and thus did not provide HS^- ions at a rate comparable to that of the intrinsic reaction rate. The acidic pH values resulting from these higher flowrates indicated that the sulphide in solution was present as $H_2S(aq)$ species and, hence, was unable to contribute to the removal of nickel from solution.

A small portion of $H_2S(aq)$ dissociates to HS^- and H^+. The concentration is not sufficient to significantly enhance the reaction rate, but the H^+ ions are sufficient to lower the pH in an unbuffered system. The partial dissociation of the weak acid causes the low pH.

After the reaction was completed the pH increased, since the reaction no longer generated protons due to NiS precipitation because all the nickel was depleted. During reaction two H^+ ions were released for each NiS precipitate molecule formed. The addition of OH^- ions neutralised protons and encouraged formation of HS^- by driving the speciation to the right

$$H_2S \rightleftharpoons HS^- + H^+ \qquad pK_1 = 6.99 \text{ (Jackson, 1986)} \qquad (1\text{-}1)$$

Once all the nickel had reacted only one H^+ ion was released for each H_2S dissolved in solution due to speciation of $H_2S(aq)$ to HS^-, and some $H_2S(aq)$ remained. As a result the pH increased as not all the OH^- ions were neutralised by H^+ liberated as H_2S dissolves.

As the pH increased more H_2S dissociates so more H^+ were released and thus there was a decrease in the rate of pH increase. The increasing sulphide concentrations indicated that the sulphide in solution had not reached the saturation concentration for the pH displayed on the graphs. After the reaction was complete the pH stabilised because the rates of alkalinity and sulphide supplied remained constant and equilibrated. As the pH stabilised and the solution was saturated with $H_2S(aq)$, the sulphide concentration in solution increased linearly at the rate of HS^- formation.

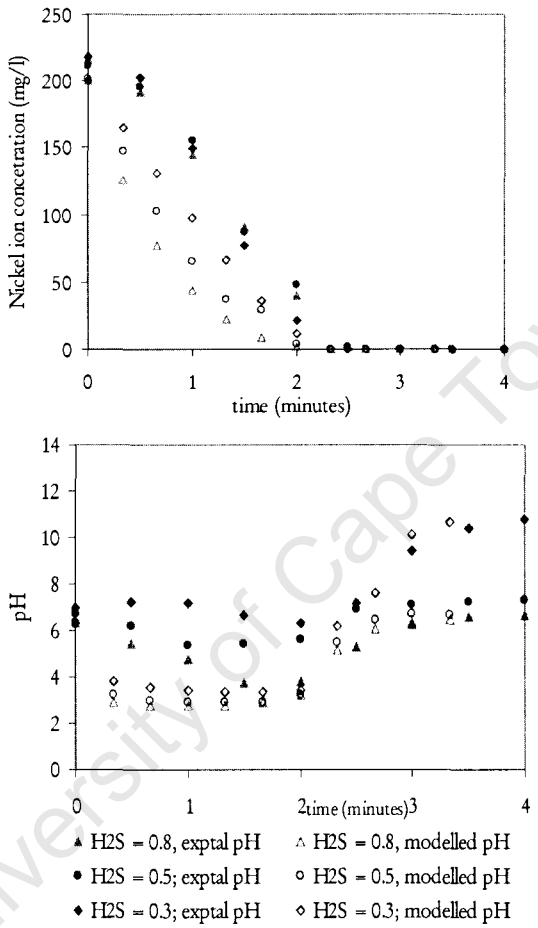

Figure 32: Nickel Precipitation with $H_2S(g)$: nickel removal and pH with time NaOH = 2.23mmol/min; $H_2S(g)$ = 0.3; 0.5; 0.8l/min [T01 – T03]

Figure 32 compares the experimental and modelled nickel concentrations and pH values with time for NaOH = 2.23mmol/min and $H_2S(g)$ = 0.8, 0.5, 0.3 and 0.1L/min. These graphs were constructed using the concentrations of NaOH and $H_2S(g)$ available for reaction after every 20s for the first 3.3 minutes of the reaction, based on their respective flowrates, and the entire Ni^{2+} concentration (200ppm). Each 20s time interval was thermodynamically modelled in OLI as a separate batch experiment, in combination resulting in a pseudo-kinetic model of the semi-batch experiment (please see Appendix C for values).

The pseudo-kinetic OLI model showed that the rate of nickel concentration derease decreased as the $H_2S(g)$ flowrate increased from 0.3L/min – 0.8L/min. During the modelled reaction there was no sulphide present in the reacting solution because the entire amount of sulphide input at the specific time (based on experimental flowrates of alkalinity and sulphide reagent) reacted with the nickel present in solution. As stated previously, the OLI model only considers the thermodynamic result whereas the experimental values include the kinetic effects.

Kinetically, not all the sulphide in the reactor at a specific time reacted because the sulphide species available were not able to precipitate nickel [ie $H_2S(aq)$]. However, the OLI model allows the nickel present at time, t, to react with all the sulphide present in solution, since, given infinite time the probability of the presence of enough reactive sulphide species (HS$^-$) allows for the complete reaction of the entire concentration of the sulphide reagent at that time. This is a deficiency in using thermodynamic models for non-equilibrium systems.

Thus, the time taken for complete nickel ion depletion takes 2 minutes at $H_2S(g)$ = 0.8L/min and 2.33min and 2.67min for $H_2S(g)$ = 0.5 and 0.3L/min, respectively, which is significantly different to the experimentally determined constant linear decrease in nickel ion concentration with complete reaction after 2.5minutes for all $H_2S(g)$ flowrates tested. The modelled pH values were lower as $H_2S(g)$ flowrates increased from 0.3L/min to 0.8L/min, which is the same trend as shown experimentally. However, the pH values are much lower, but this is expected because the rates of nickel precipitation were faster and there is no excess, unreacted sulphide present in solution in the modelled reaction. In contrast, the modelled pH values and nickel concentrations are very similar for $H_2S(g)$ = 0.1L/min. However, the nickel removal, and thus the pH change, was due to nickel hydroxide as well as nickel sulphide precipitation. Thus, when $H_2S(g)$ is limiting and the pH is sufficiently high nickel hydroxide precipitation takes place.

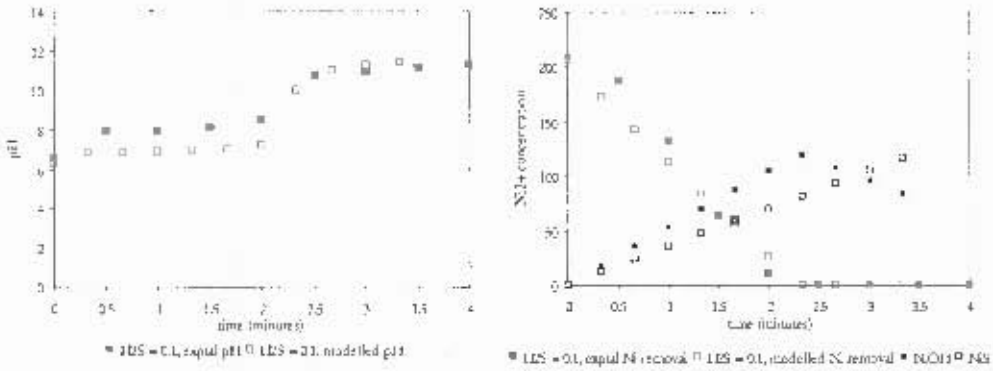

Figure 33: Pseudo-kinetic modelling of nickel precipitation from synthetic $NiSO_4$ when $H_2S(g)$ = 0.1L/min NaOH = 2.23mmol/min [TC4]

Figure 34 shows the precipitation of nickel using only NaOH at a flowrate of 1.20mmol/min for the first 4.5 minutes of the run. At 4.5 minutes $H_2S(g)$ at a flowrate of 0.3L/min was supplied to the reactor. Unfiltered samples were taken periodically to which 0.5ml of HCl and HNO_3 each were added. The samples were then filtered and sent to AAS to determine Ni^{2+} concentration. It was found that NiS precipitates do not dissolve on addition of acid. Therefore the addition of acid dissolved any nickel hydroxide precipitate formed but not nickel sulphide, and so the nickel precipitated as sulphide was able to be determined. It was found that although NiS precipitation does not occur at acidic pH values due to their high solubility values (Figure 10) dissolution of NiS precipitates did not occur upon addition of acid. Nickel hydroxide was displaced by nickel sulphide when $H_2S(g)$ was supplied after 4.5 minutes as seen in the figure, although the displacement precipitation process was slower than the precipitation of nickel by hydroxide (Figure 33) or sulphide (Figure 31). Thus, nickel sulphide preferentially precipitated over nickel hydroxide even at alkaline pH values when sulphide was not limiting.

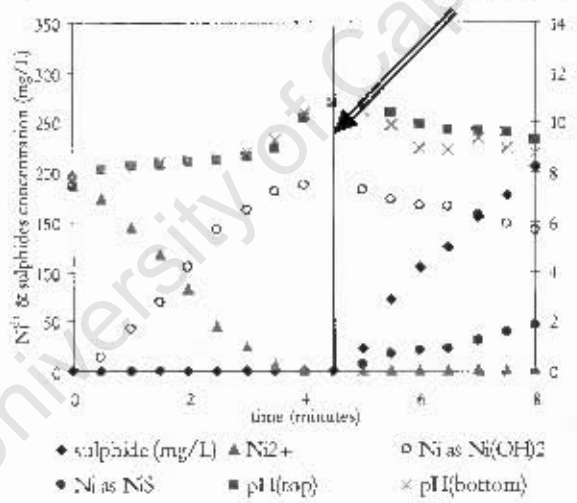

Figure 34: The precipitation of Ni using only NaOH = 1.20mmol/min for 0 - 4.5 minutes and $H_2S(g)$ = 0.3L/min for 4.5 – 8 minutes

Figure 35 below compares the effects of three different alkalinity flowrates (NaOH – 1.20, 1.75 and 2.23mmol/min) at the same $H_2S(g)$ flowrate (0.3L/min). Thus, when the alkalinity flowrate was lower, the pH was lower and there was a greater concentration of sulphide in solution present as the unreactive $H_2S(aq)$. When the rate of alkalinity provided was sufficient to convert the incoming sulphide to the reactive HS^-, then there

was no aqueous sulphide present during reaction. This represents efficient use of the added sulphide.

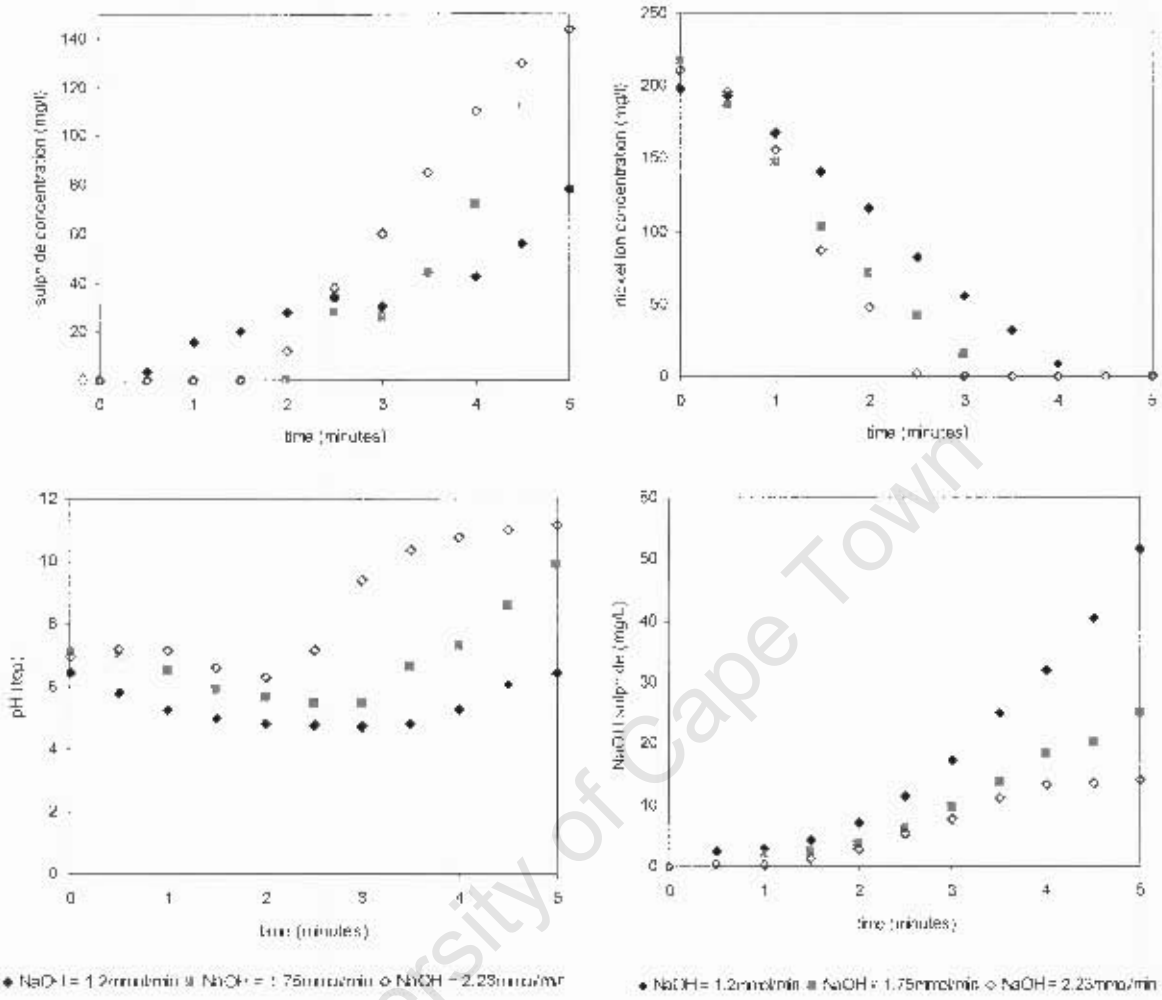

Figure 35: Semi-batch precipitation of nickel using $H_2S(g)$ = 0.3L/min and NaOH = 1.20, 1.75 and 2.23mmol/min [T03, T07 and T09]

The following diagram (Figure 36) shows the threshold above which excess sulphide was present in solution during reaction leading to sulphide reagent wastage and thus process inefficiency. The threshold is the boundary below which the rate at which NaOH enters solution was sufficient to shift the speciation to the formation of HS at a rate comparable to the entering $H_2S(g)$ flowrate. The threshold at which $H_2S(g)$ dissolution becomes apparent is significant for purposes of process optimization. Above this threshold there is significant reagent wastage, either accumulating in the reacting solution or lost as unabsorbed $H_2S(g)$ to be collected in the NaOH trap.

For the experiments where $H_2S(g)$ = 0.1L/min and NaOH = 1.20; 1.75; 2.23mmol/min and $H_2S(g)$ = 0.3L/min and NaOH = 1.75 and 2.23 mmol/min, no sulphide was present

in solution during reaction and therefore these points lie below the sulphide usage efficiency threshold. The other experiments showed significant unused sulphide in solution during reaction and are therefore points which lie above the threshold. A possibility of operating below the sulphide usage efficiency threshold is that when sulphide is limiting, $Ni(OH)_2$ precipitation may occur ($K_{SP,Ni(OH)2} = 10^{-10.4}$) (Jackson, 1983).

The threshold ratio of $H_2S(g)$ to NaOH above which excess sulphide was present in solution, thus inefficient utilisation of sulphide cations, during reaction is 1: 1.664 for the range of $H_2S(g)$ and NaOH flowrates tested. A theoretical boundary was calculated using the stoichiometry of the reaction to confirm the experimentally determined threshold. For a known NaOH flowrate, the rate of nickel precipitation was measured. The rate at which the Ni^{2+} concentration decreased during reaction was compared to the rate of NaOH input ($\frac{d[NaOH]}{dt} : \frac{-d[Ni^{2+}]}{dt}$), and then further compared the stoichiometric requirement of the sulphide to nickel reagents required to form NiS as shown in equation 7-1. Thus the nickel removal rate was related to the rate of $H_2S(g)$ consumption (See Appendix D for sample calculation). As can be seen in Figure 36, there is good agreement between the theoretically determined threshold and the experimental points. The exception was point T07, when $H_2S(g)$ = 0.3L/min and NaOH = 1.75mmol/min.

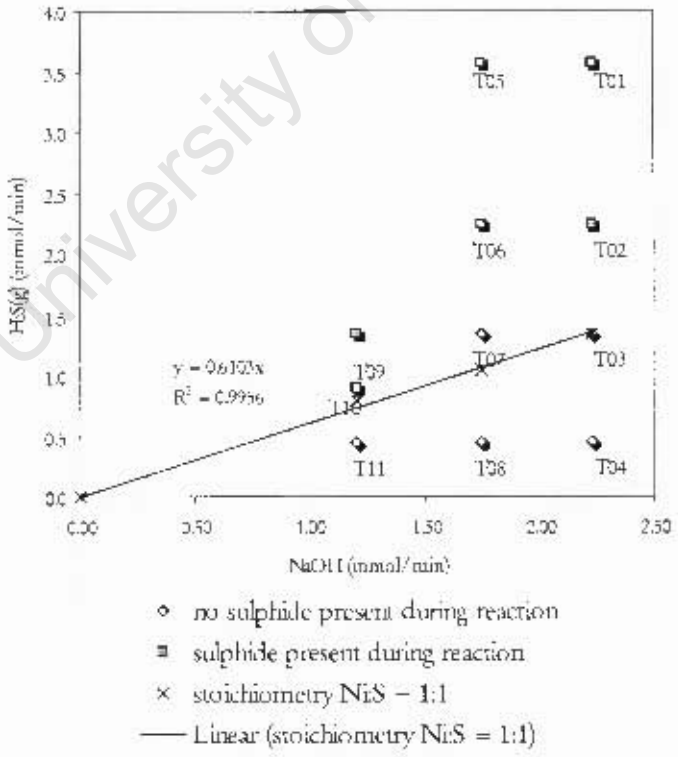

Figure 36: Sulphide usage efficiency threshold; comparing experimental and modelled regions of $H_2S(g)$ mass transfer resistance [T01 – T11]

7.2.3.1. Higbie's penetration theory

Experiments using low (L01 – L05) and high (T01 -T04) alkalinity flowrates indicated that the precipitation of NiS from the synthetic $NiSO_4$ solution is controlled by the rate of HS^- addition. Thus, Higbie's penetration theory was applied to semi-batch bubble column experiments T01 – T04 (Figure 37) and T03, T07 and T09 (Figure 38) to determine the controlling factor on the precipitation process. Higbie's theory was experimentally validated for the time scale of the reaction by comparing the sulphide concentration in solution experimentally determined to that predicted by the theoretical expression (Appendix E). The solution used had equivalent ionic strength to the reaction medium. The sulphide concentration was obtained from the calculated rate of sulphide diffusion from the bubble into the reacting solution as determined by Higbie's theory.

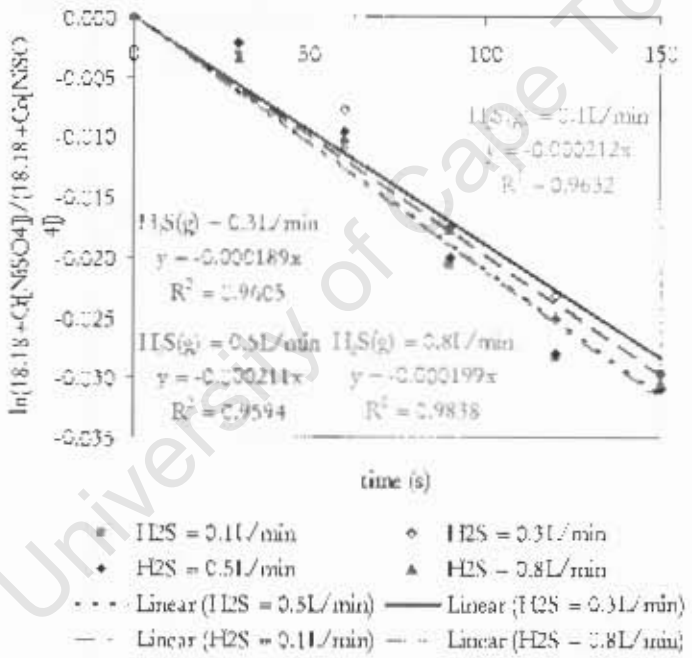

Figure 37: Higbie's penetration theory applied nickel sulphide precipitation from a synthetic nickel sulphate solution using $H_2S(g)$ promoted by alkalinity addition $\ln(18.18 + C[NiSO_4])/(18.18 + C[NiSO_4])$ vs time for different $H_2S(g)$ flowrates when NaOH = 2.23mmol/min [T01 – T04]

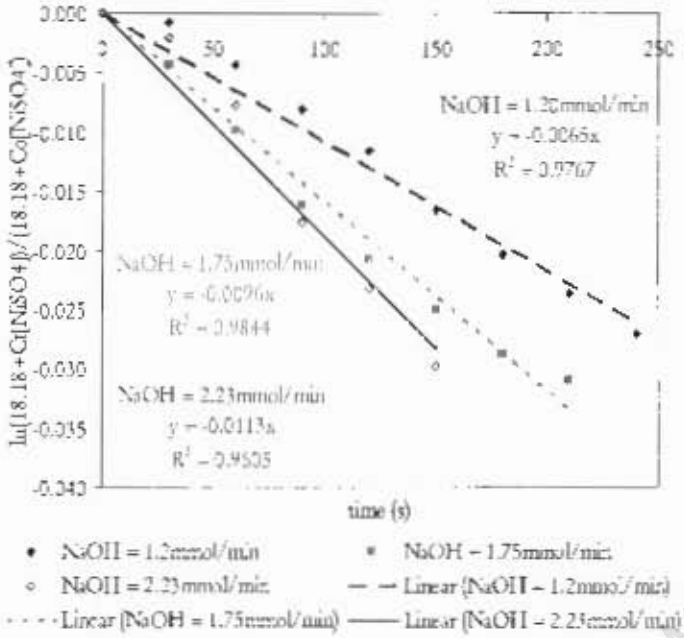

Figure 38: Higbie's penetration theory applied nickel sulphide precipitation from a synthetic nickel sulphate solution using $H_2S(g)$ promoted by alkalinity addition $\ln(18.18 + C[NiSO_4])/(18.18 + C^{\circ}[NiSO_4])$ vs time for the same $H_2S(g)$ flowrate = 0.3L/min [T03, T07 and T09]

The rate of precipitation was the same for the same NaOH flowrate at varying $H_2S(g)$ flowrates (Figure 37) and the rate of removal increased when the rate of NaOH was increased at the same $H_2S(g)$ flowrate (Figure 38) . Thus these figures confirm that the rate of precipitation expressed as $\ln(18.18 + C[NiSO_4])/(18.18 + C^{\circ}[NiSO_4])$ (Mishra and Kapoor, 1978) was controlled by the rate of alkalinity addition. Thus the mass transfer coefficient, k_c , cannot be calculated from the graphs constructed above since the rate of reaction is limited by alkalinity addition and not by the rate of $H_2S(g)$ diffusion into solution. Thus, in order to calculate supersaturations the theoretical value for the mass transfer coefficient, k_c , is used (equation 5-19). While the rate of sulphide absorption into solution is a function of $H_2S(g)$ flowrate, the availability of reaction HS^- ions is controlled by alkalinity addition. The results confirm the batch findings and therefore supersaturation cannot be calculated using the total sulphide in solution.

Comparing the graphs above to those constructed by Mishra and Kapoor (1978) further confirms that NaOH flowrate dictated the rate of removal of nickel. Mishra and Kapoor (1978) found that the rate of precipitation decreased with decreasing gas flowrate at constant bubble size and that the rate of precipitation increased with decreased bubble size. Since gas bubble sizes were constant (± 0.45mm) for all $H_2S(g)$ flowrates tested and

the bisulphide species responsible for precipitation were liberated by the addition of hydroxyl ions, the rate of alkalinity addition controlled the precipitation process.

7.2.3.2. Supersaturations

Supersaturations were based on HS^- ion values since these are primarily responsible for the precipitation of nickel in the system. The NiS precipitation system was modelled in Excel® to obtain initial supersaturation values since the first measurements during reaction were at 30s, which was too long an interval to evaluate supersaturation over considering the speciation and reaction were almost instantaneous. Supersaturations for the semi-batch precipitation of nickel sulphide were calculated and are displayed below in Table 14 (Appendix F). Only the initial supersaturation values at t = 0.01s are shown because it is assumed that supersaturations decreased as the run progressed since the concentration of nickel decreased. For the semi-batch gaseous experiments, as the $H_2S(g)$ flowrate increased the initial supersaturation increased. The rate of nickel removal was strongly dependent on the alkalinity flowrate, thus the supersaturations were smaller when the flowrates of alkalinity were lower.

Table 14: Supersaturations at time, t = 0.01s, using HS- for experiments T01, T02, T03, T07 and T09

Run	NaOH mmol/min	$H_2S(g)$ L/min	Supersaturation t = 0.01s
T01	2.23	0.8	4.94E+06
T02	2.23	0.5	2.35E+06
T03	2.23	0.3	1.15E+06
T07	1.75	0.3	9.76E+05
T09	1.20	0.3	6.45E+05

The batch aqueous supersaturations (Figure 30) were higher (10^{13} - 10^{14}) than the gaseous semi-batch ones (10^5 - 10^6) due to the mass transfer resistance in the gaseous system which slowed the rate of sulphide availability (Hammack, 1994).

As stated earlier, supersaturations cannot be related to settling times. The presence of excess sulphide in solution caused dissolution of precipitates, leading to decreased precipitate sizes, preventing flocculation (based on batch settling results), and thus causing increased settling times. Dissolution of precipitates was not apparent during reaction but probably occurred during settling due to the large excess of sulphide present in solution. Settling of larger precipitate particles was not observed, again due to the

opacity imparted to solution by the smaller precipitates suspended in solution. Settling as a phase separation process was not effective for precipitates resulting from the use of gaseous $H_2S(g)$, taking over 1 week to completely settle.

7.2.3.3. Particle size distributions (PSDs)

It was attempted to obtain PSDs of particles formed from both batch (Appendix G) and semi-batch reactor configurations using aqueous and gaseous sulphide reagents, respectively. PSDs were desired so that a population balance model could be generated. The desire was to confirm which particle processes dominated in the various systems. However, neither reactor configuration utilised yielded particles stable enough to be measured because both settling and flocculation of particles presented PSD measurement difficulties.

Particle measurement techniques employed were laser diffraction using the Malvern Mastersizer® and the electrical sensing zone method employed by the Beckman Coulter® Counter. The following graphs are PSDs for the semi-batch precipitation of NiS using $H_2S(g)$ = 0.3L/min and NaOH = 1.75mmol/min (T07).

The PSDs obtained from the Coulter® Counter decreased in particle size and number with time after the sample was obtained from reaction solution, as seen in Figure 39 for experiment T07 (NaOH = 1.75mmol/min, $H_2S(g)$ = 0.3L/min).

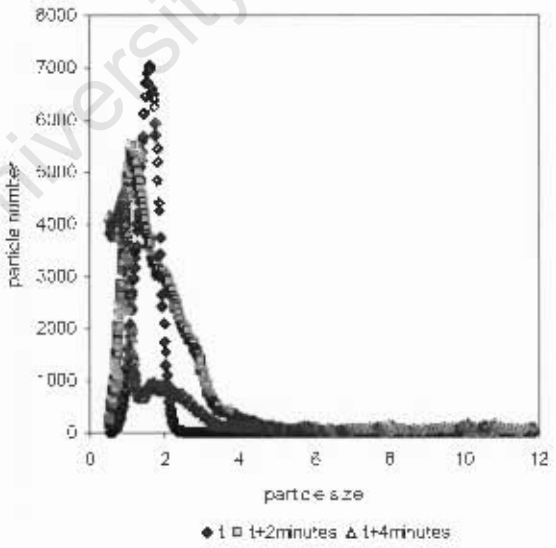

Figure 39: Repeat PSDs measured using the Beckman Coulter® Counter 1 minutes after complete reaction when NaOH = 1.75mmol/min, $H_2S(g)$ = 0.3L/min [T07]

PSDs taken by the Beckman Coulter® Counter were measured t minutes after reaction was complete, where t was between 5 – 10 minutes. A 20 micron aperture tube was used with a measuring range of 0.6 – 12 μm. Thus, the PSDs were discontinued below 0.6 μm which is undesirable since information on particle sizes below the lower limit was omitted, as apparent when the time after reaction was t + 4 minutes showing that the peak was severed. Particle numbers decreased with increasing time after the run commenced, which indicates that settling occurred because the size of particles also decreased. PSDs became increasingly bimodal as the time after reaction increased which indicates flocculation occurred as well (Adi et al., 2007).

Thus the Malvern Mastersizer® was used since there is a stirrer present to create a dynamic environment and thus prevent settling of particles within the sample volume. Samples were analysed for PSDs t1 minutes after reaction was complete, where t1 was between 20 - 25minutes. It was found that the obscuration decreased as the time after sampling increased indicating that particles were flocculating with time in the sample holder. Particle sizes increased as the time after sampling progressed, shown on the graphs as a shift in the peak from below 1μm to approximately 2μm. Particle numbers decreased with time after sampling.

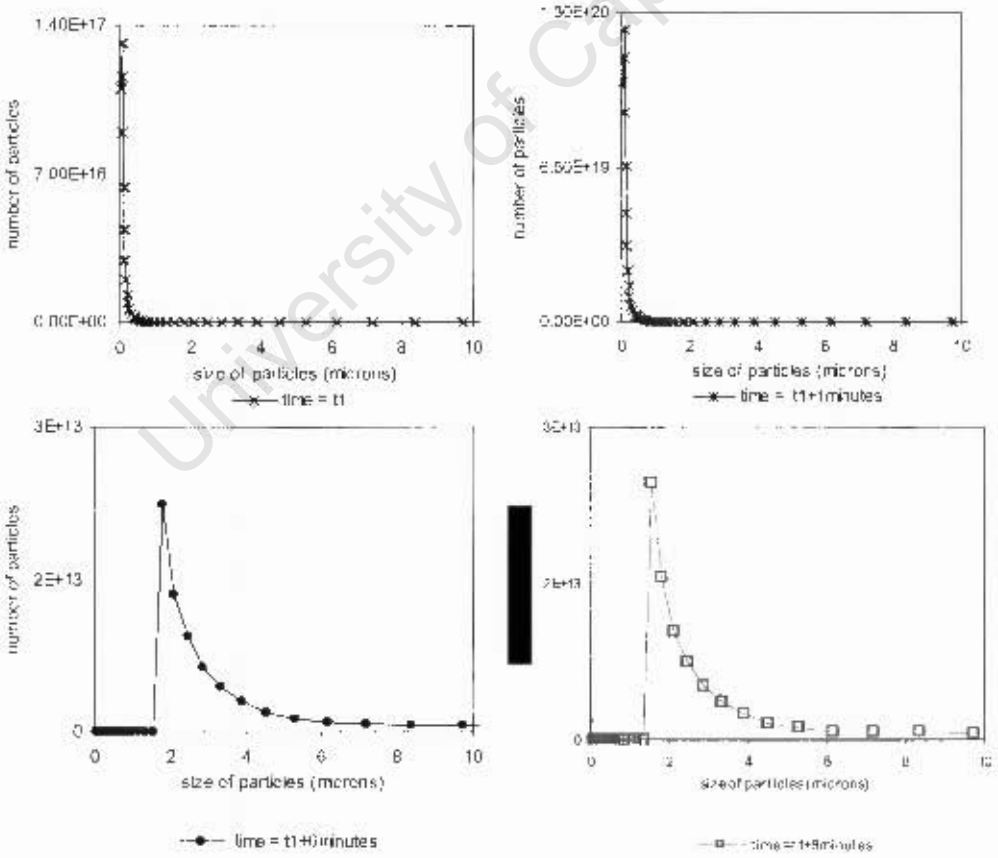

Figure 40: Repeat PSDs measured using the Malvern Mastersizer® t1 minutes after complete reaction when NaOH = 1.75mmol/min, $H_2S(g)$ = 0.3L/min [107]

PSDs measured in the Malvern Mastersizer® (range 0.1-1000μm) were cut off at the lower limit as seen in PSDs obtained at t1 and t1 + 1 minutes (Figure 40) and is undesirable since valuable information on nucleation, which produces the smallest particle sizes, is lost. An incomplete PSD prevents interpretation of particle rate processes occurring within the reaction solution. The overall decreased particle number and increased particle size, as well as the simultaneous decreased obscuration as the time after reaction progressed indicated flocculation of precipitates in the sample volume, despite stirring. It was found that sonification amplified flocculation effects for metal sulphide precipitates and therefore it was not used.

The lower limit of detectable particle sizes is smaller in the Malvern Mastersizer® than by the Beckman Coulter® Counter and thus many more particles were detected by the Malvern Mastersizer®. The PSDs from both measurement techniques are not comparable, which is a further indication of precipitate instability.

The robustness of measurement is indicated by no PSD change with time after the sample is obtained (Adi et al., 2007) and so both methods were ineffective at measuring PSDs of NiS precipitates formed in the semi-batch gaseous reactor (Figure 39 and Figure 40) and the batch aqueous reactor (Appendix G).

Similar relationships between the particle size and number and the time of measurement after sampling and for both the Beckman Coulter® Counter and the Malvern Mastersizer® are seen when NaOH = 2.23mmol/min and $H_2S(g)$ = 0.8L/min (T01) (Appendix H).

Since sample characterisation was not successful using settling and PSD measurement, X-ray diffraction (XRD) was attempted. However, due to the amorphous nature of the precipitates the XRD data did not show consistent peaks, thus ruling out the use of this method to identify precipitates formed. The XRD data as well as SEM pictures are shown in Appendix I to qualitatively support this argument.

7.2.4. Reduction End Solution (RES)

The graphs below show the results of the precipitation of nickel and cobalt from diluted RES using $H_2S(g)$.

The precipitation of nickel was incomplete when no alkalinity was provided to the reacting solution (Figure 41). Cobalt was present in small amounts (25ppm) and was

completely precipitated. There was significantly greater removal of nickel (75%) than when synthetic $NiSO_4$ was used as the nickel source (5%) (Figure 24), because the ammonium ion of the $Ni(NH_3)_2SO_4$ complex acted as a buffer against the pH change. Thus, more HS^- ions were able to be released before the pH dropped too low for the reaction to take place. The buffering effect was noted by the more gradual decrease of pH to a higher final value (pH 4.62) after 20 minutes than when using the synthetic $NiSO_4$ solution (pH 4.07). However, the buffering capacity of the NH_4^+ complex was insufficient to facilitate complete precipitation of Ni^{2+} in the diluted RES. The buffering capacity is shown graphically in Appendix J.

During precipitation of nickel and cobalt from the diluted RES, the sulphide concentration in solution reached an approximately constant value of 205ppm after 20 minutes which was due to the pH of the solution approaching a constant value since the pH dictates the saturation sulphide concentration by controlling the speciation.

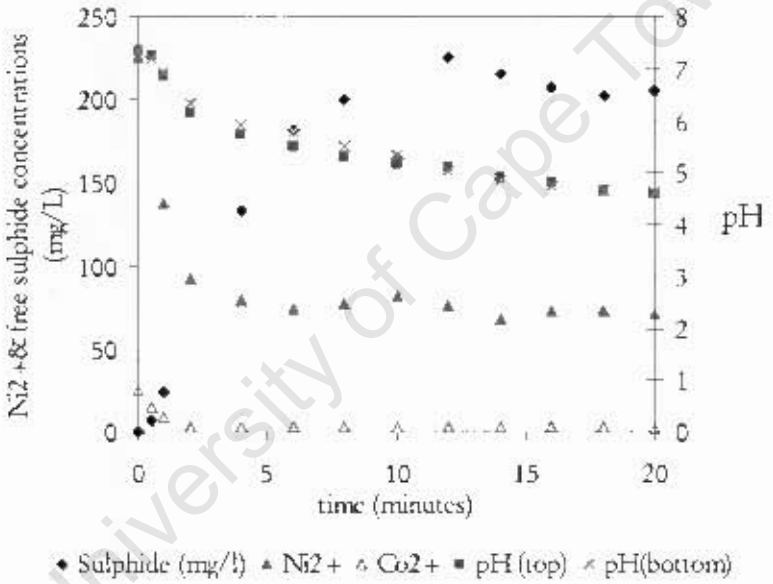

Figure 41: Sulphide precipitation of nickel and cobalt from RES using $H_2S(g)$ without alkalinity addition [RES01]

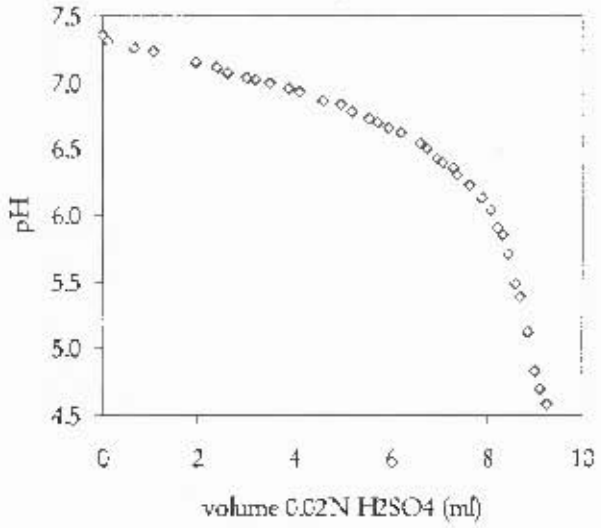

Figure 42: Amount of acid needed to facilitate pH change in the diluted RES solution to quantify buffering capacity using alkalinity (equivalent mg of $CaCO_3$/L)

The H^+ ions released during reaction, determined via alkalinity quantification, was used in an attempt to confirm that the hydrogen ions liberated from precipitation of NiS (equation 7-1) and speciation of $H_2S(aq)$ to HS^- (equation 1-1) matched the pH decrease during reaction. The calculated value of alkalinity for the diluted RES was 462mg/L $CaCO_3$ equivalents in the 750ml reaction solution for the pH change from 7.26 to 4.62 during reaction. To effect a pH change equivalent to that seen in the diluted RES 6.75mmol required H^+ ions to be released. The H^+ ions released due to reaction were calculated as 4.52 mmol thus there was a 33% discrepancy between values (Appendix J). Therefore, insufficient protons were released by only NiS precipitation to effect the pH decrease suggesting that an additional reaction releasing H^+ ions occurred in the bubble column. It is possible that the formation of $NH_3(g)$ occurred during reaction, releasing H^+ ions which effect the further pH decrease.

$$NH_4^+ \rightleftharpoons NH_3 + H^+ \qquad (7\text{-}2)$$

In order to facilitate rapid, controllable, complete removal of nickel and cobalt as sulphides from the diluted RES, alkalinity was provided as NaOH with a flowrate of 1.20mmol/L. The pH of the reacting solution remains in the neutral range between pH 7.39 – 6.67, owing to NaOH input and the buffering capacity of the ammonium ions.

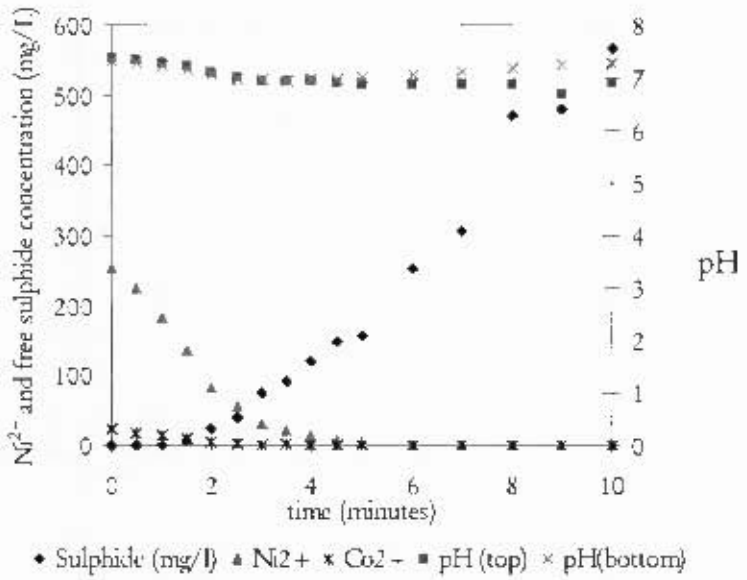

Figure 43: Sulphide precipitation of nickel and cobalt from RES using $H_2S(g)$ (0.3L/min) with alkalinity addition NaOH = 1.20mmol/min [RES02]

There was significantly less wastage of unabsorbed, unreacted sulphide to the NaOH trap compared to when no added alkalinity was used to aid precipitation of the nickel and cobalt from the diluted RES (Figure 44). After the reaction stopped, sulphide was present in larger concentrations in the reacting solution when NaOH was used to facilitate reaction (Figure 43) than when no NaOH was used (Figure 41). Thus, suggesting that sulphide is utilised more efficiently during the reaction when alkalinity was added to facilitate reaction.

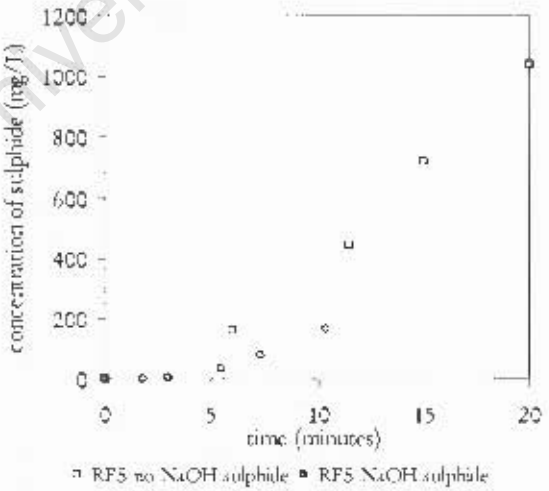

Figure 44: Comparison of sulphide in the NaOH trap for semi-batch precipitation of Ni^{2+} and Co^{2+} from diluted RES without NaOH input where NaOH = 1.20mmol/min

Comparison of the precipitation of nickel and cobalt from RES and that of nickel from the synthetic $NiSO_4$ solution are shown in the graphs below. Complete precipitation occurred after 4.5 minutes for both solutions therefore the rate of nickel removal was not affected by the solution matrix as long as the alkalinity was supplied at the same rate.

The rate of precipitation from the diluted RES was initially rapid and then slowed after three minutes as the nickel concentration in solution decreased probably because the nickel became more strongly complexed to the ammonium sulphate,. From the synthetic nickel solution the precipitation was in general linear throughout the run, slowing only slightly in the last 30s.

The sulphide concentration in the synthetic $NiSO_4$ reaction solution was greater than that of the diluted RES in the first 1.5 minutes of the run as predominantly $H_2S(aq)$ was present, which is unable to precipitate nickel. Also, the pH of the synthetic $NiSO_4$ solution was lower during reaction, limiting the amount of sulphide in solution. Conversely, no excess sulphide was present in the diluted RES precipitating system during reaction.

Because the pH was close to neutral and varied marginally (pH 6.67 – 7.39) throughout the duration of the run, the sulphide in solution speciated to HS^- and therefore was able to precipitate nickel. In the synthetic nickel sulphate system the pH was lowered to acidic values since the system was not buffered and thus the excess sulphide in solution during reaction was $H_2S(aq)$. Thus, the sulphide entering the RES precipitating system was utilised more efficiently within the first 1.5 minutes because as it entered solution it speciated to HS^- and was consumed by reaction. From 2.5 minutes until the end of the run there was more sulphide in the reacting solution in the diluted RES system because the pH was higher and thus more sulphide was able to enter solution.

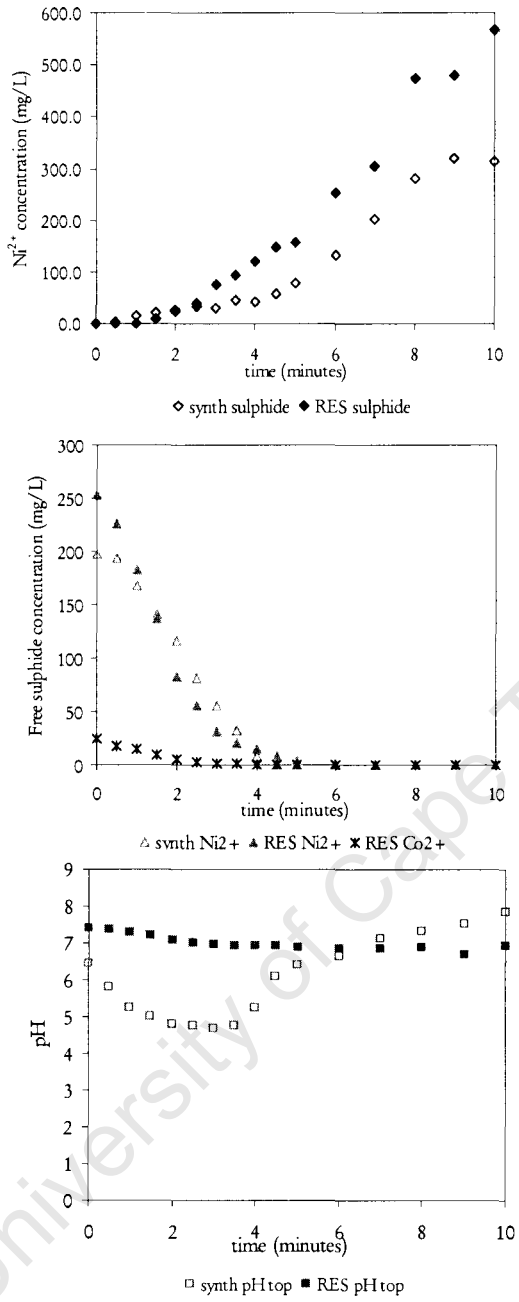

Figure 45: Comparison of the precipitation of nickel and cobalt from diluted RES and nickel from synthetic $NiSO_4$, NaOH = 1.2mmol/L $H_2S(g)$ = 0.3L/min

8. Conclusions and recommendations

Batch experiments were inconclusive in determining whether HS^- or S^{2-} species were responsible for the precipitation of NiS, but sufficient evidence exists to confirm that the $H_2S(aq)$ sulphide species cannot precipitate Ni^{2+} at ambient conditions. The most recent pK_2 value of 17.4 (Midgisov et al., 2001), used in this study, suggests that the bisulphide ion (HS^-) was responsible for NiS precipitation because the sulphide ion (S^{2-}) was not present at significant concentrations for the extent of the real pH scale (0-14). It was found that sulphide precipitation of Ni^{2+} using $H_2S(g)$ decreased the pH and limited the extent of reaction as the supply of reactive sulphide ions (HS^-) was exhausted.

In this study, the use of gaseous sulphide to precipitate Ni^{2+} from an aqueous solution was facilitated by the addition of alkalinity, in the form of an independent NaOH source, to provide the bisulphide ions necessary for the reaction. Gaseous sulphide slowed the rate of the precipitation due to the mass transfer delay of sulphide entering solution. Therefore, provided sufficient sulphide has diffused into solution, it can be said that the control of Ni precipitation by gaseous sulphide is dictated by the rate at which HS^- species are made available. In this study, this was controlled by the rate at which NaOH (alkalinity) was supplied. As a result, supersaturation calculations were carried out using the HS^- species as opposed to the total free sulphide concentration measured in solution. Initial supersaturations of the gaseous semi-batch system in the range of 10^5 – 10^6 compared to the aqueous "slug-dosed" batch system at supersaturations of 10^{13} – 10^{14}.

When the flowrates of NaOH and $H_2S(g)$ were such that the supplied alkalinity was an order of magnitude lower than the sulphide, Ni precipitation occurred at a linear rate and was complete after 25 – 40 minutes. In this case, the rate of precipitation was not dependent on the sulphide flowrate but rather on the rate of NaOH addition. Aqueous sulphide accumulated in the system during the precipitation phase and increased as the $H_2S(g)$ increased. In all cases, the pH reached a relatively stable value of approximately 3.5 during the precipitation phase indicating that the accumulated sulphide was the $H_2S(aq)$ species. Where sulphide and hydroxide continued to be added after precipitation was complete, the pH and accumulated sulphide increased with time, the sulphide concentration to values greater than the previous stable concentration as more dissociated to HS^-. Thus, sulphide was supplied in excess and did not limit the reaction. The controlled pH values were between pH 3 and 4. Previously precipitated nickel was observed to re-enter solution during this period. This was attributed to the formation of nickel polyusulphide complexes.

Batch experiments in which excess sulphide was provided relative to the stoichiometric dosage of Ni:S (1:1), demonstrated the dissolution of precipitates. In the well-mixed system the amount of resolubilised nickel exceeded 10ppm after 10 minutes and then continued to increase linearly with time. This phenomenon was observed to a lesser extent where the Ni: S stoichiometry was 1:1 and could most likely be attributed to local HS^- excess during the precipitation reaction.

Where the $H_2S(g)$ flowrate was significantly greater than rate of NaOH addition, it was observed that the majority of added sulphide did not dissolve and was accumulated in the sulphide trap. In an industrial precipitation context, process economics dictate efficient reagent unitisation and this was not achieved under conditions of low alkalinity addition. Increasing the alkalinity flowrate such that the flowrates of NaOH and $H_2S(g)$ were of equal magnitude resulted in significantly faster removal of nickel and decreased sulphide wastage. The molar ratio of $H_2S(g)$ and NaOH addition at which mass transfer limitations ensured minimal sulphide in solution and no excess $H_2S(g)$ passing through the solution, but at which HS^- availability still controlled the rate of nickel removal was determined to be 1: 1.66. When experiments were performed at sulphide to hydroxide ratios below this threshold value the precipitation of nickel as $Ni(OH)_2$, as well as NiS, occurred because in the absence of sulphide the hydroxide ions accumulated to the point where the solution became supersaturated with respect to $Ni(OH)_2$.

When the hydroxide addition rate was 2.23mmol/min, the rate of Ni pptn was still largely independent of gas flowrate over the range tested. When the NaOH rate was 0.1L/min $Ni(OH)_2$ precipitation occurred since insufficient sulphide was supplied. When NaOH was increased to 0.3L/min the flowrates of sulphide and hydroxide caused a neutral pH and the precipitation was in close proximity of the threshold between NiS and $Ni(OH)_2$ formation. When the NaOH flowrate was 0.5 and 0.8L/min NiS precipitation occurred but the pH decreased due to the speciation of the excess accumulated sulphide in solution. Therefore, at these higher flowrates an increase in NaOH flowrate would probably result precipitation becoming dependent on H2S gas flowrate. This would result in an undesirable increase in supersaturation.

A thermodynamic software package, OLI Stream Analyzer (OLI© 2006), was used in an attempt to generate a pseudo-kinetic model. However, it allowed the reaction to reach thermodynamic equilibrium over each time scale resulting in overestimations of precipitation efficiency and inaccurate pH predictions. Therefore, thermodynamic models are not suitable to predict system performance.

Higbie's Penetration Theory was applied to calculate the rate of $H_2S(g)$ dissolution. The model prediction was validated experimentally and held until the solution approached saturation wrt $H_2S(aq)$. When applied to the reaction system, this model indicated that over the range of flowrates tested the bubble diameter did not significantly affect the precipitation rate. The model confirms experimental observations that precipitation was predominantly affected by NaOH flowrate. Application of this model allowed more accurate determination of supersaturation values.

A number of methods were attempted to determine PSD during the reaction process. The nature of the precipitate formed occluded the collection of reproducible PSD data predominantly due to flocculation of precipitates within the counting chambers. A number of dispersants and pre-treatment options were investigated but this problem could not be overcome. The lack of representative PSD data meant that a meaningful population balance analysis could not be performed; therefore the predominant particle rate process could not be confirmed. However, based on the high SS values even in the gaseous system it is likely that the precipitation process is dominated by nucleation and aggregation rather than nucleation and growth.

In the absence of meaningful PSD data particle settling rate was investigated as a technique to relate supersaturation values to particle size. This data did not produce conclusive results partly due to the formation of polysulphide complexes which made observation of phase separation difficult. In addition, for batch precipitation, flocculation of precipitate particles occurred immediately after reaction resulting in rapid settling and thus could not be described by Stokes' Law (settling for single particle grains).

Using diluted RES, to obtain a nickel concentration of 200ppm in order to compare results to the synthetic solution, showed that the RES had significant buffering capacity and in excess of 50% nickel and all cobalt could be precipitated without addition alkalinity. However, for complete efficient precipitation addition, alkalinity was required. The rates of nickel removal using $H_2S(g)$ were comparable for the synthetic $NiSO_4$ solution and the diluted RES for the same flowrate of NaOH. The precipitation mechanism described in the simple synthetic system holds for the diluted RES so it is a good model system for investigating phenomena which have potential significance in a process environment.

Based on the above conclusions, it is recommended that various aspects of NiS precipitation using $H_2S(g)$ assisted by alkalinity addition are further investigated.

- It is recommended that additional methods for characterisation of precipitates be undertaken.
- Modelling of mixed hydroxide/sulphide precipitation under these conditions should be performed to determine the dominant precipitate formed.
- Robust PSD measurement techniques are necessary in order to quantitatively and critically compare the effect of decreasing the supersaturations, in the gaseous system, with the batch system. Obtaining PSDs during the reaction will enable determination of the dominant particle forming mechanisms. By measuring zeta potentials of the NiS precipitates it may be possible to identify suitable dispersants to minimise flocculation of precipitates during PSD measurement.
- Process optimisation was not the intention of this study. However, identifying the sulphide usage efficiency threshold was the first step towards process optimisation. Further research is required to optimise the process in terms of efficiency of sulphide utilisation and particle characteristics.
- Despite reduced supersaturations obtained in the gaseous system, phase separation of precipitate particles from the mother liquor remained relatively inefficient. Additional research into solid-liquid phase separation is necessary.
- The use of thermodynamic based modelling was not suitable to predict process performance. Initial attempts at modelling the precipitation of NiS from the synthetic $NiSO_4$ solution, based on observed kinetic parameters, was attempted in both Microsoft Excel® and Matlab® . Initial indications suggest this approach will yield a more applicable model and current work on model development is continuing.

9. References

Adi, H., Larson, I., and Stewart, P. (2007). Laser diffraction particle sizing of cohesive lactose powders, *Powder Technology*, doi:10.1016/j.powtec.2007.01.018 Article in Press

Al-Farawati, R. and van den Berg, C.M.G. (1999). Metal complexation in sea water, *Marine Chemistry* **63** pp331-352

Baldyga, J., and Bourne J.R. (1989). Simplification of micromixing calculations, II, New applications, *The Chemical Engineering Journal*, Volume **42**, Issue 2, November 1989, pp93-101

Berry, E.W. (1967). Cloud droplet growth by collections, *Journal of Atmospheric Science*, **24** pp688

Bhagat, M., Burgess, J.E., Antunes, A.P.M., Whitely, C.G. and Duncan, J.R. (2004). Precipitation of mixed metal residues from wastewater utilising biogenic sulphide, *Minerals Engineering* **17** pp925-932

Bhattacharyya, D., Jumawan., A.B., Sun, G. (1981). Precipitation of heavy metals by with sodium sulphide: bench-scale and full-scale experiments, *Water-1980 AIChe Symposium Series*, vol. **77**

Bramley, A.S., Hounslow, M.J., Ryall, R.L. (1996). Aggregation during precipitation from solution: A method for extracting rates from experimental data, *Journal of Colloid and Interface Science* **183**, pp155-165

Bryson, A.W., and Bijsterveld, C.H. (1991). Kinetics of the precipitation of manganese and cobalt sulphides in the purification of a manganese sulphate electrolyte, *Hydrometallurgy*, **27** pp75-84

Chadwell S.J., Rickard, D.T, and Luther, G.W. III (1999). Electrochemical evidence for pentasulphide complexes with Mn^{2+}, Fe^{2+}, Co^{2+}, Ni^{2+}, Cu^{2+} and Zn^{2+}, *Aquatic Geochemistry* **5** pp29-57

Chadwell S.J., Rickard, D.T, and Luther, G.W. III (2001). Electrochemical evidence for metal polysulphide complexes: Tetrasulphide (S42-) reactions with Mn^{2+}, Fe^{2+}, Co^{2+}, Ni^{2+}, Cu^{2+} and Zn^{2+}, *Electroanalysis* **13** pp21-29

Cooke, E.G., 1966, *Krist. U. Technic.* 1, 119

Costodes, V.C.T., Lewis, A.E. (2005). Reactive crystallisation of nickel hydroxyl-carbonate in fluidized-bed reactor: Fines production and column design, *Chemical Engineering Science* **61** pp1377-1385

Cotton, F.A., Wilkinson, G., Murillo, C. A. and Bochmann M. (1999). *Advanced inorganic chemistry*, 6th edition, John Wiley, New York

Coulson, J.M., and Richardson, J.F. (2002). *Coulson and Richardson's Chemical Engineering* Volume 2, Pergamon press Ltd. Oxford, England

Denk, E.G. (1970). Ph.D. Thesis. Tufts University, Medford, M.A.

Drake, R.L. (1972). *Agglomeration effects in aluminium trihydroxide precipitation*, Ph.D. Thesis. University of Queensland, Australia

Esposito, G., Veeken, A., Weijma, J. and Lens., P.N.L. (2006). Use of biogenic sulphide for ZnS precipitation, *Separation and purification technology*, 51, 1 pp31-39

Frank, F.C. (1949). Crystal Growth, *Symposium on Crystal Growth, Discussions of the Faraday Society*, no. 5

Franke, J. and Mersmann, A. (1995). The influence of operational conditions on the precipitation process, *Chemical Engineering Science*, **50** pp1737-1753

Gosele, W. and Kind, M. (1991). Study on the influence of mixing on the quality of continues precipitating products. *Chemie Ingenieur Technik*, **63** pp59-61.

Guillard, D. (2001). *Nickel hydroxyl-carbonate precipitation in a pellet reactor*, MSc. Thesis. Cape Town, South Africa: University of Cape Town

Hammack, R.W., Dvorak, D.H., Edenborn, H.M. (1993). The use of biogenic hydrogen sulphide to selectively recover copper and zinc from severely contaminated mine drainage. In: Torma, A.E., Wey, J.E. Lakshmann, V.L. (Eds.), *Biohydrometallurgy Technologies. The Minerals, Metals and Materials Society*, pp631 - 639.

Hammack, R.W., Edenborn, H.M. and Dvorak, D.H. (1994). Treatment of waste from an open-pit copper mine using biogenic sulphide and limestone: a feasibility study. *Water Research* **28**, pp2321-2329

Hounslow, M.J., Pearson, J., Instone, T. (2001). Tracer studies of high-shear granulations: II. Population balance modelling, *AIChE, Journal* **47** pp1984-1999

Hounslow, M. J., Lewis, A. E., Sanders, S. J. and Bondy, R. (2005). A generic crystalliser model: I. A model framework for a well-mixed compartment *AIChEJ,* **51**, 11 pp2942-2955

Jackson, E. (1986). *Hydrometallurgical Extraction and Reclamation*, Ellis Horwood Limited, Chichester, Chapter 4, pp147-200

Jandová, J., Lisá, K., Vu, H., and Vranda, F. (2005). Separation of copper and cobalt-nickel sulphide concentrates during processing of manganese deep ocean nodules *Hydrometallurgy* **77** pp75-79

Jones, A.G. (2002) *Crystallisation process systems*, Butterworth-Heinemann, Boston, Oxford

Koltoff, I.M. and Moltzau, D.R. (1935). Induced precipitation and properties of metal sulphides *Chemical Reviews* **17** pp293-325

Lewis, A.E., and Butler, B.K. (2001). An investigation into the precipitation of nickel and cobalt sulphides, *Research Report*, (unpublished data)

Lewis, A.E. and van Hille, R.P. (2005). An exploration into the sulphide precipitation method and its effect on metal removal, *Hydrometallurgy*, **81**, pp197 – 204

Lewis, A.E. and van Hille, R.P. (2005). Complexity in Sulphide Precipitation, In: T. Subbaiah (eds) Emerging trends in *Mineral Processing and Extractive Metallurgy*, 13-14 June, Bhubaneswar, India. pp298-305

Licht, S. (1988). Aqueous solubilities, solubility products and standard oxidation-reduction potentials of the metal sulphides, *Journal of the electrochemical society*, **135**, 22, pp2971-2975

Low, G.C. (1972) in Topics in current aerosol research (G.M. Hiddy, and J.R. Brocks), Part 2, No. 3, p201, Pergammon, New York

Luther, G.W. III, Therberge, S.M., Rickard, D.T, and Oldroyd, A. (1996). Determination of bisulphide stability constants of Mn, Fe, Co, Ni, Cu and Zn by voltammetric methods, *Environmental Science and Technology* **30**, pp671-679

Luther, G.W. III, Therberge, S.M., and Rickard, D.T (1999). Evidence for aqueous clusters as intermediates during zinc sulphide formation, *Geochimica et Cosmochimica Acta*, **36**, 19/20, pp3159-3169

Luther, G.W. III, et al. (2002). Aqueous copper sulphide clusters as intermediates during copper sulphide formation, *Environmental Science and Technology*, **36**, 3 pp394-402

McNally, S., Benefield, L. and Reed, R.B. (1984). Nickel removal from a synthetic nickel-plating wastewater using sulphide and carbonate precipitation and coprecipitation, *Separation Science and Technology*, **19**, 2 and 3, pp191-217

Mersmann, A. and Braun, B. (2001). In: *Crystallisation Technology handbook* (2001) 2nd edition, Marcel Dekker, New York, USA

Migdisov A.A, Williams-Jones A.E., Lakshtanov L.Z., Alekhin Y.V. (2001). Estimates of the second dissociation constant of H_2S from the surface sulfidation of crystalline sulphur *Geochmica et Cosmochimica* **66**, 10, pp1713 – 1725

Milligan, T.G. (1995). An examination of the settling behaviour of a flocculated suspension *Netherlands Journal of Sea Research*, **33**, 2, pp163 - 167

Mishra, K.K. and Kapoor, M.L. (1978). Kinetics of liquid-gas reactions through bubbles, *Hydrometallurgy* **3** pp75-83

Mishra, P.K. and Das, R.P. (1991). Kinetics of zinc and cobalt sulphide precipitation and its application in hydrometallurgical separation, *Hydrometallurgy* **28** pp373-379

Mullin, J.W., *Crystallization* (1972). 2nd edition, Butterworth-Heinemann, Oxford, UK

Mullin, J.W., *Crystallization* (2001). 4th edition, Butterworth-Heinemann, Oxford, UK, Chapters 5- 6, pp181 - 309

Myerson A.S. (2002). *Handbook of Industrial Crystallisation*, 2nd edition, Butterworth-Heinemann, Boston, USA

Nielsen, A.E. (1964) *Kinetics of precipitation*, Pergamon, Oxford

Oktaybus, C., Açma, E., Arslan, C. and Addemir, O. (1994). Kinetics of copper precipitation by H_2S from sulphate solutions, *Hydrometallurgy* **35** pp129-137

Ohara and Reid (1973). *Modelling crystal growth rates from solution*, Prentice Hall, Englewood Cliffs

Pulles, W., Heath, R., and Howard, M. (1996). *A manual to assess and manage the impact of gold mining operations on the surface water environment*, Pretoria

Randolph, A.D. and Larson, M.A. (1988). Theory of particulate processes, 2nd edition, Academic Press Inc. Limited, New York

Rickard, D., and Luther, G.W. III (2006). Metal sulphide complexes and clusters, Reviews in Mineralogy and Geochemistry, **61,** pp421-504

Schöller, M. and von Dijk, J.C. (1987). *Recovery of heavy metals by crystallisation in the pellet reactor*, Proceedings of the second conference on environmental technology, production and the environment, pp294-303

Seader, J.D. and Henley, E.J. (1998). *Separation Process Principles*, John Wiley and sons, New York, USA, Chapter 3

Shea, D and Helz G.R. (1988). The solubility of copper in sulfidic waters: Sulfide and polysulphide complexes in equilibrium with covellite, *Geochemica et Comochimica Acta* **52** pp1815-1825

Simons, C.S. (1963). Hydrogen Sulphide as a hydrometallurgical reagent, *Metallurgical Society Conference*, **24,** pp592-616

Söhnel, O. and Garside, J. (1992). *Precipitation: Basic principles and applications*, Butterworth-Heinemann, Oxford,

Söhnel, O., and Mullin, J.W. (1987). Influence of mixing on batch precipitation, *Crystal Research and Technology*, **22** pp1235-1240

Smoluchowski, M.V. (1917). Mathematical theory of the coagulation of colloidal solutions, *Zeitschrift für Physikalische Chemie* **92** pp92 – 129

Stumm, W. and Morgan, J.J. (1996). Aquatic chemistry: chemical equilibria and rates in natural waters, 3rd edition, John Wiley and sons, New York

Thompson, P.D. (1968). in *Proceedings International Conference Cloud Physics, Toronto* pp115

Van Hille, R.P., Peterson, K.A., and Lewis, A.E. (2005). Copper sulphide precipitation in a fluidised bed reactor, *Chemical Engineering Science* **60**, pp2571 – 2578

Veeken, A.H.M., Atoko, L., Pol, L.W.H. and Weijma, J. (2003). Control of the sulphide concentration for optimal zinc removal by sulphide precipitation in a continuously stirred tank reactor, *Water Research* **37** pp3709-3717

Vergouw, J.M. et al. (1998). An agglomeration study of sulphide minerals using zeta-potential and settling rate. Part I: Pyrite and Galena, *Minerals Engineering*, **97**, 2, pp159-169

Vergouw, J.M. et al. (1998). An agglomeration study of sulphide minerals using zeta-potential and settling rate. Part II: Sphalerite/Pyrite and Sphalerite/Galena, *Minerals Engineering*, 11, 7, pp605-614

Vicum, L., Ottiger, S., Mazzotti, M., Makowski, L. and Baldyga, J. (2004). Multi-scale modelling of a reactive mixing process in a semi-batch stirred tank, *Chemical Engineering Science*, **59**, pp1767-1781

Zhang, J-Z, and Millero, F.J. (1994). Investigation of metal sulphide complexes in sea-water using cathodic stripping square-wave voltametry. *Anal. Chem. Acta.* 284 pp497-504

OLI Systems Inc. Support systems viewed 15 March, 2007 <http://support.olisystems.com/Documents/Manuals/ >

Appendices

Appendix A

Sulphide species available in reaction at various pHi values, as modelled in OLI.

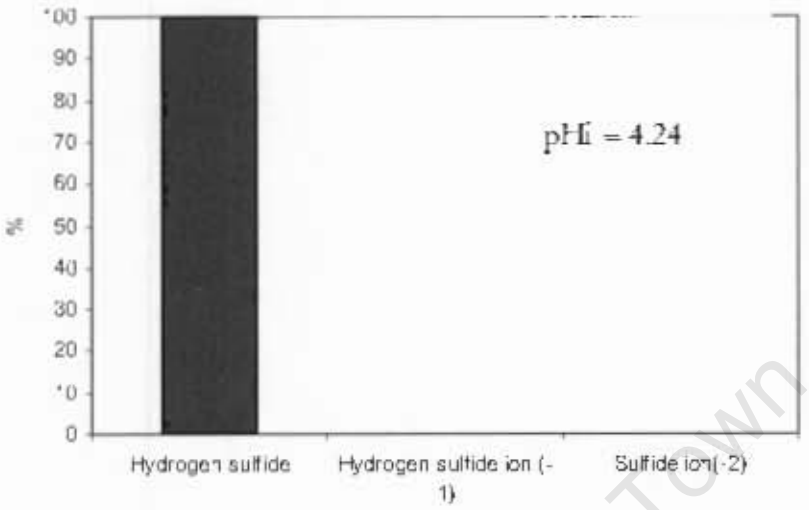

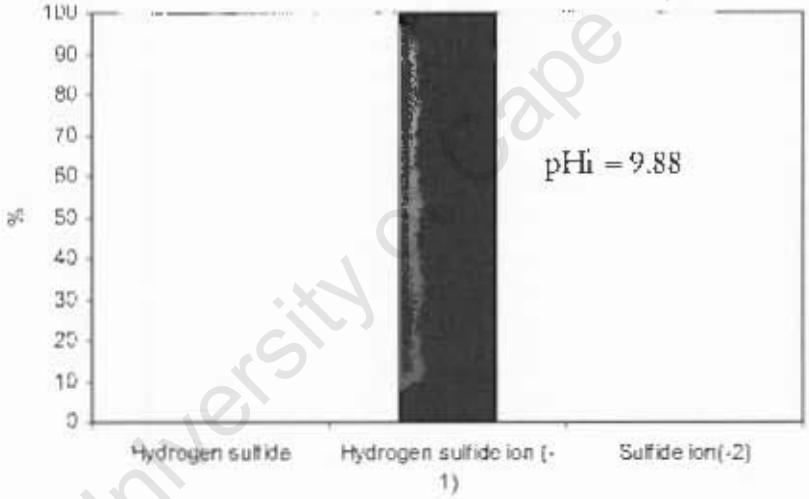

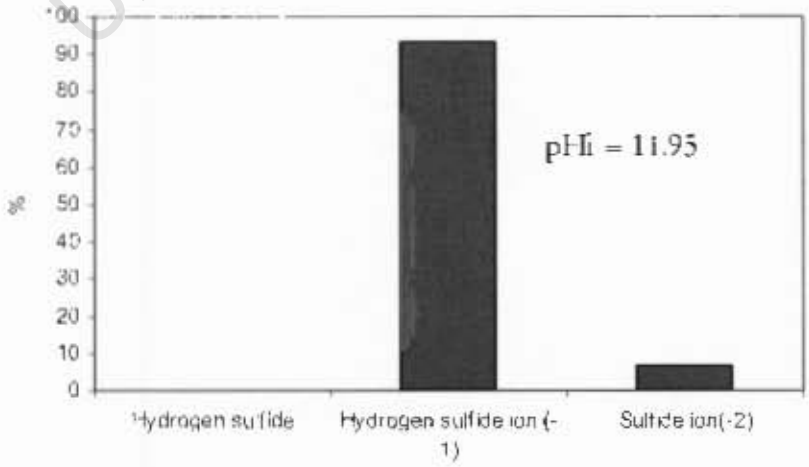

Appendix B

Low alkalinity flowrate showing relative error in measurements [LOS = NaOH -- 0.100, $H_2S(g)$ = 0.8L/min]

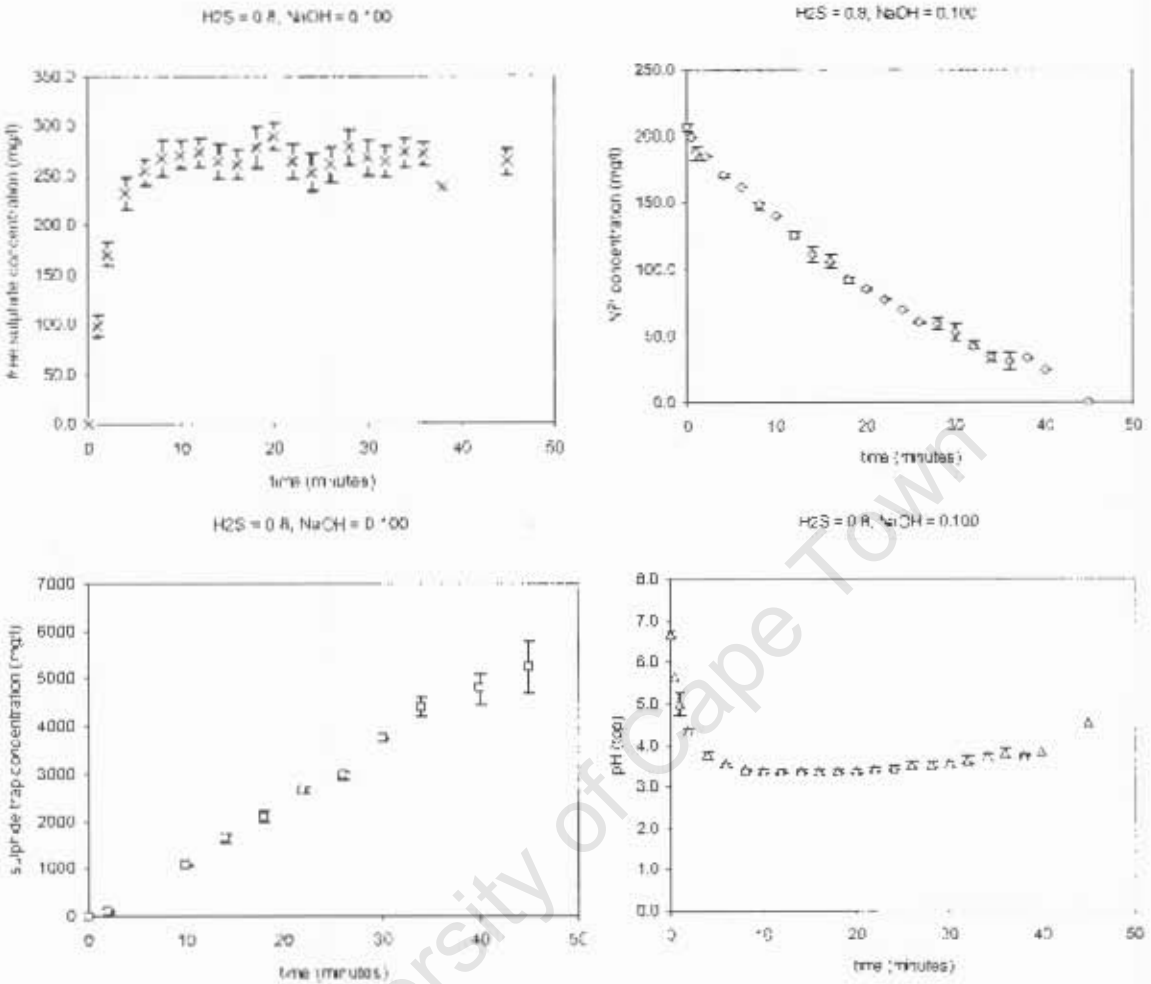

Time (min)	pH (top)	pH(bottom)	Ni^{2+}(mg/L)	Time (min)	Sulphide (mg/l)	Time (minutes)	NaOH sulphide
0	6.52	6.62	210.4	0	0	0	0
1	4.50	4.53	180.7	1	73.3	2	80
2	4.22	4.28	184.3	2	150.0	10	1120
4	3.64	3.67	167.9	4	186.7	14	1740
6	3.46	3.49	161.5	6	226.7	18	2000
8	3.36	3.38	144.5	8	210.0	22	2600
10	3.32	3.35	139.9	10	253.3	26	2860
12	3.31	3.34	123.1	12	235.0	30	3740
14	3.3	3.33	104.03	14	226.7	34	4620
16	3.29	3.33	99.14	16	230.0	38	4467
18	3.31	3.35	88.87	20	261.7	40	4700
20	3.31	3.36	83.03	22	220.0		
22	3.33	3.39	77.2	24	210.0		
24	3.38	3.44	69.42	26	223.3		
26			61.41	28	245.0		
28	3.41	3.49	63.97	30	238.3		
30	3.45	3.51	59.88	32	245.0		
32	3.5	3.6	45.96	34	228.3		
34	3.6	3.73	37.46	36	245.0		
36	3.64	3.74	39.43	38	238.3		
38	3.72	3.85	33.27	40			
40			23.47				

Time (min)	Sulphide (mg/l)	pH (top)	pH(bottom)	Ni^{2+}(mg/L)	NaOH sulphides
0	0.00	6.78	6.77	203.20	0
0.5	49.05	5.63	5.53	199.00	
1	117.14	5.44	5.38	193.90	98.33
2	200.48	4.48	4.49	185.60	
4	272.38	3.89	3.90	172.70	
6	286.67	3.65	3.64	162.40	
8		3.45	3.44	151.40	1080
10	293.81	3.46	3.45	140.40	
12	306.19	3.46	3.44	128.10	1650
14	303.81	3.43	3.44	118.00	
16	300.00	3.44	3.45	112.30	2100
18	290.00	3.45	3.46	94.37	
20	292.86	3.48	3.50	86.03	2650
22		3.51	3.54	77.71	
24	289.05	3.55	3.56	68.70	2950
26	288.10	3.59	3.62	59.01	
28	290.48	3.64	3.70	52.70	3730
30		3.71	3.76	45.01	
32	297.14	3.80	3.88	38.52	4410
34	307.14	3.90	4.09	30.45	
36	291.90	4.02	4.10	22.64	

time (min)	sulphides (mg/l)	pH(top)	pH(bottom)	Ni^{2+} (mg/L)	NaOH sulphides
0	0.00	6.64	6.58	206.80	0
1	95.00	5.00	5.10	199.00	
2	158.33	4.29	4.39	187.30	116.67
4	216.67	3.71	3.78	184.95	263.33
6	231.67	3.5	3.55	170.30	540
8	253.33	3.41	3.43	161.95	780
10	255.00	3.36	3.36	147.95	1040
12	263.33	3.34	3.35	140.15	1300
14	243.33	3.33	3.33	125.60	1560
16	250.00	3.33	3.33	111.02	1760
18	230.00	3.34	3.34	105.72	2200
20	265.00	3.36	3.36	91.62	2420
22	265.00	3.38	3.38	84.53	2700
24	243.33	3.40	3.41	77.46	2760
26	255.00	3.43	3.44	69.06	3040
28	248.33	3.47	3.49	60.21	3320
30	261.67	3.52	3.55	58.34	3720
32	231.67	3.57	3.60	52.45	4560
34	266.67	3.64	3.66	42.24	4200
36	268.33	3.72	3.75	33.96	4400
38		3.77	3.81	31.04	4800
40	263.33	3.83	3.93	33.27	5080
45	263.33	4.51	4.66	23.47	5760

High alkalinity flowrate showing relative error in measurements [T05 = NaOH = 1.75, $H_2S(g)$ = 0.8L/min]

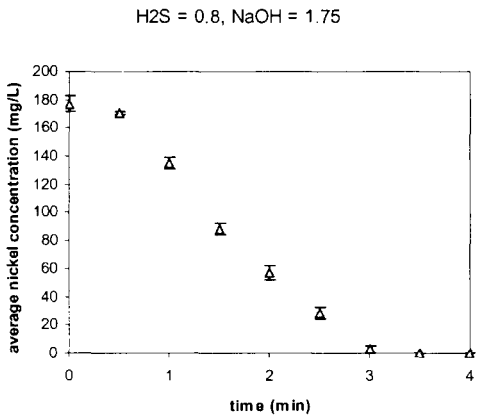

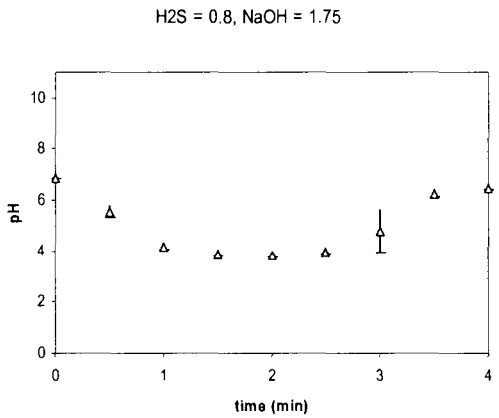

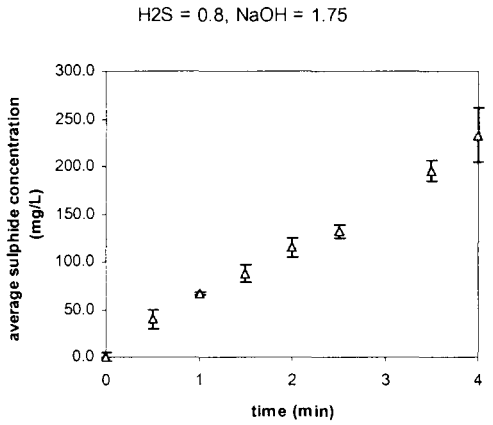

Time (minutes)	Sulphide (mg/l)
0	0.0
0.5	36.0
1	56.0
1.5	86.0
2	106.0
2.5	122.0
3.5	188.0
4	222.0
5	282.0
6	353.3
7	443.3
8	533.3
9	613.3
10	723.3

Time (minutes)	pH (top)	pH(bottom)	$Ni^{2+}(aq)$
0	6.85	6.81	182.6
0.5	5.80	5.72	171.5
1	4.28	4.70	138.9
1.5	3.97	4.61	91.9
2	3.83	4.41	61.6
2.5	3.96	4.53	32.21
3	3.94	5.97	5.49
3.5	6.36	6.49	0.15
4	6.49	6.58	0.15
4.5	6.71	6.78	0.13
5	6.82	6.90	0.21
6	7.02	6.99	0.13
7	7.13	7.14	0.16
8	7.21	7.20	0.17
9	7.27	7.30	0.18
10	7.24	7.33	0.20

Time (minutes)	Sulphide (mg/l)	pH (top)	pH(bottom)	$Ni^{2+}(aq)$
0	0.0	6.85	6.81	171.3
0.5	44.0	5.34	5.49	169.2
1	76.0	4.04	4.81	131.0
1.5	90.0	3.81	4.26	84.4
2	124.0	3.75	4.28	51.63
2.5	142.0	3.9	5.02	23.87
3	170.0	5.63	5.47	0.08
3.5	202.0	6.13	6.41	0.04
4	244.0	6.4	6.53	0.1
4.5	296.0	6.58	6.71	0.07
5	338.0	6.69	6.89	0.11
6	396.7	6.9	6.91	0.07
7	470.0	7.04	7.06	0.03
8	576.7	7.14	7.16	0.06
9	646.7	7.23	7.26	0.06
10	723.3	7.3	7.31	0.07

Appendix C

Tabulated values for high flowrate alkalinity experiments T01 –T04

NaOH = 2.23mmol/min $H_2S(g)$ = 0.1 L/min

Time (minutes)	Sulphide (mg/l)	pH (top)	pH(bottom)	$Ni^{2+}(aq)$
0	0.0	6.65	6.56	208.9
0.5	0.0	7.88	7.93	187.3
1	0.0	7.95	7.99	131.8
1.5	0.0	7.77	8.14	63.4
2	0.0	8.54	8.49	9.7
2.5	14.0	10.14	10.75	0.52
3	20.0	10.75	10.94	0.03
3.5	30.0	10.98	11.12	0.05
4	36.0	11.13	11.27	0.03
4.5	48.0	11.25	11.35	0.07
5	54.0	11.34	11.43	0
6	76.0	11.44	11.51	0.04
7	80.0	11.57	11.63	0.07
8	96.0	11.66	11.72	0.14
9	94.0	11.73	11.79	0.08
10	100.0	11.79	11.85	0.06

NaOH = 2.23mmol/min $H_2S(g)$ = 0.3 L/min

Time (minutes)	Sulphide (mg/l)	Time (minutes)	pH (top)	pH(bottom)	$Ni^{2+}(aq)$	NaOH sulphide(mg/L)
0	0.0	0	6.94	6.91	210.5	0.0
0.5	12.50	0.5	7.21	7.5	195.8	0.2
1	12.50	1	7.14	7.19	155.7	0.5
1.5	12.50	1.5	6.62	7.55	86.58	1.3
2	27.50	2	6.30	6.95	47.6	2.8
2.5	30.00	2.5	7.15	8.03	2.25	5.4
3	40.00	3	9.42	10.08	0.20	7.7
3.5	140.00	3.5	10.37	10.55	0.28	11.3
4	187.50	4	10.75	10.79	0.42	13.2
4.5	237.50	4.5	10.98	10.98	0.35	13.5
6	260.00	5	11.13	11.06	0.42	14.0
7	282.50	6	11.36	11.26	0.63	
		7	11.50	11.42	0.60	

NaOH = 2.23mmol/min $H_2S(g)$ = 0.5 L/min

Time (minutes)	Sulphide (mg/l)	pH (top)	pH(bottom)	$Ni^{2+}(aq)$	NaOH sulphide(mg/L)
0	0.0	7.11	6.71	217.4	0.0
0.5	12.5	6.47	6.17	201.8	1.2
1	27.5	5.53	5.36	149.9	5.7
1.5	47.5	4.91	5.42	76.78	10.3
2	52.5	4.6	5.62	21.32	21.5
2.5	62.5	6.41	6.88	0.32	38.8
3	117.5	6.83	7.11	0.17	49.0

3.5	170.0	7.11	7.22	0.15	65.0
4	195.0	7.4	7.30	0.17	78.0
4.5	287.5	7.89	7.49	0.16	
5	330.0	7.67	7.68	0.19	

NaOH = 2.23mmol/min $H_2S(g)$ = 0.8 L/min

Time (minutes)	Sulphide (mg/l)	Time (minutes)	pH (top)	pH(bottom)	Time (minutes)	$Ni^{2+}(aq)$
0	0.00	0	6.83	6.89	0	215.5
0.5	32.50	0.5	5.41	5.29	0.5	191.1
1	42.50	1	4.76	4.09	1	144.6
1.5	57.50	1.5	3.71	4.11	1.5	91.18
2	80.00	2	3.78	5.31	2	40.12
2.5	135.00	2.5	5.31	6.25	2.5	1.99
3	155.00	3	6.24	6.53	3	0.27
3.5	195.00	3.5	6.56	6.80	3.5	0.29
4	270.00	4	6.62	6.84	4	0.30
5	357.50	4.5	6.74	6.94	5	0.37
		5	6.82	7.03		

High flowrate alkalinity experiments showing complete reaction [T05 – T11]

NaOH = 1.75mmol/min $H_2S(g)$ = 0.1, 0.3, 0.5 and 0.8L/min

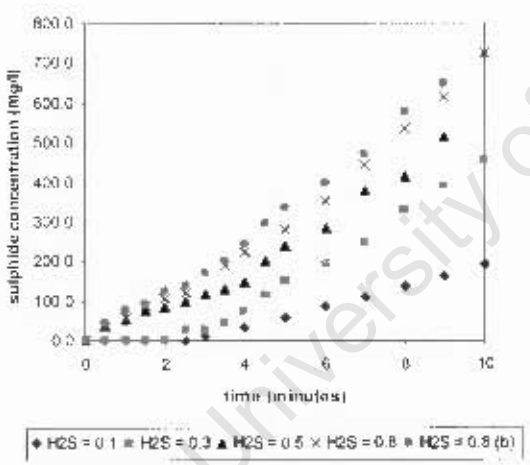

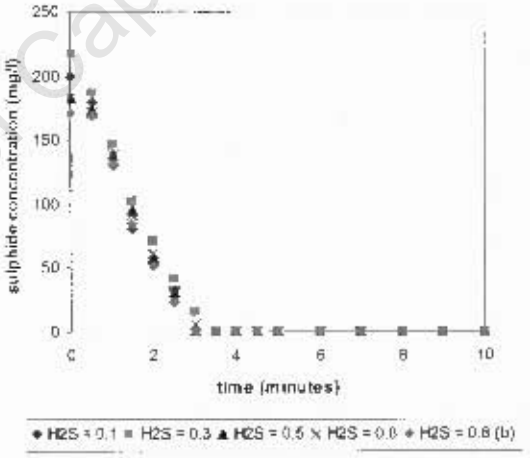

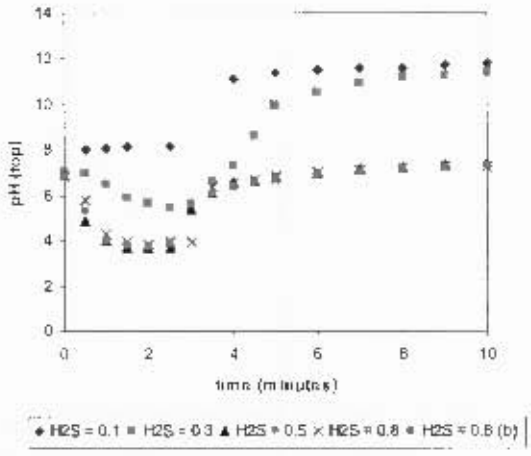

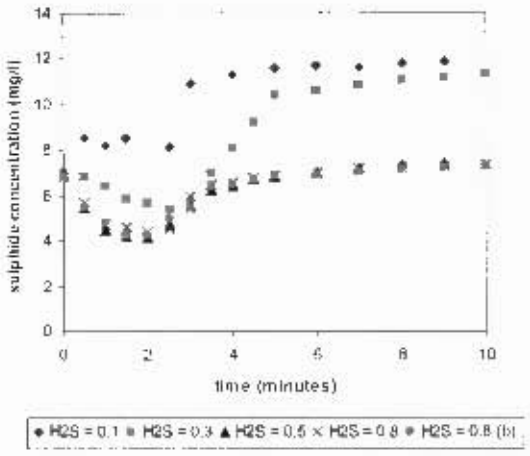

$H_2S(g)$ = 0.1L/min, NaOH = 1.75mmol/min

Time (minutes)	Sulphide (mg/l)	Time (minutes)	pH (top)	pH(bottom)	Time (minutes)	$Ni^{2+}(aq)$
0	0.0	0	6.99	6.99	0	199.7
0.5	0.0	0.5	8.00	8.53	0.5	179.1
1	0.0	1	8.10	8.21	1	130.4
1.5	0.0	1.5	8.16	8.53	1.5	81.2
2.5	0.0	2.5	8.15	8.15	2.5	32.28
3	13.0	4	11.08	10.88	3	0.22
4	35.0	5	11.35	11.33	4	0.19
5	56.0	6	11.50	11.56	5	0.2
6	88.0	7	11.57	11.68	6	0.19
7	110.0	8	11.54	11.61	7	0.2
8	138.0	9	11.69	11.80	8	0.24
9	164.0	10	11.75	11.88	9	0.16
10	194.0				10	0.24

$H_2S(g)$ = 0.3L/min, NaOH = 1.75mmol/min

Time (minutes)	Sulphide (mg/l)	pH (top)	pH(bottom)	$Ni^{2+}(aq)$
0	0.0	7.08	7.09	217.0
0.5	0.0	6.98	6.85	186.3
1	0.0	6.50	6.44	147.0
1.5	0.0	5.92	5.85	102.5
2	0.0	5.63	5.66	70.74
2.5	28.0	5.43	5.38	40.86
3	26.0	5.45	5.73	15.33
3.5	44.0	6.65	6.94	0.18
4	72.0	7.30	8.06	0.04
4.5	112.0	8.61	9.22	0.15
5	152.0	9.91	10.41	0.07
6	192.0	10.54	10.61	0.11
7	248.0	10.94	10.87	0.14
8	330.0	11.16	11.02	0.09
9	390.0	11.26	11.16	0.09
10	456.0	11.36	11.28	0.09

$H_2S(g)$ = 0.5L/min, NaOH = 1.75mmol/min

Time (minutes)	Sulphide (mg/l)	pH (top)	pH(bottom)	$Ni^{2+}(aq)$
0	0.0	6.89	6.98	183.2
0.5	38.0	4.88	5.46	173.9
1	52.0	3.99	4.46	138.2
1.5	76.0	3.70	4.18	94.6
2	82.0	3.67	4.15	57.6
2.5	98.0	3.69	4.67	30.52
3	118.0	5.38	5.50	0.39
3.5	130.0	6.13	6.22	0.03
4	148.0	6.59	6.47	0.07
4.5	202.0	6.67	6.72	0.09
5	238.0	6.80	6.84	0.07
6	286.0	6.97	7.01	0.02
7	380.0	7.14	7.2	0.03

8	418.0	7.25	7.34	0.05
9	514.0	7.34	7.44	0.04
10		7.46	7.50	0.07

NaOH 1.20mmol/min H_2S = 0.1, 0.2 and 0.3L/min

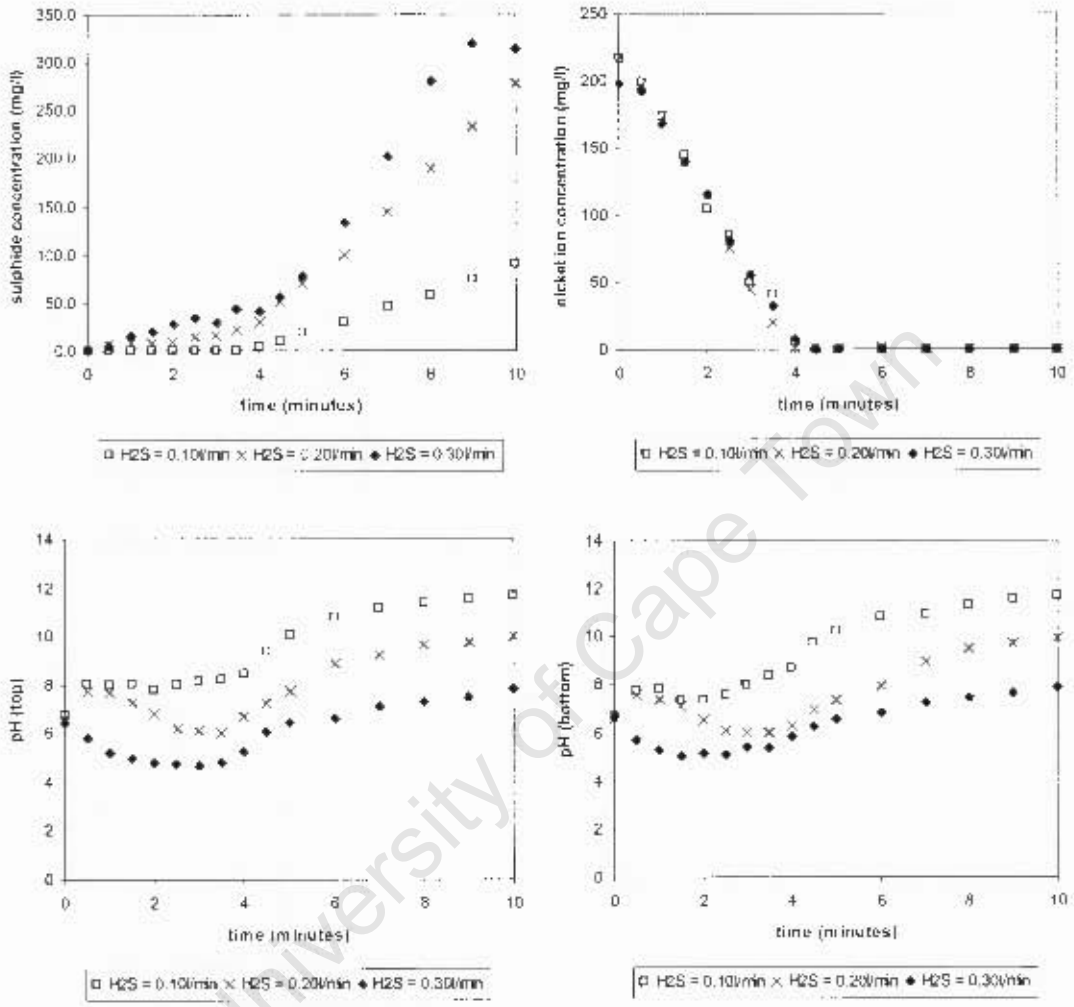

$H_2S(g)$ = 0.1L/min, NaOH = 1.20mmol/min

Time (minutes)	Sulphide (mg/l)	pH (top)	pH(bottom)	Ni^{2+}(aq)
0	0.0	6.76	6.71	217.1
0.5	0.0	8.03	7.78	198.6
1	0.0	7.98	7.81	173.3
1.5	0.0	8.07	7.33	144.1
2	0.0	7.80	7.42	103.9
2.5	0.0	8.06	7.60	85.80
3	0.0	8.17	8.02	49.60
3.5	0.0	8.24	8.42	40.56
4	4.0	8.46	8.73	5.58
4.5	10.0	9.40	9.79	0.26
5	18.0	10.06	10.27	0.08
6	30.0	10.81	10.81	0.10

7	46.0	11.17	10.96	0.09
8	58.0	11.38	11.30	0.07
9	74.0	11.54	11.55	0.09
10	90.0	11.64	11.68	0.18

$H_2S(g)$ = 0.2L/min, NaOH = 1.20mmol/min

Time (minutes)	Sulphide (mg/l)	pH (top)	pH(bottom)	$Ni^{2+}(aq)$
0	0.0	6.64	6.61	217.4
0.5	6.0	7.76	7.61	196.2
1	8.0	7.70	7.43	173.1
1.5	8.0	7.27	7.10	138.6
2	10.0	6.79	6.53	115.0
2.5	14.0	6.19	6.11	75.62
3	16.0	6.09	6.01	44.42
3.5	22.0	6.01	6.02	20.54
4	30.0	6.69	6.27	1.58
4.5	52.0	7.25	6.98	0.11
5	70.0	7.76	7.33	0.42
6	100.0	8.88	7.99	1.78
7	144.0	9.22	8.93	0.57
8	190.0	9.61	9.50	0.54
9	234.0	9.79	9.73	0.44
10	278.0	10.01	9.93	0.39

$H_2S(g)$ = 0.3L/min, NaOH = 1.20mmol/min

Time (minutes)	Sulphide (mg/l)	pH (top)	pH(bottom)	$Ni^{2+}(aq)$
0	0.0	6.43	6.67	197.7
0.5	4.0	5.81	5.72	192.6
1	16.0	5.25	5.27	167.3
1.5	20.0	5.00	5.05	140.5
2	28.0	4.81	5.17	115.8
2.5	34.0	4.75	5.13	81.47
3	30.0	4.68	5.44	55.14
3.5	44.0	4.78	5.43	32.06
4	42.0	5.26	5.84	8.08
4.5	56.0	6.07	6.27	0.24
5	78.0	6.42	6.58	0.32
6	134.0	6.66	6.86	0.32
7	202.0	7.12	7.28	0.32
8	280.0	7.33	7.48	0.37
9	320.0	7.52	7.67	0.33
10	314.0	7.86	7.91	0.41

Values from OLI modelling of T01 – T04

NaOH = 2.23mmol/min $H_2S(g)$ = 0.1 L/min

Appendix D

Relationship between NaOH and Ni^{2+} removal (ie ignoring the steps of NaOH effect on sulphide solubility)

Example:

NaOH = 2.23mmol/min, $H_2S(g)$ = 0.8L/min

Ni^{2+} removal rate $= \frac{197.7\,ppm}{58.69\,g/mol} \times \frac{g}{1000\,mg} \div 2.5\,\text{min} = 1.34\,\text{mmol/min}$

$\therefore$ Ratio of $\frac{d[NaOH]}{dt} : \frac{-d[Ni^{2+}]}{dt}$

$\Rightarrow \frac{2.23}{1.34} : \frac{1.34}{1.34}$

= 1.664:1

Appendix E

Comparison of Higbie's penetration theory prediction for sulphide in solution compared with experimentally determined values.

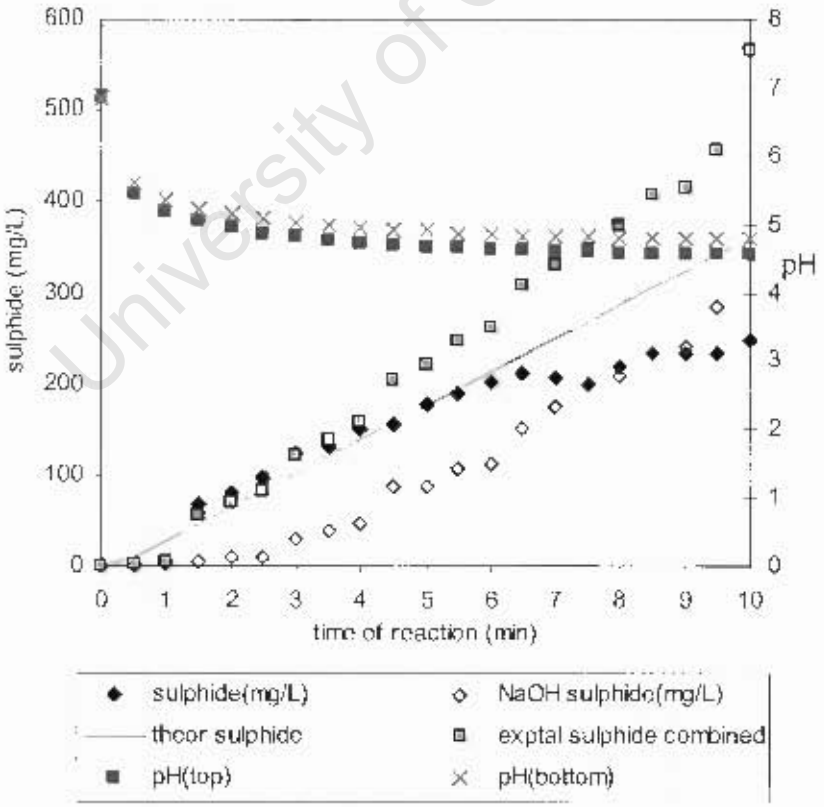

time(min)	pH(top)	pH(bottom)	Sulphide (mg/L)	NaOH sulphide (mg/L)	total sulphide (mg/L)
0	6.86	6.85	0	0	0
0.50	5.43	5.59	2.1	0.65	2.2
1.00	5.17	5.36	4.8	1.25	4.9
1.50	5.05	5.22	68	3.70	54.7
2.00	4.95	5.15	80	9.40	69.4
2.50	4.87	5.08	98	9.40	82.9
3.00	4.82	5.02	124	29.5	122.5
3.50	4.77	4.98	132	40.0	139.0
4.00	4.73	4.94	150	45.0	157.5
4.50	4.7	4.91	156	86.5	203.5
5.00	4.68	4.91	178	88.0	221.5
5.50	4.65	4.87	190	106.0	248.5
6.00	4.64	4.85	202	112.0	263.5
6.50	4.62	4.84	212	150.0	309.0
7.00	4.61	4.82	206	176.0	330.5
7.50	4.6	4.82	200	198.0	348.0
8.00	4.58	4.80	218	210.0	373.5
8.50	4.58	4.79	232	234.0	408.0
9.00	4.57	4.79	234	240.0	415.5
9.50	4.56	4.78	232	283.3	457.3
10.00	4.56	4.78	248	380.0	566.0

Appendix F

Supersaturation calculation using HS^-.

The expression for supersaturation is,

$$S = \frac{\gamma_{Ni^{2+}}[Ni^{2+}]\gamma_{HS^-}[HS^-]}{K_{SP,NiS}}$$

where the activity coefficients $\gamma_{Ni^{2+}}$ an d γ_{HS^-} = 0.807 (OLI), the solubility product $K_{SP,NiS} = 10^{-19.4}$ and the concentrations of Ni^{2+} and HS^- depend on experimental data.

The rate at which HS^- becomes available in solution depends on the rate of diffusion per unit interfacial area of bubbles in the column $\overline{R}$, where

$$\overline{R} = \frac{N_A}{t}$$

t is the contact time of a single bubble travelling the length of the bubble column (approximately 2s to travel 40cm). To convert $\overline{R}$ to the rate of diffusion independent of bubble area, multiply by the interfacial area, A. The interfacial area is calculated from the

observed number of bubbles in solution wrt $H_2S(g)$ flowrate. By counting the number of bubbles in the reactor volume and multiplying by their average diameter (R_B = 0.2mm, measured from observation), the interfacial area is determined as 0.0216m^2 when $H_2S(g)$ = 0.3L/min. The bubble diameter remained the same but the frequency of bubbles increased with increasing $H_2S(g)$ flowrate.

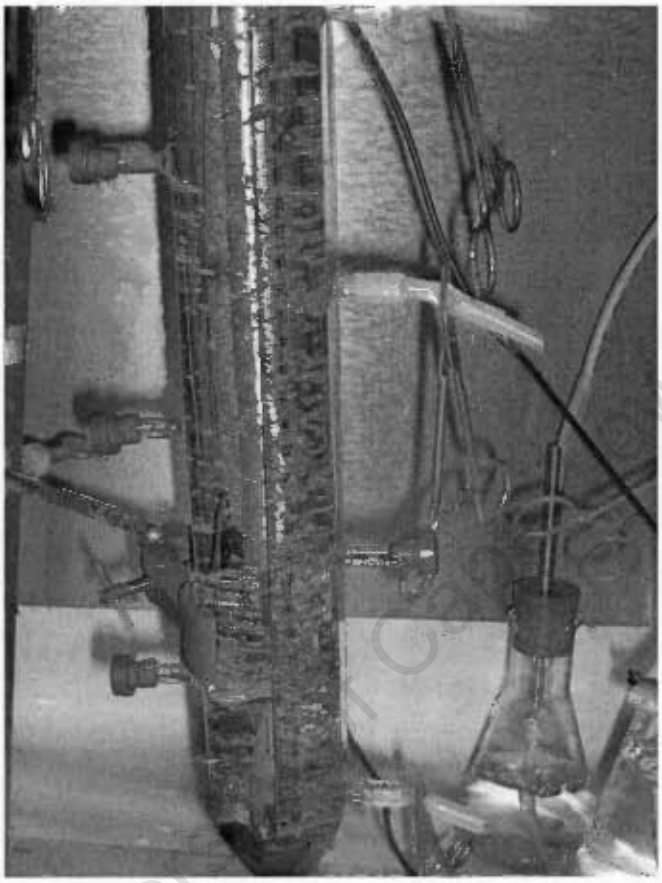

The flux of $H_2S(g)$ into solution is quantified in the following expression

$$N_A = 2k_c(c_{Ai} - c_{Ab})$$

where c_{Ai} is the interfacial concentration of $H_2S(aq)$ with a value of c_{Ai} = 18.18kg/m^3 (Perry, 2005), and c_{Ab} is the experimentally measured bulk concentration of sulphide in solution.

k_c is the mass transfer coefficient of $H_2S(g)$ into solution and was determined from the equation below

$$k_c = 0.82\sqrt{D_{H_2S}}\left(\frac{g}{R_B}\right)^{1/4}$$

Where g is acceleration due to gravity = 9.81 m/s^2 and D_{H_2S} = 1.61 x 10^{-9}m^2/s (Perry, 2006). The value of k_c was found to be 0.00049m/s.

From c_{Ab} and the corresponding measured pH, the concentration of HS^- is determined using the pH dependent speciation of H_2S, where K_1 = 9.12 x 10^{-8} and K_2 = 3.98 x 10^{-18}.

$$[HS^-] = \frac{[S]_{total}}{\frac{[H^+]}{K_1} + 1 + \frac{K_2}{[H^+]}}$$

Example: Calculation of the rate of diffusion when H_2S(g) = 0.3L/min, NaOH = 2.23mmol/min (experimental data shown below).

Time (min)	Time (s)	[Ni^{2+}](aq) (measured) (ppm)	[Ni^{2+}](aq) (measured) (g/L)	[Ni^{2+}](aq) (measured) (mol/L)	Sulphide (measured) (mg/l)	Sulphide (measured) (kg/m3)	pH
0	0	210.5	2.11E-01	3.59E-03	0	0	6.94
0.5	30	195.8	1.96E-01	3.34E-03	0	0	7.21
1	60	155.7	1.56E-01	2.65E-03	0	0	7.14
1.5	90	86.6	8.66E-02	1.48E-03	0	0	6.62
2	120	47.60	4.76E-02	8.11E-04	12.0	0.012	6.30
2.5	150	2.25	2.25E-03	3.83E-05	38.0	0.038	7.15
3	180	0.20	2.00E-04	3.41E-06	60.0	0.060	9.42
3.5	210	0.28	2.80E-04	4.77E-06	85.0	0.085	10.37
4	240	0.42	4.20E-04	7.16E-06	110.0	0.110	10.75
4.5	270	0.35	3.50E-04	5.96E-06	130.0	0.130	10.98
5	300	0.42	4.20E-04	7.16E-06	144.0	0.144	11.13

The concentration of HS^- at 2 minutes calculated using

$$[HS^-] = \frac{[S]_{total}}{\frac{[H^+]}{K_1} + 1 + \frac{K_2}{[H^+]}} = \frac{0.012/32 mol/L}{\frac{-\log(6.30)}{9.12\times10^{-8}} + 1 + \frac{3.98\times10^{-18}}{-\log(6.30)}} = 5.77 \text{ x } 10^{-5}\text{mol/L } (= c_{Ab})$$

Using the concentration of HS^-, calculated above, the flux of H_2S(g) into solution, N_A, is calculated

$$N_A = 2k_c(c_{Ai} - c_{Ab}) = 2 \text{ x } 0.00049[\text{m/s}](18.18 - 1.85 \text{ x } 10^{-6})[\text{kg/m}^3] = 8.90 \text{ x } 10^{-3}$$

To convert the flux into a rate, multiply by the total bubble interfacial area = 0.0261m^2. To calculate the concentration of HS^- based on the rate at which "HS^-" enters solution. The rate at which "HS^-" enters solution is a combination of the rate at which sulphide enters solution and speciates, since speciation is taken as instantaneous. The driving force of the diffusion is thus the difference in concentration between the bubble (18.18kg/m3) and the HS^- ions in solution, since this ion is consumed by reaction, and again assuming that speciation is instantaneous.

Therefore the rate of diffusion becomes

$$\overline{R} = \frac{N_A}{t} = \frac{8.90 \times 10^{-3} kg/m^3}{0.2 m/s} = 3.42 \times 10^{-5} \text{mol/L.s}$$

The diffusion rates at the other $H_2S(g)$ flowrates are shown in the table below

$H_2S(g)$	$\overline{R}$, Rate of diffusion
L/min	mol/L.s
0.1	1.68e-05
0.3	3.42e-05
0.5	4.88e-05
0.8	7.08e-05

A schematic diagram of the modelling algorithm used to determine the HS^- concentration and the pH during the NiS precipitation is shown below

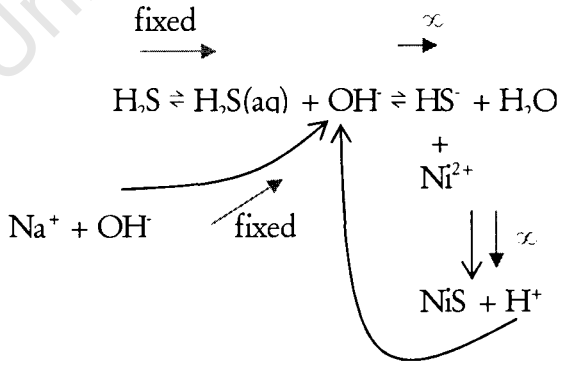

The steps of the algorithm are shown below

1. Initial pH gives H^+ ions in solution (pHi = 6.94)

2. H_2S diffusion rate from Higbie's Theory quantifies sulphide in solution in time interval specified which is from t = 0s to t1 = 0.01s (Δt).
3. Initial speciation to obtain the bisulphide concentration for the concentration of sulphide which has diffused into solution in the time interval Δt_1 is calculated

$$[HS^-] = \frac{[S]_{total}}{\frac{[H^+]}{K_1} + 1 + \frac{K_2}{[H^+]}}$$

4. The nickel precipitated is equivalent to HS^- ion concentration. The remaining nickel in solution (Ni^{2+}remain2) is equivalent to initial nickel concentration (200ppm) – initial HS^- concentration.
5. The concentration of H^+ ions released from reaction are equivalent to the nickel concentration reacted and from speciation are equivalent to the HS^- ion concentration
6. The pH (pH2) for the second time (t2) is calculated from released H^+ ions (step5)
7. pH2 gives H^+ ions in solution for the second time interval
8. Add NaOH in time interval t1 to t2 (Δt)
9. Calculate new pH (pH2mix) resulting from the combination of OH^- ions in solution and H^+ ions as a result of pH2
10. Calculate sulphide which diffuses into solution in the time interval Δt for the new time t2 and add sulphide which remains from time t1. Speciate sulphide in solution using pH2mix calculated.
11. React HS^- with Ni^{2+}remain2 in solution. Nickel reacting equivalent to HS^- in solution.
12. H^+ ions in solution equivalent to Hmix (H^+ initially in solution at pH2mix) + HS^- speciated (H^+ ions liberated by speciation of sulphide to HS^-) + Ni^{2+} reacted (H^+ liberated by reaction of nickel) to give pH3.
13. Repeat from step 7 for duration of reaction.
14. Calculate the supersaturation using the equation below and the concentrations of nickel and sulphide calculated for each time t1, t2 etc.

$$S = \frac{\gamma_{Ni^{2+}}[Ni^{2+}]\gamma_{HS^-}[HS^-]}{K_{SP,NiS}}$$

The table below shows the calculations for Ni^{2+} and HS^- during the first 0.1s (for each Δt) of the precipitation of Ni2$^+$ using $H_2S(g)$ = 0.3L/min and NaOH = 1.20mmol/min.

Time	pHi	[H+]	H+	OH added	[H+] mix	pH mix	H2S diss	Total S	H2S(aq)	HS-	S2-	H2S ppm	Ni ppt	Ni2+	Ni ppm	H+ spec	H+ ppt	[H+] ppt	pH ppt	supersaturation
0	6.94	1.15E-07	8.61E-08	0	1.15E-07	6.94	0	0	0	0	0	0.000	0	3.41E-03	200.00	0	0	1.15E-07	6.94	0.00E+00
0.01	6.94	1.15E-07	8.61E-08	2.00E-07	6.59E-08	7.18	2.565E-07	2.565E-07	1.076E-07	1.489E-07	9.004E-18	0.004	1.489E-07	3.41E-03	199.99	1.489E-07	1.49E-07	4.63E-07	6.33	6.45E+05
0.02	6.33	4.63E-07	3.47E-07	2.00E-07	1.96E-07	6.71	2.565E-07	3.641E-07	2.486E-07	1.155E-07	2.340E-18	0.008	1.155E-07	3.41E-03	199.98	1.151E-07	1.15E-07	5.04E-07	6.30	3.88E+05
0.03	6.30	5.04E-07	3.78E-07	2.00E-07	2.38E-07	6.62	2.565E-07	5.051E-07	3.650E-07	1.401E-07	2.348E-18	0.012	1.401E-07	3.41E-03	199.98	1.40E-07	1.40E-07	6.11E-07	6.21	5.71E+05
0.04	6.21	6.11E-07	4.58E-07	2.00E-07	3.45E-07	6.46	2.565E-07	6.2149E-07	4.914E-07	1.301E-07	1.503E-18	0.017	1.301E-07	3.41E-03	199.97	1.30E-07	1.30E-07	6.91E-07	6.16	4.92E+05
0.05	6.16	6.91E-07	5.19E-07	2.00E-07	4.25E-07	6.37	2.565E-07	7.4791E-07	6.157E-07	1.322E-07	1.239E-18	0.021	1.322E-07	3.41E-03	199.96	1.32E-07	1.32E-07	7.77E-07	6.11	5.08E+05
0.06	6.11	7.77E-07	5.83E-07	2.00E-07	5.11E-07	6.29	2.565E-07	8.7221E-07	7.400E-07	1.322E-07	1.030E-18	0.025	1.322E-07	3.41E-03	199.95	1.32E-07	1.32E-07	8.63E-07	6.06	5.08E+05
0.07	6.06	8.63E-07	6.47E-07	2.00E-07	5.966E-07	6.22	2.565E-07	9.9654E-07	8.644E-07	1.322E-07	8.822E-19	0.029	1.322E-07	3.41E-03	199.95	1.32E-07	1.32E-07	9.49E-07	6.02	5.08E+05
0.08	6.02	9.49E-07	7.12E-07	2.00E-07	6.82E-07	6.17	2.565E-07	1.1209E-06	9.887E-07	1.322E-07	7.713E-19	0.034	1.322E-07	3.41E-03	199.94	1.32E-07	1.32E-07	1.03E-06	5.99	5.08E+05
0.09	5.99	1.03E-06	7.76E-07	2.00E-07	7.68E-07	6.11	2.565E-07	1.2452E-06	1.113E-06	1.322E-07	6.851E-19	0.038	1.322E-07	3.41E-03	199.93	1.32E-07	1.32E-07	1.12E-06	5.95	5.08E+05
0.1	5.95	1.12E-06	8.40E-07	2.00E-07	8.54E-07	6.07	2.565E-07	1.3695E-06	1.237E-06	1.322E-07	6.163E-19	0.042	1.322E-07	3.41E-03	199.92	1.32E-07	1.32E-07	1.21E-06	5.92	5.08E+05

Appendix G

PSD from the Malvern Mastersizer® for batch precipitation of NiS using Na_2S(aq) ratio of Ni:S = 1:1, pHi = 11.59

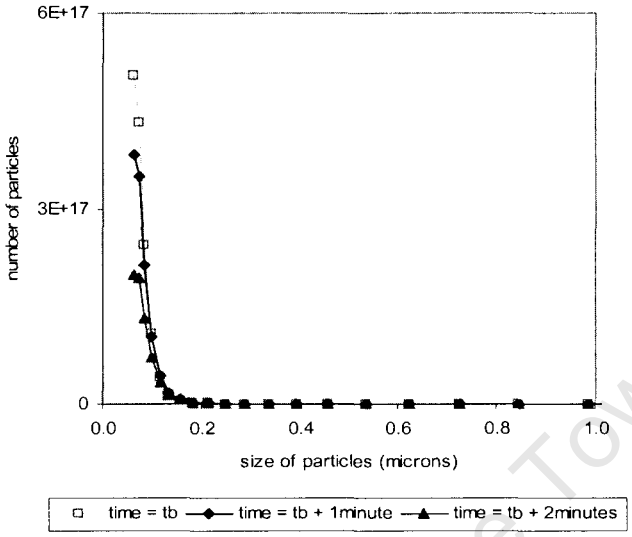

Appendix H

PSD for semi-batch precipitation of NiS using H_2S(g) when H_2S(g) = 0.8L/min NaOH = 2.23mmol/min

Beckman Coulter® Counter

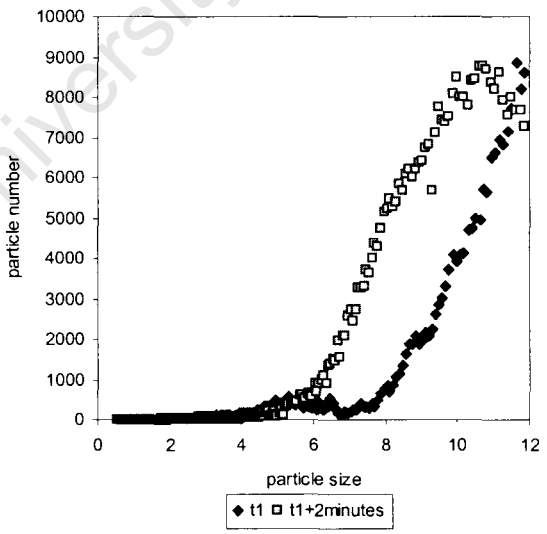

Malvern Mastersizer®

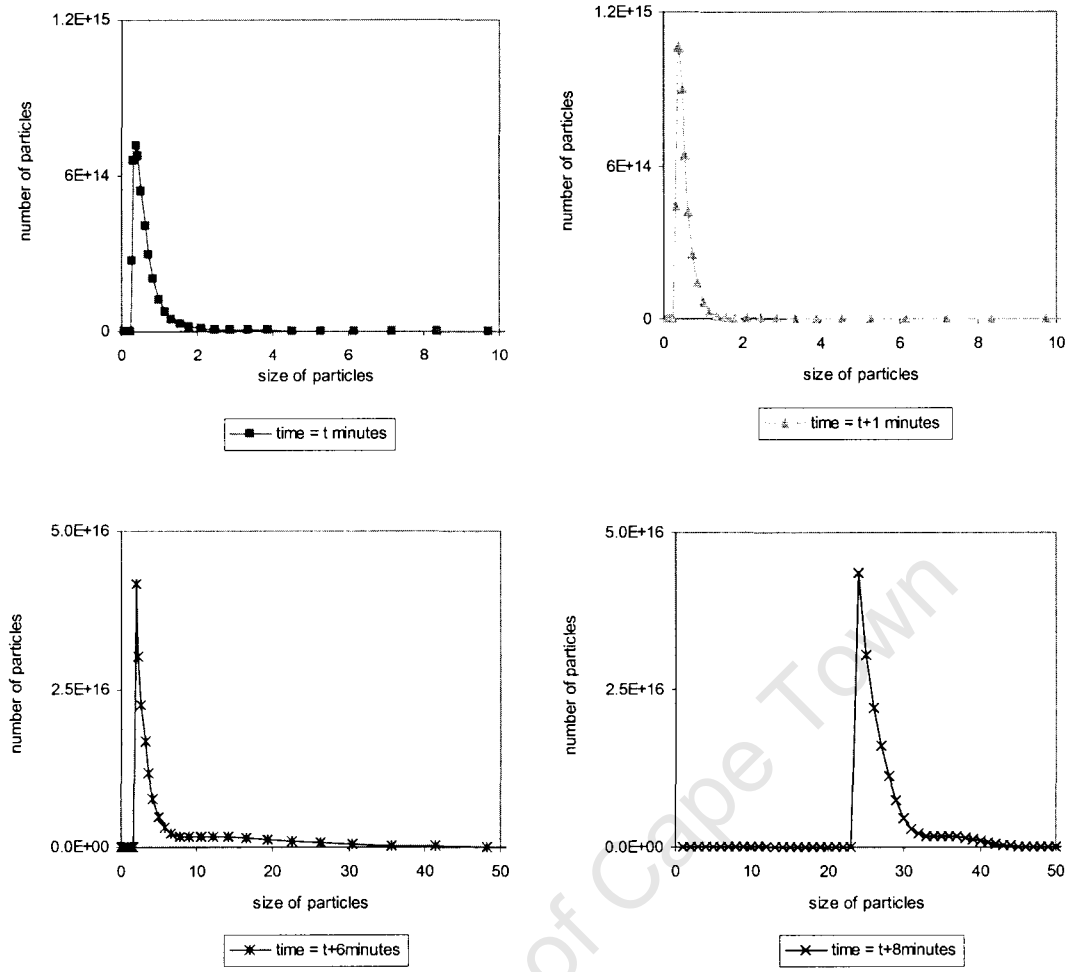

Appendix I

XRD data for NiS precipitates formed

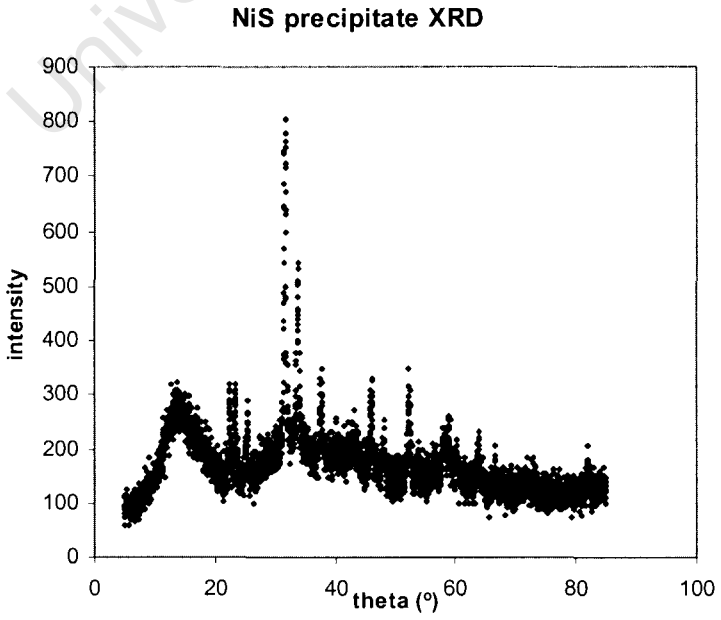

SEM pictures taken of NiS precipitates formed

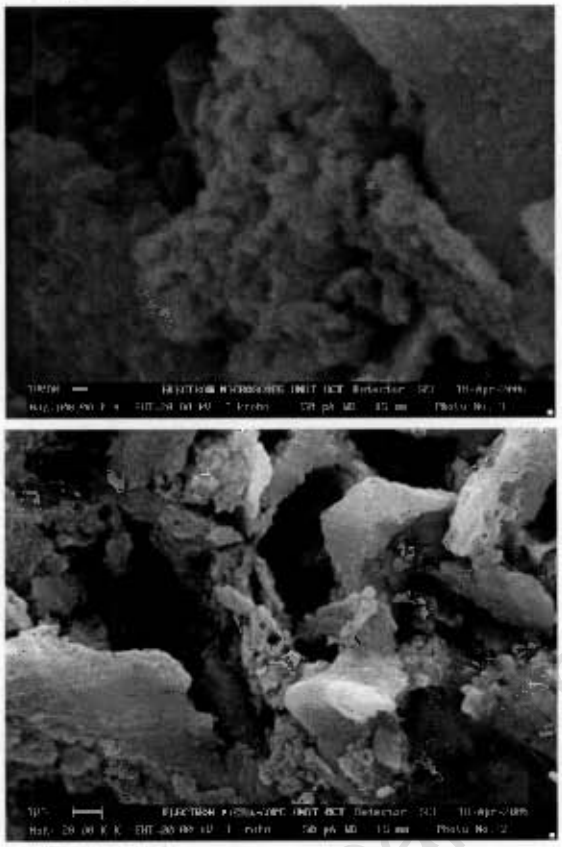

Appendix J

H^+ ion mass balance between pH change due to reaction of diluted RES and protons liberated by reaction of nickel and cobalt ions (experimental run below; RES01 – no NaOH used)

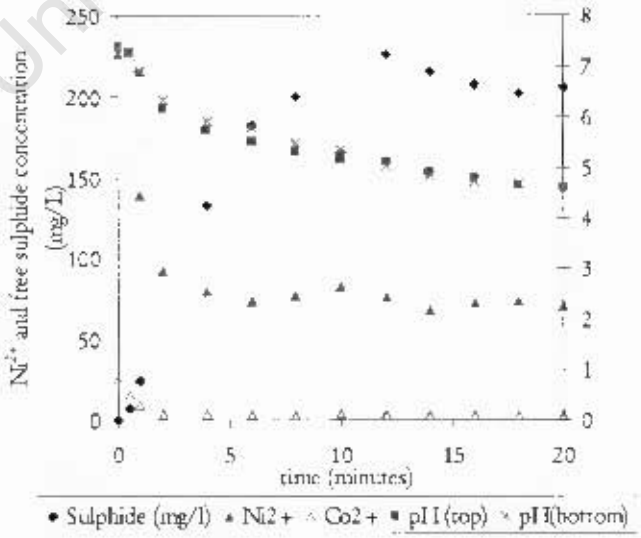

Time (minutes)	Sulphide (mg/l)	pH (top)	pH(bottom)	Ni^{2+}(aq)	Co^{2+}(aq)

0	0	7.36	7.35	225.6	25.04
0.5	7	7.26	7.20	276.7	14.79
1	24	6.86	6.92	138.7	9.21
2		6.16	6.35	92.0	3.49
4	133	5.73	5.91	79.6	3.55
6	182	5.50	5.78	73.78	3.23
8	200	5.31	5.48	76.80	3.02
10	165	5.16	5.33	82.07	3.15
12	226	5.10	5.03	76.58	3.05
14	215	4.9	4.84	67.94	2.64
16	207	4.8	4.74	72.99	2.61
18	202	4.65	4.66	73.4	2.80
20	205	4.6	4.62	71.21	2.53

Alkalinity for diluted RES to quantify buffering capacity;

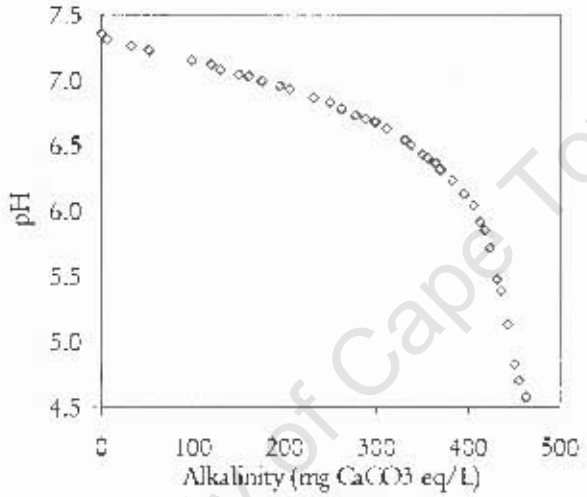

pH	ml	ml 0.02N H_2SO_4 required	mmol protons per ml RES sample for DpH	cumulative protons	alkalinity
7.35	0.00	0.00	0	0	0
7.31	0.10	0.10	1.00E-04	1.00E-04	5.0
7.26	0.65	0.55	5.50E-04	6.50E-04	32.5
7.23	1.05	0.40	4.00E-04	1.05E-03	52.5
7.15	1.95	0.90	9.00E-04	1.95E-03	97.5
7.11	2.40	0.45	4.50E-04	2.40E-03	120.0
7.08	2.60	0.20	2.00E-04	2.60E-03	130.0
7.04	3.00	0.40	4.00E-04	3.00E-03	150.0
7.02	3.20	0.20	2.00E-04	3.20E-03	160.0
6.99	3.50	0.30	3.00E-04	3.50E-03	175.0
6.95	3.90	0.40	4.00E-04	3.90E-03	195.0
6.93	4.10	0.20	2.00E-04	4.10E-03	205.0
6.86	4.60	0.50	5.00E-04	4.60E-03	230.0
6.83	4.95	0.35	3.50E-04	4.95E-03	247.5
6.78	5.20	0.25	2.50E-04	5.20E-03	260.0
6.73	5.55	0.35	3.50E-04	5.55E-03	277.5
6.70	5.75	0.20	2.00E-04	5.75E-03	287.5
6.67	5.95	0.20	2.00E-04	5.95E-03	297.5
6.62	6.20	0.25	2.50E-04	6.20E-03	310.0
6.54	6.60	0.40	4.00E-04	6.60E-03	330.0
6.50	6.75	0.15	1.50E-04	6.75E-03	337.5

6.43	7.00	0.25	2.50E-04	7.00E-03	350.0
6.40	7.10	0.10	1.00E-04	7.10E-03	355.0
6.36	7.30	0.20	2.00E-04	7.30E-03	365.0
6.31	7.40	0.10	1.00E-04	7.40E-03	370.0
6.22	7.65	0.25	2.50E-04	7.65E-03	382.5
6.13	7.90	0.25	2.50E-04	7.90E-03	395.0
6.04	8.10	0.20	2.00E-04	8.10E-03	405.0
5.91	8.25	0.15	1.50E-04	8.25E-03	412.5
5.85	8.35	0.10	1.00E-04	8.35E-03	417.5
5.71	8.45	0.10	1.00E-04	8.45E-03	422.5
5.48	8.60	0.15	1.50E-04	8.60E-03	430.0
5.39	8.70	0.10	1.00E-04	8.70E-03	435.0
5.12	8.85	0.15	1.50E-04	8.85E-03	442.5
4.83	9.00	0.15	1.50E-04	9.00E-03	450.0
4.70	9.10	0.10	1.00E-04	9.10E-03	455.0
4.58	9.25	0.15	1.50E-04	9.25E-03	462.5
4.48	9.30	0.05	5.00E-05	9.30E-03	465.0
4.38	9.45	0.15	1.50E-04	9.45E-03	472.5
4.27	9.60	0.15	1.50E-04	9.60E-03	480.0
4.22	9.70	0.10	1.00E-04	9.70E-03	485.0
4.15	9.85	0.15	1.50E-04	9.85E-03	492.5
4.11	9.90	0.05	5.00E-05	9.90E-03	495.0
4.06	10.10	0.20	2.00E-04	1.01E-02	505.0
4.02	10.20	0.10	1.00E-04	1.02E-02	510.0
3.96	10.45	0.25	2.50E-04	1.05E-02	522.5
3.90	10.65	0.20	2.00E-04	1.07E-02	532.5
3.85	10.90	0.25	2.50E-04	1.09E-02	545.0
3.82	11.10	0.20	2.00E-04	1.11E-02	555.0
3.79	11.20	0.10	1.00E-04	1.12E-02	560.0
3.74	11.50	0.30	3.00E-04	1.15E-02	575.0
3.69	11.80	0.30	3.00E-04	1.18E-02	590.0
3.65	12.15	0.35	3.50E-04	1.22E-02	607.5
3.59	12.65	0.50	5.00E-04	1.27E-02	632.5
3.54	13.10	0.45	4.50E-04	1.31E-02	655.0
3.50	13.50	0.40	4.00E-04	1.35E-02	675.0
3.45	14.10	0.60	6.00E-04	1.41E-02	705.0
3.39	14.80	0.70	7.00E-04	1.48E-02	740.0
3.35	15.55	0.75	7.50E-04	1.56E-02	777.5
3.28	16.85	1.30	1.30E-03	1.69E-02	842.5
3.23	18.00	1.15	1.15E-03	1.80E-02	900.0
3.18	19.05	1.05	1.05E-03	1.91E-02	952.5
3.15	19.95	0.90	9.00E-04	2.00E-02	997.5
3.10	21.50	1.55	1.55E-03	2.15E-02	1075.0
3.04	23.50	2.00	2.00E-03	2.35E-02	1175.0
3.00	25.35	1.85	1.85E-03	2.54E-02	1267.5
2.97	26.80	1.45	1.45E-03	2.68E-02	1340.0
2.94	28.40	1.60	1.60E-03	2.84E-02	1420.0
2.90	30.45	2.05	2.05E-03	3.05E-02	1522.5
2.87	33.70	3.25	3.25E-03	3.37E-02	1685.0
2.80	38.00	4.30	4.30E-03	3.80E-02	1900.0
2.77	39.75	1.75	1.75E-03	3.98E-02	1987.5
2.76	41.65	1.90	1.90E-03	4.17E-02	2082.5
2.74	43.95	2.30	2.30E-03	4.40E-02	2197.5
2.71	46.15	2.20	2.20E-03	4.62E-02	2307.5

2.70	47.80	1.65	1.65E-03	4.78E-02	2390.0
2.68	50.00	2.20	2.20E-03	5.00E-02	2500.0

MASS BALANCE FOR H^+ ions

IN		alkalinity	
initial pH	7.35	0	
final pH	4.62	9.10E-03	pH
Δ pH	2.73		

from alkalinity calcs # H^+ ions for D pH =

(dil RES) $\Delta pH_{dil\ RES}$ =

ΔH^+	0.009	mmol/ml sample	
	6.75	mmol/750ml	

OUT

initial Ni2+	225.6	ppm		
final Ni2+	71.21	ppm		
ΔNi^{2+}	154.39	ppm	2.63	mmol/L
			1.97	mmol/750ml
initial Co2+	25.04			
final Co2+	2.53			
ΔCo^{2+}	22.51	ppm	0.382	mmol/L
			0.286	mmol/750ml

based on $Ni^{2+} + HS^- \rightarrow NiS + H^+$

H^+ released =	3.01	ppm	
	6.03	mmol/L	
	4.52	mmol/750ml	
In - out |%	% error = 32.8	%	